ENGINEERED CRAC CHANNEL FOR OPTICAL CONTROL OF CALCIUM SIGNALING

A Dissertation

by

LIAN HE

Submitted to the Office of Graduate and Professional Studies of
Texas A&M University
in partial fulfillment of the requirements for the degree of

DOCTOR OF PHILOSOPHY

Chair of Committee,	Yubin Zhou
Committee Members,	Michael X. Zhu
	David J. Reiner
	Fen Wang
Head of Program,	Warren E. Zimmer

May 2018

Major Subject: Medical Sciences

ABSTRACT

Calcium (Ca^{2+}) acts as a universal second messenger to regulate a myriad of biological processes, including gene expression, cell metabolism, lymphocyte activation and cell growth. In non-excitable cells such as cells of the immune system, store-operated Ca^{2+} entry (SOCE) through the Ca^{2+} release-activated Ca^{2+} (CRAC) channel is primarily coordinated by two components: the ER-resident Ca^{2+} sensor protein stromal interaction molecule 1 (STIM1) and the pore subunit ORAI1 on the plasma membrane. To meet the demand of chemical biology tools for remote control of Ca^{2+} signaling in mammals with high precision, we set out to engineer photo-sensitivities into either STIM1 (OptoSTIM1) or ORAI1 (OptoORAI1) to generate photoswitchable CRAC channels.

OptoSTIM1 was engineered by combining STIM1-ORAI1 activation region (SOAR) of STIM1 with the light-reactive light-oxygen-voltage (LOV2) domain. The light-inducible effects were assessed by Ca^{2+} influx with genetically-encoded calcium indicators, degrees of NFAT translocation, and expression levels of Ca^{2+}/NFAT downstream targets. To generate OptoORAI1, LOV2 was inserted into the loop region of ORAI1 and thus acted as an allosteric switch to induce structural rearrangement within ORAI1 to open the channel. Through several rounds of randomized screening and optimization, we identified one OptoORAI1 variant exhibiting a high dynamic change in the light-induced Ca^{2+} response without noticeable dark activity. In parallel, to enable more flexible and versatile optogenetic engineering of proteins, we developed a series of engineered LOV2 variants (cpLOV2) through circular permutation. cpLOV2 creates new interfaces to cage protein function, thus enabling broader applications of LOV2-based optogenetic tools to targets that are otherwise not photo-controllable.

In summary, our single-component OptoCRAC tools provide new opportunities to remotely and precisely control the Ca^{2+} signaling at high spatial and temporal resolution. We have successfully demonstrated the use of OptoCRAC to photo-tune Ca^{2+}/NFAT-dependent gene expression, as well as transcriptional reprogramming of endogenous genes when coupled with the CRISPR/Cas9 genome editing technique.

DEDICATION

I would like to dedicate this dissertation to my parents, husband and my son for their unconditional and continuous supports and loves.

NOMENCLATURE

AAV	Adeno Associated Viruses
BLINK	Light-gated potassium channel
Ca^{2+}	Calcium
CAD	CRAC activation domain
CatCh	Calcium translocating channelrhodopsin
CC1	Coiled-coil 1
ChR	Channelrhodopsin
CoIP	Co-immunoprecipitation
cpLOV2	Circularly permuted LOV2
CRAC	Calcium release-activated calcium channel
Cry2	Cryptochrome 2
CT	C-terminus
dCas9	Catalytically deactivated CRISPR associated protein 9
DMEM	Dulbecco's modified Eagle's medium
ER	Endoplasmic reticulum
ESC	Embryonic stem cell
FBS	Fetal bovine serum
FMN	Flavin mononucleotide
HEPES	N-2-hydroxyethylpiperazine-N-2-ethane sulfonic acid
ID	Inactivation domain
IFN-γ	Interferon-γ

IL-2	Interleukin 2
IP_3	Inositol trisphosphate
IP_3R	Inositol trisphosphate receptor
IRES	Internal ribosome entry site
iSH2	Inter-SH2
LOV	Light, oxygen and voltage
Luc	Luciferase
Lyn	Tyrosine-protein kinase Lyn
mCh	mCherry
MBP	Maltose binding protein
Na^+	Sodium
NES	Nuclear export signal
NFAT	Nuclear factor of activated T-cells
NIR	Near-infrared
NLS	Nuclear localization signal
ORAI1	Calcium release-activated calcium channel protein 1
PAS	Per-ARNT-Sim
PBS	Phosphate buffered saline
pH	Potential of hydrogen
PHR	Photolyase homology region
PI3K	Phosphoinositide 3-kinase
$PI(4,5)P_2$	Phosphatidylinositol 4,5-bisphosphate
$PI(3,4,5)P_3$	Phosphatidylinositol (3,4,5)-trisphosphate

PKC	Protein kinase C
PKI- α	Protein kinase inhibitor-α
PM	Plasma membrane
PMA	Phorbol 12-myristate-13-acetate
PS	Pro/Ser-rich domain
RIPA	Radioimmunoprecipitation assay buffer
ROI	Region of interest
SAM	sterile α-motif
SCID	Severe combined immunodeficiency
SDS	Phosphate buffered saline
SDS-PAGE	Sodium dodecyl sulfate-polyacrylamide gel electrophoresis
SOAR	STIM-ORAI activation region
SOCE	Store-operated Ca^{2+} entry
SP	Signal peptide
STIM1	Stromal interaction molecule 1
TG	Thapsigargin
TIRF	Total internal reflection fluorescence
TM	Transmembrane domain
UAS	Upstream activator sequence
UCNP	Upconversion nanoparticles
VPR	VP64-p65-Rta
Zdk	Zdark

CONTRIBUTORS AND FUNDING SOURCES

This work was completed in Dr. Yubin Zhou's Lab. This work was supported by a dissertation committee consisting of Professors Yubin Zhou, Fen Wang and David Reiner of the Center for Translational Cancer Research in Texas A&M Institute of Biosciences and Technology, Professor Michael Zhu of the Department of Integrative Biology and Pharmacology in the University of Texas Health Science Center at Houston McGovern Medical School, Professor Dekai Zhang (former committee member) of Center for Infectious and Inflammatory Diseases in Texas A&M Institute of Biosciences and Technology.

The STIM1 and ORAI1 fragments described in Chapter II were provided by Dr. Guolin Ma of the Center for Translational Cancer Research in Texas A&M Institute of Biosciences and Technology. The statistical analyses for NFAT-GFP nuclear translocation depicted in Chapter IV were conducted by Reid Powell of the Center for Translational Cancer Research in Texas A&M Institute of Biosciences and Technology.

Funding Sources

This work was supported by the National Institutes of Health grants (R01GM112003 and R21GM126532), the Welch Foundation (BE-1913), the American Cancer Society ((RSG-16-215-01-TBE), and the Cancer Prevention and Research Institutes of Texas (RP170660).

TABLE OF CONTENTS

Page

LIST OF FIGURES

Page

LIST OF TABLES

Page

CHAPTER I

INTRODUCTION AND LITERATURE REVIEW

The calcium ion (Ca^{2+}) serves as a versatile and universal second messenger to control many biological processes, such as muscle contraction, neurotransmitter transmission and lymphocyte activation [1-3]. Calcium release-activated calcium (CRAC) channel is one of the primary Ca^{2+} entry routes in mammals and is widely expressed in non-excitable tissues [4-6].The CRAC channel is among the most selective Ca^{2+} channels with an estimated selectivity of 1000 for Ca^{2+} over Na^{+}, and it is best characterized in non-excitable cells such as T cells to control lymphocytes activation [7]. Abnormal CRAC channel activity is closely related to human diseases [8]. Loss of STIM1 or ORAI1 function causes severe combined immunodeficiency (SCID) in humans. The infants with this immunodeficiency disease often die at the very early age of life due to compromised immune function and recurrent infections [9, 10]. ORAI or STIM depletion in mice causes defective cytokines production in T cells [11, 12]. And this signaling pathway has been validated as a therapeutic target for suppressing immune response [13-15]. Gain-of-function mutations in ORAI1 and STIM1 have been reported to cause tubular aggregate myopathy (TAM) [16, 17], and augmented ORAI-STIM signaling is implicated in cardiac hypertrophy [18].

In resting T cells, the Ca^{2+} concentration is tightly controlled. The cytosolic Ca^{2+} level is maintained in the range of 50-100 nM, and the internal Ca^{2+} store such as endoplasmic reticulum (ER) can maintain the concentration up to 400–600 μM Ca^{2+}. By contrast, the extracellular Ca^{2+} concentration can reach 1–2 mM. As a prototypical example of store-operated Ca^{2+} entry (SOCE), the CRAC channel is activated upon ER Ca^{2+} store depletion. In T cells, antigen

presentation to T cell receptor in the plasma membrane triggers calcium store depletion in the ER, which induces the oligomerization of the ER-resident calcium sensor STIM1 to ultimately enable its interaction with ORAI1 on the plasma membrane [5, 19]. Calcium influx through ORAI1 causes a substantial elevation in the cytosolic Ca^{2+} level to further activate calcineurin, a downstream Ca^{2+}-dependent phosphatase that in turn dephosphorylates the transcriptional factor-nuclear factor of activated T-cells (NFAT) to cause NFAT nuclear translocation for target gene transcription (**Figure 1**).

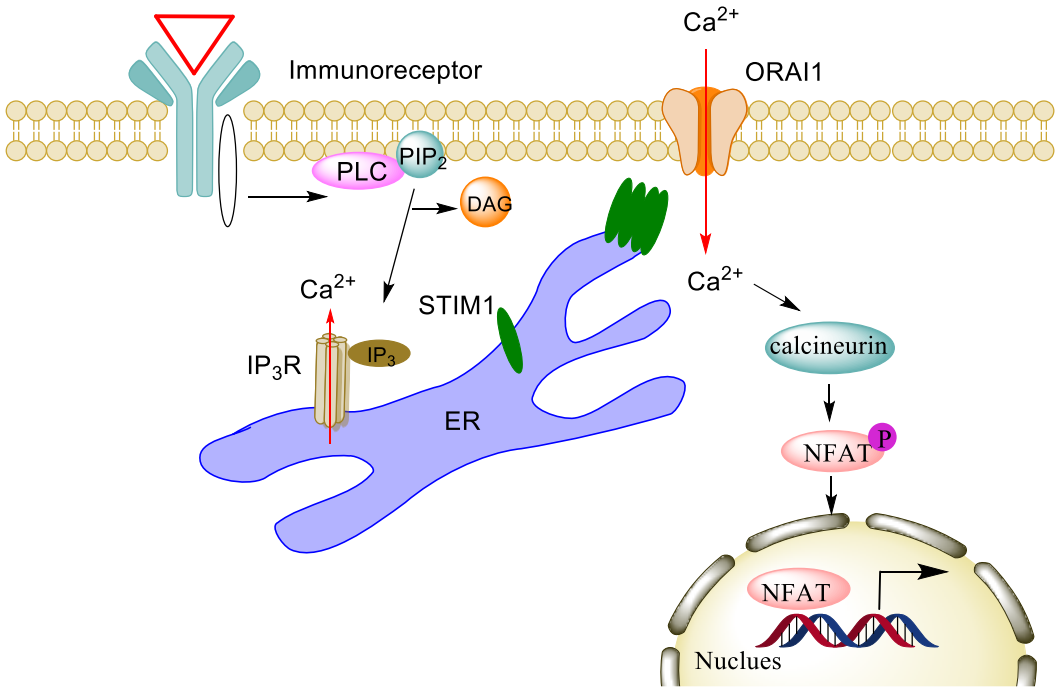

Figure 1. Scheme of ORAI-STIM signaling in lymphocytes.
The Ca^{2+} concentration gradient exists in resting T cells, and the cytosolic Ca^{2+} concentration is tightly kept at approximately 50-100 nM. Upon antigen binding to T cell receptor, the protein tyrosine kinase activation produces IP_3, which binds and opens IP_3R on ER. The Ca^{2+} releasing from intracellular Ca^{2+} store leads to ER Ca^{2+} sensor STIM1 moving and activating Ca^{2+} channel ORAI1, resulting in the intracellular Ca^{2+} elevation. The downstream effectors such as calcineurin are activated and trigger NFAT nuclear translocation to regulate genes expression.

Sarcoplasmic-endoplasmic reticulum Ca^{2+} pump inhibitor, thapsigargin (TG) and Ca^{2+} ionophore, ionomycin, are two commonly pharmacological tools to induce store depletion, which causes STIM1 to accumulate at ER-plasma membrane (PM) junctions where it traps and activates ORAI1 channels [20]. Ionomycin is also commonly used in conjunction with phorbol myristate acetate (PMA) to activate the transcription factors AP-1 and NFAT, leading to the production of the cytokines, such as IL-2 and IFN-γ, in T cells [7]. However, the irreversibility and off-target toxicity of these compounds call for the development of next-generation calcium actuators [15, 21]. The rapidly developing optogenetic toolkit provides a new direction to overcome the disadvantages associated with chemical compounds. Compared with traditional pharmacological agents, optogenetic tools have several unique features [22-24]: i) spatial and temporal control, ii) photo-tunable response to deliver customized signals, iii) less toxicity, and iv) superior reversibility. Light switches can reversely activate or deactivate protein in a timely manner to prevent the compensation pathways. Photoreceptors respond to light in a way of conformational change as a result of energy transfer by an incorporated exogenous cofactor or chromophore capable of transmitting light into energy. The light-sensitive ion channel channelrhodopsin-2 (ChR2) [25] has been widely used in the neuroscience field through a combination of Cre-dependent adeno-associated viruses (AAV) delivery system to study neural circuits *in vivo* [26]. Yet, the ChR2 is a non-selective cation channel that can cause membrane depolarization in excitable tissues upon photostimulation. But it is not suitable for manipulating Ca^{2+} signals given its lack of ion selectivity and the relative inertia of non-excitable cells to membrane depolarization. ChR2 is permeable to not only Ca^{2+} but also other monovalent cations such as H^+ and Na^+. Although a more Ca^{2+}-selective variant of ChR2, designate as calcium translocating channelrhodopsin (CatCh) [27], has been presented, it is not selective enough to

prevent the permeation of other cations, thus confounding the interpretation of observed cellular behaviors. The flow of proton into cells will also perturb intracellular PH and cause unpredicted side effects [25]. CRAC channel is highly Ca^{2+} selective and thus can serve as an ideal engineering target to achieve optical control of Ca^{2+} signaling in mammals. In order to engineer a photo-controllable CRAC channel, I review herein the existing photoreceptors and photosensitive modules that can be exploited for optogenetic engineering.

(1) Protein-protein interaction modules

a) UVR8-COP1: In *Arabidopsis thaliana*, photoreceptor UV-resistance locus 8 (UVR8) comprises light-absorbing tryptophans, Trp233 (W233) and Trp285 (W285) residues at the homodimer interface as self-chromophore that play a vital role in perception of UV-B light to disrupt the cation- π interaction, resulting in transition from homodimer to monomer and association with constitutively photomorphogenic 1 (COP1) [28].

b) CRY2-CIB: the N-terminal photolyase homology region (PHR, 1-498aa) of *A. thaliana* cryptochrome 2 (CRY2) bearing the flavin adenine dinucleotide (FAD) as cofactor can reversibly interact with CIB1 in response of blue light stimulation [29]. Improvements of the CRY2-CIB-based optical dimerizers have been optimized for tighter control of light-mediated hetero-dimerization. One truncated CRY2 variant (1-535aa) shows tighter light control than CRY2 (PHR). In addition, the mutants L348F or W349R can prolong or shorten the CRY2 photocycle, respectively [30].

c) LOVpep-ePDZ: the light-oxygen-voltage 2 (LOV2) domain from *Avena sativa* phototropin 1 contains a C-terminal helical extension (Jα) that exhibits light-dependent unfolding (LOV2-Jα, aa 404-546). In the dark, the C-terminal Jα helix tightly docks to the core of LOV2,

termed as Period/ARNT/Single-minded (PAS) domain. Upon blue light illumination, the formation of a covalent bond between Cys450 (C450) and the C4a atom of the flavin mononucleotide (FMN) leads to a weakened interaction between the core PAS domain and the C-terminal Jα helix, ultimately causing the unfolding and unwinding of the Jα helix [31]. By fusing a peptide epitope that can be specifically recognized by an engineered PDZ domain (ePDZ) downstream of the Jα helix, the uncaging of Jα helix upon blue light illumination exposes LOVpep to interact with ePDZ [32].

d) iLID-SspB: By fusing the *Escherichia coli* SsrA peptide to the C-terminus of Jα helix (LOV2-SsrA), this fusion construct shows light-dependent interaction with a 13KDa adaptor protein SspB. Light-inducible heterodimer (LID) can be formed through the photo-triggered association between LOV2-SsrA and SspB. An improved version (iLID) has been developed by introducing mutation to the two-component LID system: SspB (R73Q) and LOV2 (G528A, N538E), which significantly increased the affinity while reducing the dark activity [33].

e) VVD+ VVD-: Vivid (VVD) is a LOV domain photoreceptor derived from *Neurospora crassa* and rapidly forms a homodimer in response to blue light [34].

f) EL222-DNA: EL222, a 222-residue bacterial transcriptional factor containing an N-terminal LOV domain and a C-terminal helix-turn-helix (HTH) DNA binding domain. LOV domain binds to the HTH domain in the dark and dissociates with blue light illumination, thus allowing EL222 to dimerize and bind DNA [35, 36].

g) FKF1-GIGANTEA: In *Arabidopsis*, Flavin-binding/Kelch repeat/F-box1 (FKF1) forms a complex with GIGANTEA in a blue-light-dependent manner to promote daytime CONSTANS (CO) gene expression for time measurement in the control of photoperiodic flowering [37].

h) PhyB-PIF: In *A. thaliana*, phytochrome B (PhyB) responds to red light (650 nm), with the chromophore undergoing a switch from the inactive form (Pr) to the active form (Pfr), and binds to phytochrome interaction factor (PIF) and translocates to the nucleus as a heterodimer to modulate gene expression, a process that requires the presence of an exogenous cofactor bilin (open-chain tetrapyrrole) chromophore, phycocyanobilin (PCB) or phytochromobilin (PΦB), which can be converted back to Pr by infrared light (750 nm) [38]. The N-terminal photosensory module (PSM) of PhyB contains a PAS with a long N-terminus extension (NTE), a cGMP phosphodiesterase/adenylyl cyclase/Fh1A (GAF) domain and a Phy-specific (PHY) domain [39].

(2) Protein multimerization modules

(a) Dronpa: Dronpa is a fluorescent protein that switches off under cyan light (500nm) to promote monomerization, and switches on under violet light (400nm), resulting in multimerization. Similar to UVR8, Dronpa uses tryptophan for light sensing without the need of small-molecule cofactors [40].

(b) Aureochrome LOV2: Aureochrome-1 from *Vaucheria frigida* (vfAU1-LOV) or Aureochrome-1a from *Phaeodactylum tricornutum* (ptAU1-LOV) harbors an N-terminal basic leucine zipper (bZIP) domain and a LOV domain. Blue light illumination triggers intramolecular bZIP-LOV dissociation with subsequent LOV dimerization [41, 42].

(c) CRY2: The light-induced interaction of CRY2-CIB does not preclude CRY2 self-clustering. Light-insensitive mutant CRY2 (D387A) abolishes the clustering ability of CRY2. A E490G mutant significantly enhances the light-mediated CRY2 oligomerization (CRY2oligo) when compared to wild type (WT) CRY2 [29, 43].

(d) CPH1S: Similar to PhyB, the N-terminal sensory domain of phytochrome protein Cph1 (Cph1S) from *Cyanobacteria* undergoes light-dependent changes in the oligomerization state. Cph1S stays as homodimer in its Pfr state with red light stimulation but switches to a monomeric Pr state in far-red light [44].

(3) Allosteric regulation or conformational switch: AsLOV2

As briefly mentioned above, the LOV2 Jα helix undergoes light-dependent conformational switch to expose the effector domain fused to the C-terminus [45]. LOV2 derived from phototropin has been exploited most widely to cage protein function through steric hindrance imposed to the fused partner in the dark. With photostimulation, the unfolding of the Jα helix often restores the effector domain activity [46]. Phototropins are photoreceptors which have the functions to mediate responses such as phototropism [47] and chloroplast movement [48] in higher plants. Phototropins consist of N-terminal LOV domains and C-terminal kinase domains; while light sensor LOV domains regulate the activity of kinase domains. The structure of LOV2 (residues 404-546) from the *Avena sativa* (oat) phototropin 1 has been determined [31]. It contains an N-terminal core domain (green region), which has a classical Per-ARNT-Sim (PAS) fold, and a C-terminal Jα helix (purple area) (**Figure 2a**). The ubiquitously expressed endogenous flavin mononucleotide (FMN) serves as the light-absorbing cofactor of LOV2. In the dark state, FMN is non-covalently bound to the PAS core. Upon blue light (470 nm) absorption, FMN forms a covalent bond with a conserved cysteine residue (C450) in the LOV2, which causes the reorganization of the PAS domain [49, 50], and induces the Jα undocking from the core domain. As a result, effector protein fused to the C-terminus of LOV2 will be uncaged with functional restoration (**Figure 2b**). LOV2 has been widely used in mammalian cells for

photoactivatable control of cell motility [51], protein nuclear translocation [52, 53], and protein degradation [54].

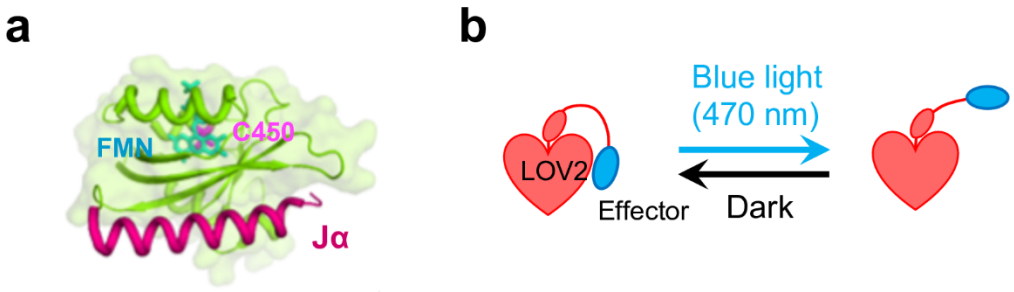

Figure 2. Structure of LOV2 domain and the working principle.
(a) 3D structure of LOV2 (PDB entry: 2V0W) with co-factor FMN bound. The C-terminal Jα-helix (magenta) docks toward the LOV2 core PAS domain (green) along with its co-factor FMN (cyan sticks) in the dark state. **(b)** The effector or binding partner is fused to and caged by LOV2 in the dark state. The blue light absorption induces the Jα-helix of LOV2 domain undocking from the core domain and leads to uncaging of the effector domain.

In this study, we selected LOV2 domain for photo-modulation of CRAC channel (designated as OptoCRAC). The schematic of OptoCRAC (OptoSTIM1 and OptoORAI1) is shown in **Figure 3**. STIM1 cytosolic fragments (STIM1-CT) are sufficient to activate ORAI1. The design of OptoSTIM1 is to directly cage the function of STIM1-CT through fusion to the C-terminus of LOV2. In addition, circularly permuted LOV2 (cpLOV2) was generated to provide new caging interfaces to regulate the STIM1-CT activity. For OptoORAI1, insertion of LOV2 into the only intracellular loop of ORAI1 channels was made to tune the channel activity with light through allosteric control.

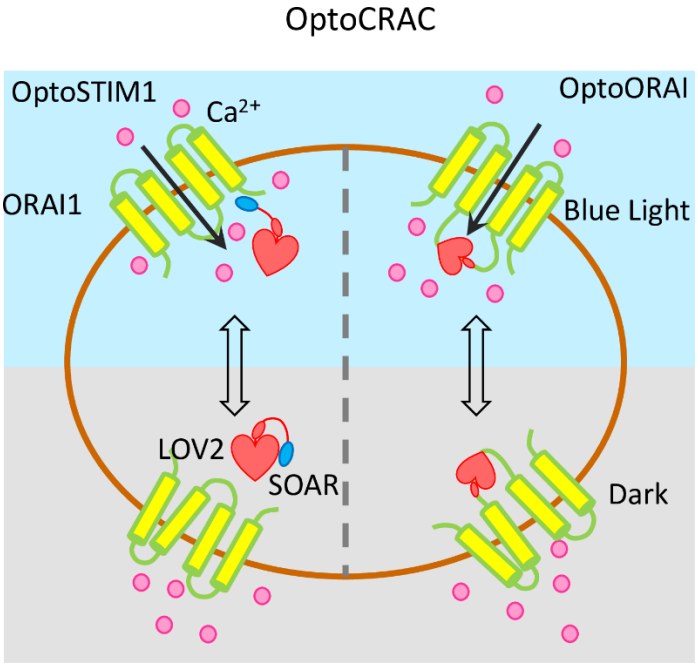

Figure 3. Schematic of light-operated Ca^{2+} entry through engineered STIM1 and ORAI.
Both designs are based on the photosensitive LOV2 domain from *Avena sativa* phototropin 1, which exhibits light-dependent conformational changes. OptoSTIM1: Fusion of ORAI1-activating STIM1-CT fragments with LOV2. Upon blue light illumination, the undocking of LOV2 C-terminal Jα helix leads to the exposure of STIM1-CT fragments, enabling their interaction with ORAI1 Ca^{2+} channels to trigger Ca^{2+} influx across the plasma membrane. OptoORAI: The LOV2 domain is directly inserted into the intracellular loop of ORAI1. Photo-triggered conformational changes in LOV2 propagate to nearby TMs in engineered ORAI1 to cause Ca^{2+} influx.

CHAPTER II

PHOTOACTIVATABLE CONTROL OF CALCIUM SIGNALING THROUGH OPTOSTIM1[1]

Introduction

STIM1 is an ER-localized transmembrane protein that can detect the depletion of ER Ca^{2+} store and directly gate ORAI1 Ca^{2+} channel. The functional domains and activation model of STIM1 are shown in **Figure 4**. STIM1 signal peptide (SP) is located at the N-terminus of STIM1 and is cleaved during translocation. The luminal EF-SAM domain (EF-hand and sterile α-motif) is responsible for Ca^{2+} sensing and initiation of STIM1 self-oligomerization. Upon ER Ca^{2+} depletion, EF-SAM oligomerization further triggers the conformational change in the STIM1 coiled-coil 1 (CC1) domain, with consequent exposure of the STIM-ORAI activating region (SOAR) or the CRAC-activation domain (CAD) to gate ORAI channels at ER-PM junctions. The polybasic domain (Lys-rich) in the C-terminus stabilizes the STIM1-ORAI complex through interacting with PM-embedded negatively charged phospholipid. In addition, the sequence Thr-Arg-Ile-Pro (TRIP) in the C-terminus of STIM1 is responsible for the direct binding to EB1, which engages STIM1 with the plus end of microtubules during ER remodeling. In a recent study, the light-sensitive photolyase homology region (PHR) domain of cryptochrome 2 (CRY2) was used to induce oligomerization of STIM1-CT to activate Ca^{2+} [55]. However, since the STIM1-CT can constitutively activate ORAI channels, the construct will likely show some dark activity (with leaky calcium entry in the dark) to limit its application.

---

[1] Part of this chapter is reprinted with permission from "Near-infrared photoactivatable control of Ca^{2+} signaling and optogenetic immunomodulation" by Lian He, Yuanwei Zhang, Guolin Ma, *et al*. eLife 2015;4:e10024, Copyright [2015] by Lian He; and "Rewiring calcium signaling for precise transcriptional reprogramming" by Nhung T. Nguyen, Lian He, *et al*. ACS Synthetic Biology, 2018;7(3):814-821

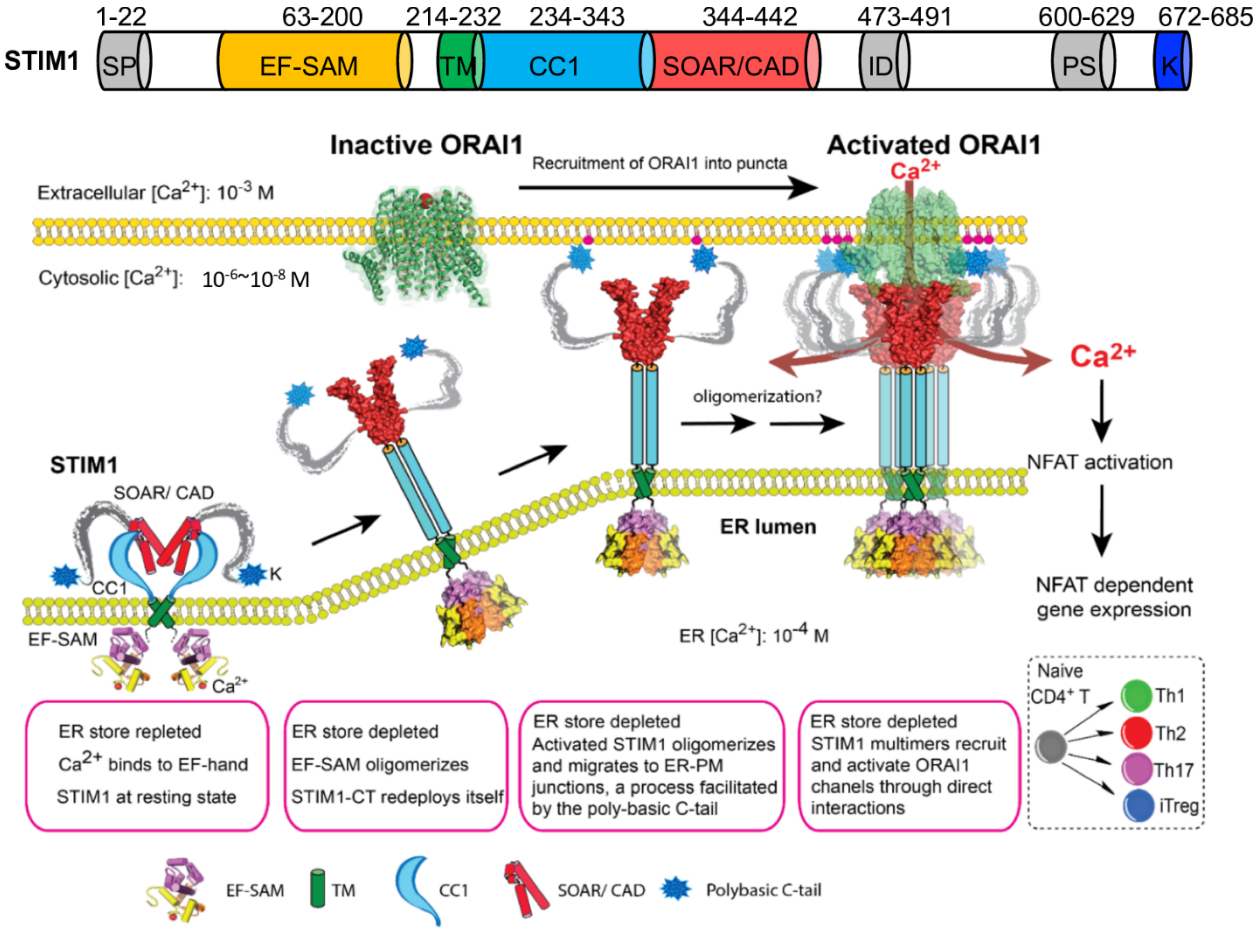

Figure 4. The domain architecture and activation model of STIM1[56]. Reprinted from "Inside-out Ca^{2+} signalling prompted by STIM1 conformational switch", by Guolin Ma, Ming Wei, Lian He, *et al*., Nature communications, 2015, 6: 7826. Copyright [2015] by Nature communications.
SP, signal peptide; EF-SAM, EF-hand and sterile α-motif; TM, transmembrane domain; CC1, coiled-coil 1; SOAR, STIM-ORAI activation region; CAD, CRAC activation domain; ID, inactivation domain; PS, Pro/Ser-rich domain; K, polybasic domain.

I will describe herein the development of OptoSTIM1 by fusing LOV2 to STIM1-CT fragments so as to mimic the CC1-SOAR authoinhibition that traps STIM1 in an inactive configuration. The LOV2-based OptoSTIM1 shows a fast decay half-time (within seconds). The relatively smaller size of LOV2 makes it feasible for facile packages of viral particles and *in vivo* delivery. We further demonstrated that OptoSTIM1 can be used to remotely control cytosolic

Ca^{2+} oscillations, and Ca^{2+} dependent genes expression. In parallel, we have improved the prototypical OptoSTIM1 through combined use with Zdk [57, 58], an engineered protein that can dock to LOV2 in the dark but will dissociate upon light irradiation. This strategy imposes an additional lock to OptoSTIM1 to reduce dark activation while increase the dynamic changes of light-induced Ca^{2+} signals in mammalian cells.

Materials and Methods

Constructs for fluorescence imaging and luciferase assays

Human STIM1-CT fragments (aa 336-450, 336-460, 336-473, 336-486, 342-486, 344-486) were amplified and inserted into the pTriEx-mCheerry-PA-Rac1 vector to replace Rac1 (Addgene #22027) by using HindIII and XhoI restriction sites to produce mCh-LOV2-STIM1 constructs. The KOD hot start DNA polymerase (EMD Millipore) was used for gene fragments amplification. mCh-OptoSTIM1(LOV2$_{404-546}$-STIM1-CT) constructs with various linkers were generated by inserting the linkers as follows, HindIII-XhoI sites for the KL linker and NotI-XhoI sites for the KLAAA linker. LOV2 mutations in mCh-OptoSTIM1 were introduced by QuikChange Lightning Multi Site-Directed Mutagenesis Kit (Agilent Technologies). For OARI1-T2A/IRES-mCh-OptoSTIM1$_{336-486}$, ORAI1 was first inserted between the PacI and NcoI sites upstream of mCh. Then, T2A/IRES were fused by using the Gibson Assembly (NEBuilder® HiFi DNA Assembly Master Mix, NEW ENGLAND Biolabs Inc). LOVSoc was inserted to replace mCh in pTriEx-mCh-LOVSoc to make pTriEx-(LOVSoc)$_2$ by using NcoI and BamHI restriction sites. The Zdk templates (Zdk1 and Zdk2) were a gift from Dr. Klaus M Hahn at University of North Carolina at Chapel Hill, USA. The Zdk genes with various linkers were amplified and fused after mCh-LOVSoc by Gibson Assembly. The following plasmids used were obtained from Addgene: LOVS1K (#31981), pGP-CMV-GCaMP6m (#40754), pGP-CMV-GCaMP6s-CAAX (#52228), CMV-R-GECO1.2 (#45494). The pN1-R-CaMP2 was a gift from Dr. Haruhiko Bito at the University of Tokyo, Japan. The Flag-ORAI1 was a gift from Dr. Youjun Wang at Beijing Normal University, China. The pGL4.30[luc2P/NFAT-RE/Hygro] for

NFAT dependent luciferase reporter and the pRL-TK for *Renilla* luciferase reporter control were purchased from Promega. All the plasmids used in this chapter were listed in Table 1.

Table 1. Plasmids used in Chapter II

Given name	Plasmids	Source
	pTriEx-mCh-LOV2(404-546)-STIM1$_{336-450}$	This study
	pTriEx-mCh-LOV2(404-546)-STIM1$_{336-460}$	This study
	pTriEx-mCh-LOV2(404-546)-STIM1$_{336-473}$	This study
LOVSoc	pTriEx-mCh-LOV2(404-546)-STIM1$_{336-486}$	This study
	pTriEx-mCh-LOV2(404-546)-STIM1$_{342-486}$	This study
	pTriEx-mCh-LOV2(404-546)-STIM1$_{344-486}$	This study
	pTriEx-mCh-LOV2-(No linker)-STIM1$_{336-486}$	This study
	pTriEx-mCh-LOV2-KLAAA-STIM1$_{336-486}$	This study
	pTriEx-mCh-PA-Rac1	Addgene #22027
	pTriEx-mCh-LOV2(404-546, C450A)-STIM1$_{336-486}$	This study
	pTriEx-mCh-LOV2(404-546, G528A)-STIM1$_{336-486}$	This study
	pTriEx-mCh-LOV2(404-546, I532A)-STIM1$_{336-486}$	This study
	pTriEx-mCh-LOV2(404-546, N538E)-STIM1$_{336-486}$	This study
	pTriEx-mCh-LOV2(404-546, I539E)-STIM1$_{336-486}$	This study
	pTriEx-Lyn11-mCh-LOV2-STIM1$_{336-486}$	This study
T2A	pTriEx-ORAI1-T2A-mCh-LOV2-STIM1$_{336-486}$	This study
IRES	pTriEx-ORAI1-IRES-mCh-LOV2-STIM1$_{336-486}$	This study
$(LOVSoc)_2$	pTriEx-LOV2-STIM1$_{336-486}$-LOV2-STIM1$_{336-486}$	This study
ORAI1-$(LOVSoc)_2$	pTriEx-ORAI1-LOV2-STIM1$_{336-486}$-LOV2-STIM1$_{336-486}$	This study
	pTriEx-mCh-LOV2-STIM1$_{336-486}$-GS linker1-Zdk1	This study
	pTriEx-mCh-LOV2-STIM1$_{336-486}$- GS linker1-Zdk2	This study
	pTriEx-mCh-LOV2-STIM1$_{336-486}$- GS linker2-Zdk1	This study
	pTriEx-mCh-LOV2-STIM1$_{336-486}$- GS linker2-Zdk2	This study
	Flag-ORAI1	Gift from Dr. Youjun Wang

Table 1. Continued

Given name	Plasmids	Source
	LOVS1K	Addgene #31981
	pGP-CMV-GCaMP6m	Addgene #40754
	pGP-CMV-GCaMP6s-CAAX	Addgene #52228
	CMV-R-GECO1.2	Addgene #45494
	pN1-R-CaMP2	Gift from Dr. Haruhiko Bito
	pGL4.30[luc2P/NFAT-RE/Hygro]	Promega
	pRL-TK	Promega
	pMCSG9-MBP	This study
	pMCSG9-MBP- LOV2-STIM1$_{336-486}$	This study
	pProEx-HTb-GB1- ORAI1$_{259-301}$	This study

Constructs for recombinant protein expression

The gene fragment of LOVSoc was cloned into pMCSG9 between BamHI and XhoI sites to make the MBP-LOVSoc. ORAI1-CT (residues 259-301) fragment flanked with BamHI and XhoI sites was inserted into pProEx-HTb, with a B1 domain of streptococcal protein G (GB1) tag fused between NcoI-BamHI sites. The GB1 tag here is used to enhance ORAI1-CT solubility.

Cell culture and transfection

HeLa and HEK293T cells were cultured in Dulbecco's modified Eagle's medium (DMEM, Sigma-Aldrich) supplemented with 10% fetal bovine serum (FBS) under 37 °C in a 5%

CO_2 atmosphere. For live cell imaging, cells were seeded on 35-mm glass bottom dishes and transfected using Lipofectamine 3000 (Life Technologies) according to the manufacturer's instructions.

Live-cell fluorescence Imaging and total internal reflection fluorescence (TIRF) microscopy

The Nikon A1R confocal module mounted onto an inverted Nikon Eclipse Ti-E body was used for confocal imaging. Nikon Multi-line Argon Laser sources (405/488/561 nm) were used for excitation. The 40x and 60x objectives (Nikon) were used for imaging acquisition. The same microscope system connected to a Ti-TIRF E motorized illuminator unit with a 60x objective (NA 1.49 oil-immersion) was used for TIRF imaging. The live cell imaging caged platform was used to maintain the proper temperature, CO_2 and humidity to keep cells healthy during the imaging process.

To monitor the light-inducible plasma membrane translocation of mCh-LOVSoc, 50-100 ng plasmid was transfected into HEK293-ORAI1 stable cells using Lipofectamine 3000. An external blue light (470 nm, 40 $\mu W/mm^2$, ThorLabs, Inc.) was used for photo-stimulation. Pulsed light cycles (100 sec light, 140 sec dark) were applied with the mCherry signals acquired by using the 561 nm laser channel.

For Ca^{2+} imaging, 50-100 ng mCh-LOVSoc was co-transfected with cytosolic or membrane-tethered GCaMP6s into HeLa or HEK293T cells pre-seeded on the 35-mm glass bottom dish. 24 h post-transfection, fluorescence signals were monitored by exciting at the GFP (488 nm) and mCherry (561 nm) channels with intervals of 1-5 sec. The 488 nm laser source for GCaMP6s signal recording is sufficient for mCh-LOVSoc photo-activation, so no external blue light source was needed. For localized photostimulation, a region of interest (ROI) was selected,

and then pre-stimulated for 5-10 secs. The GCaMP6s signals in the whole field were subsequently recorded.

For measurements of Ca^{2+} influx with the red color genetically encoded Ca^{2+} indicators (GECIs), 100 ng mCh-LOVSoc and 200 ng R-GECO1.2 or R-CaMP2 were co-transfected into HeLa or HEK293T cells. Blue light photostimulations were performed by a ThorLabs external blue LED as described above. To assess the dark activity of the constructs, we used $NFAT_{1-460}$-GFP stable HeLa cells and the nuclear/total GFP signal ratios were calculated for mCherry positive cells. For light dependent NFAT nuclear translocation assay, mCh-LOVSoc was transfected into the same stable cell line. A blue light pulse (30 sec, 40 $\mu W/mm^2$) was applied with the pulse intervals ranging from 0.5, 1, 4, to 8 min. A total of 24 min time-lapse imaging was performed with biological triplicate.

The measurements of intracellular Ca^{2+} with Fura-2 was performed by using previous protocols [59-62]. In brief, Fura-2 AM (Life Technologies) was loaded into the cells kept in the imaging solution (107 mM NaCl, 7.2 mM KCl, 1.2 mM MgCl2, 11.5 mM glucose, 1 mM CaCl2, 20 mM HEPES-NaOH, pH 7.2) and was incubated for 30 min in a 37-degree incubator in the dark. The Fura-2 fluorescence at 509 nm was acquired by excitation at 340 nm (F340) and 380 nm (F380) light. Cells were exposed to repeated light-dark cycles (blue light for 1min) and signals were recorded every two seconds. The Ca^{2+} concentrations were determined by using the Fura-2 calcium calibration kit (ThermoFisher Scientific).

Luciferase assay

mCh-LOVSoc, NFAT-luc (firefly luciferase reporter) and pRL-TK (Renilla luciferase reporter) were transfected into HeLa cells seeded in 24-well plate with 40-50% confluence. Cells

were treated with PMA (1 μM) with or without blue light stimulation (30 sec light pulse, 30 sec off, 40 $\mu W/mm^2$) 24 hours after transfection. The Dual-Luciferase Reporter Assay System (Promega) was used to measures luciferase activity in harvested cells. Renilla luciferase was used as the control to normalize the firefly luminescence. The luciferase activity ratio (Firefly/Renilla) was calculated and normalized.

Recombinant protein expression and purification

Protein expression plasmids MBP-LOVSoc or BG1-ORAI1-CT were transformed into BL21 (DE3) *E. coli* competent cells (EMD Millipore). The transformed bacteria were cultured at 37 ºC in LB medium (100 mg/L Ampicillin) until the OD_{600} of culture reached between 0.6-0.8. 500 μM IPTG was added to induce protein expression at 16 ºC for 6-8 hours, or at 37 ºC for 3-4 hours. Cell pellets were harvested and sonicated in 1X Phosphate Buffered Saline (PBS). For MBP or MBP-LOVSoc, amylose resin (New England Biolabs) was used to enrich the MBP fusion proteins, which were eluted in PBS with 25 mM maltose. For His-GB1-ORAI1-CT, the recombinant proteins were bound to Ni^{2+}-nitrilotriacetic acid (Ni-NTA)-agarose resin (Qiagen) and eluted in PBS containing 250 mM imidazole and 1 mM TCEP. Gel filtration was performed with a Superdex 200 10/300 GL columns or a Superose 6 10/300 GL column (GE Healthcare).

Pulldown and coimmunoprecipitation (CoIP) experiments

For MBP pulldown assay, recombinant GB1-ORAI1-CT proteins (800 μg) were incubated with MBP (400 μg) or MBP-LOVSoc (400 μg) pre-immobilized on amylose resin containing PBS buffer (containing 1 mM TCEP). Half of the mixtures were kept in the dark, and another half was exposed continuously to blue light for 4 hours at 4 °C. Extensive PBS washing

was followed to minimize nonspecific binding. All the steps were performed under blue light for the experimental group and in the dark for the control group. For CoIP experiments, lysed HEK293 cells (FLAG-ORAI1 and mCh-LOVSoc transfected) with 1x RIPA buffer and protease inhibitor cocktails. Cell lysis was incubated with anti-FLAG M2 affinity resin (Sigma) for 1 h with gentle shaking. The enriched fractions were stripped off the beads by boiling in 4x SDS gel loading buffer for 10 min. The samples were then resolved on SDS-PAGE. The bound proteins were visualized by using Coomassie Brilliant Blue staining or through immunoblotting.

Data and statistical analysis

All the data collected were plotted by GraphPad Prism 5 as mean ± s.e.m unless otherwise noted. The statistical significance was assessed by using two-tailed Student's *t*-test. *P<0.05; **P<0.01; ***P<0.001. The half-lives of activation and deactivation kinetics were calculated by the same statistical software.

Results

Design and optimization of OptoSTIM1

To design a single-component optogenetic tool to enable light control over the Ca^{2+}/NFAT signaling pathway, we set out to fuse the ORAI-activating region within STIM1 with the LOV2 (residues 404-546) domain from *Avena sativa* phototropin 1. In the dark state, the STIM1-CT is caged by LOV2 and showed an even distribution across the cytoplasm. Upon exposure to blue light, the STIM1-CT is released and translocated toward plasma membrane to directly activate the ORAI1 Ca^{2+} channels (**Figure 5**).

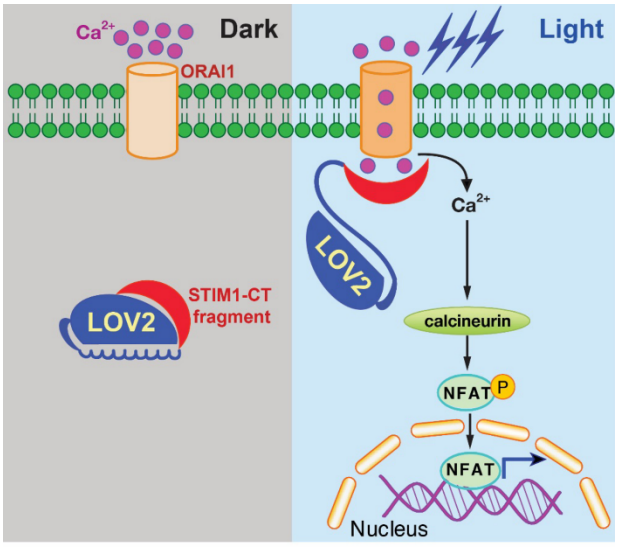

Figure 5. Diagram showing light-operated Ca^{2+} entry.
ORAI1-activating STIM1-CT fragments were fused to LOV2. In the dark state, the docking of STIM1-CT fragments toward the LOV2 domain keeps STIM1-CT inactive. Absorption of blue light by LOV2 triggers the undocking and unfolding of the C-terminal Jα helix, resulting in the release the STIM1-CT fragments. The STIM1-CT fragments further interact with ORAI1 on the plasma membrane to elicit Ca^{2+} influx.

We next optimized the system by i) testing a collection of STIM1-CT fragments capable of triggering different degrees of Ca^{2+} entry, ii) varying the linker between STIM1-CT and LOV2 domain, and iii) introducing mutations in the LOV2 domain (**Figure 6a**). To test their function, mCherry (mCh)-fused OptoSTIM1 constructs were transfected with genetically encoded green (GCaMP6s) [63] or red (R-GECO1.2) Ca^{2+} indicators [64] in HeLa cells to monitor Ca^{2+} influx. And NFAT-GFP stably expressed HeLa cells were used to test the dark activities of OptoSTIM1 variants by NFAT nuclear translocation assay (**Figure 6b**). When exposed to blue light, all the constructs except mCh-OptoSTIM1$_{336\text{-}473}$ showed light-induced Ca^{2+} entry as reported by both GCaMP6s and R-GECO1.2. The LOV2-STIM1$_{336\text{-}486}$ chimera with the linker KL was designated as "LOVSoc" in our following studies because it displayed the highest Ca^{2+} dynamic change and showed the least dark activity (**Figure 6b-d**). Notably, both two light-insensitive mutants, the inactivating mutant C450A and the constitutively active mutant I539E, attenuated the Ca^{2+} influx [51] (**Figure 6a, d**). The G528A, I532E, and N538E have been reported to cage LOV2 tighter [65] (**Figure 6d**). But in our hands, these mutations did not seem to improve the performance of LOVSoc.

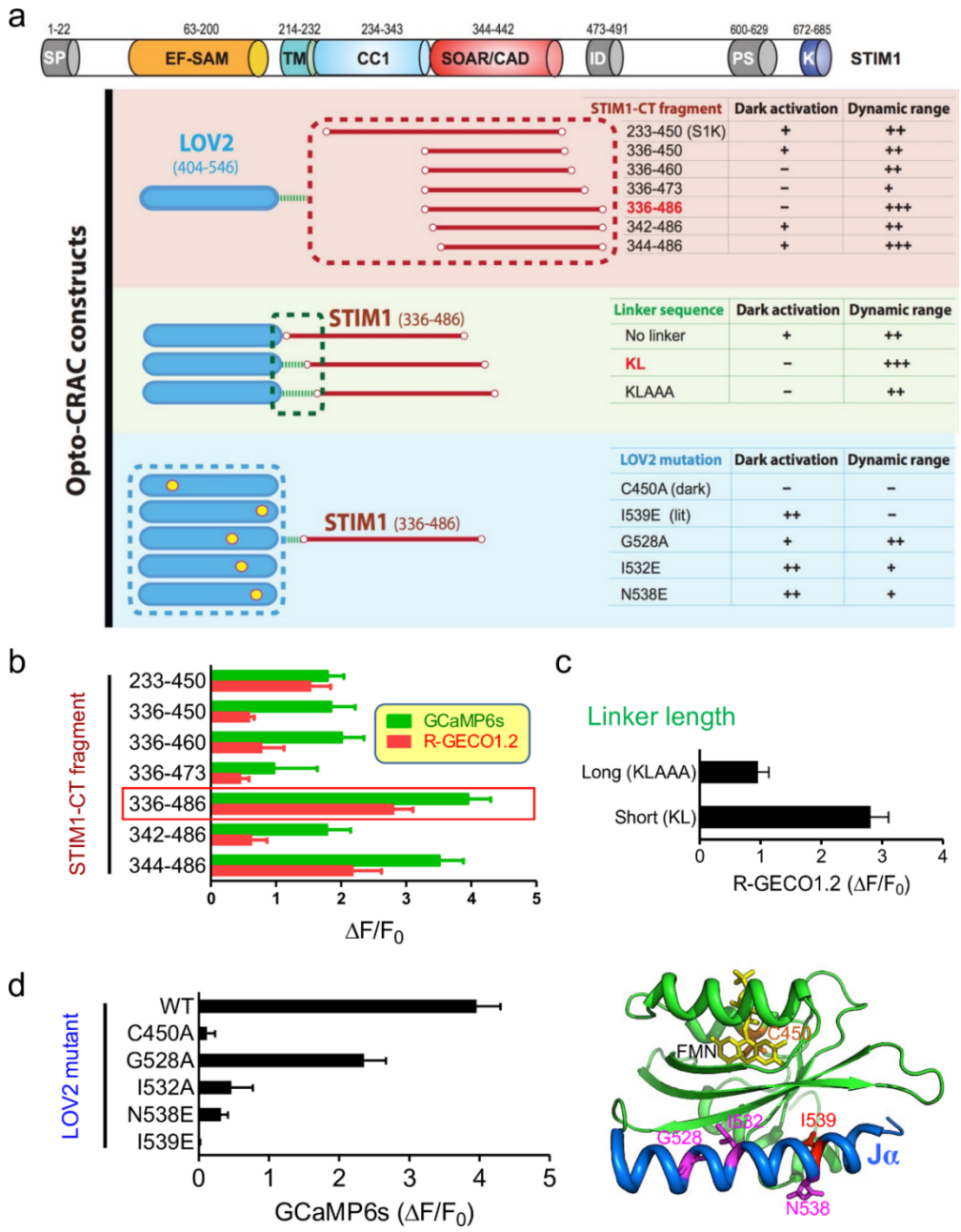

Figure 6. Design and comparison of Opto-STIM1 constructs.
(a) Design of OptoSTIM1 variants by varying the cytoplasmic domain of STIM1 (STM1-CT), the linker between LOV2 and STIM1-CT, and LOV2 mutations. The degree of NFAT-GFP translocation in the dark was used to define the dark activity of OptoSTIM1 constructs. "–", no discernible activation; "+" means less than 10% and "++" indicates more than 10%. The fluorescence changes ($\Delta F/F_0$) of green color Ca^{2+} indicator GCaMP6s was used to categorize the dynamic range: "–", <0.2; "+", 0.2-1.0; "++", 1.0-2.5; "+++", >2.5. **(b-d)** The Ca^{2+} dynamic change induced by blue light was reported by genetically-encoded Ca^{2+} sensors (R-GECO1.2 or GCaMP6s) in HeLa cells transfected with OptoSTIM1 variants. b, STIM1-CT variants; c, linker optimization; d, LOV2 domain mutants. The mutated positions were highlighted in red in the LOV2 3D structure (PDB entry: 2V0W). Yellow sticks, co-factor FMN. Data were shown as mean ± s.e.m (10-20 cells).

Light-induced reversible interaction of LOVSoc with ORAI1

Analysis of subcellular localization of mCh-LOVSoc was performed in HEK293-ORAI1 stable cells to detect the interaction of LOVSoc and ORAI1 (**Figure 7a**). When illuminated with blue light, cytosolic mCh-LOVSoc rapidly translocated to the PM and showed a light-dependent toggling between cytosol and the PM repeatedly ($t_{1/2,on}$ = 6.8 ± 2.3 s; $t_{1/2,off}$ = 28.7 ± 6.5 s). To further confirm the light-dependent interaction between LOVSoc and ORAI1, Flag-ORAI1 was used to pull-down mCh-LOVSoc with or without blue light. The binding of mCh-LOVSoc and Flag-ORAI1 was only detected in blue light-treated group but not the control group kept in the dark (**Figure 7b**).

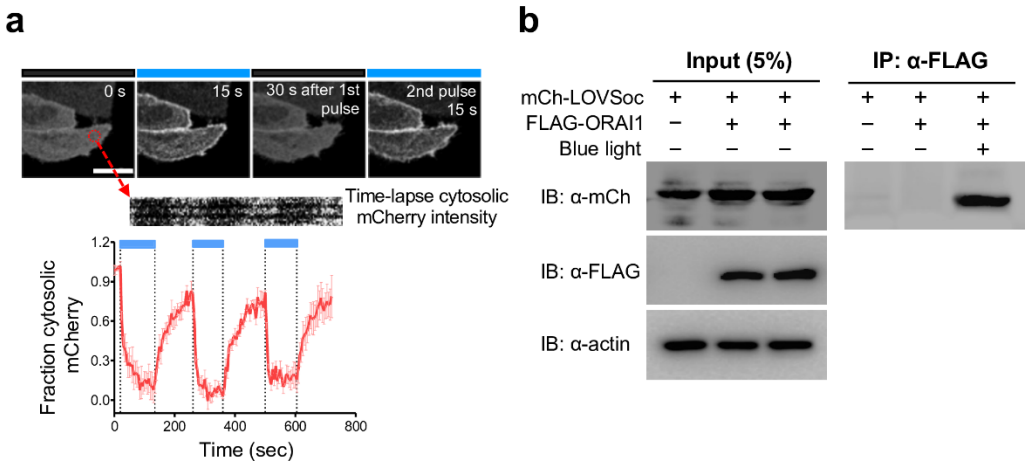

Figure 7. OptoSTIM1-V1 mediated photoactivatable ORAI1 interaction and Ca^{2+} entry.
(a) Light-inducible translocation of cytosolic OptoSTIM1-V1 (mCherry-LOV2-STIM1$_{336-486}$ or mCh-LOVSoc) to the plasma membrane in HEK293T-ORAI1 stable cells. *Upper* panel, photoexcitation of OptoSTIM1-V1 PM translocation. *Lower* panel, kymograph and quantification of mCh intensity in the circled area for over three light-dark cycles (40 μW/mm^2). n=12 from three trials. Error bars indicate s.e.m. Scale bar, 10 μm. **(b)** LOVSoc interacted with ORAI1 in a light-dependent manner. Cells were co-transfected with FLAG-ORAI1 and mCh-LOVSoc and lysed for coimmunoprecipitation (co-IP) experiment. An external blue light (470 nm, 40 μW/mm^2) was applied for all the steps after cell lysis in the light-stimulated groups.

The light-dependent interaction between LOVSoc and ORAI1-CT was further assessed *in vitro* by using recombinant proteins: MBP-LOVSoc and GB1-ORAI1 CT (residues 259-301) (**Figure 8**). The purified recombinant LOVSoc showed characteristic light-dependent changes in the absorbance spectrum (**Figure 8b**), confirming its photo-responsiveness. The *in vitro* pull-down assay by purified recombinant proteins further confirmed the light-dependent association between LOVSoc and ORAI1-CT (**Figure 8c**).

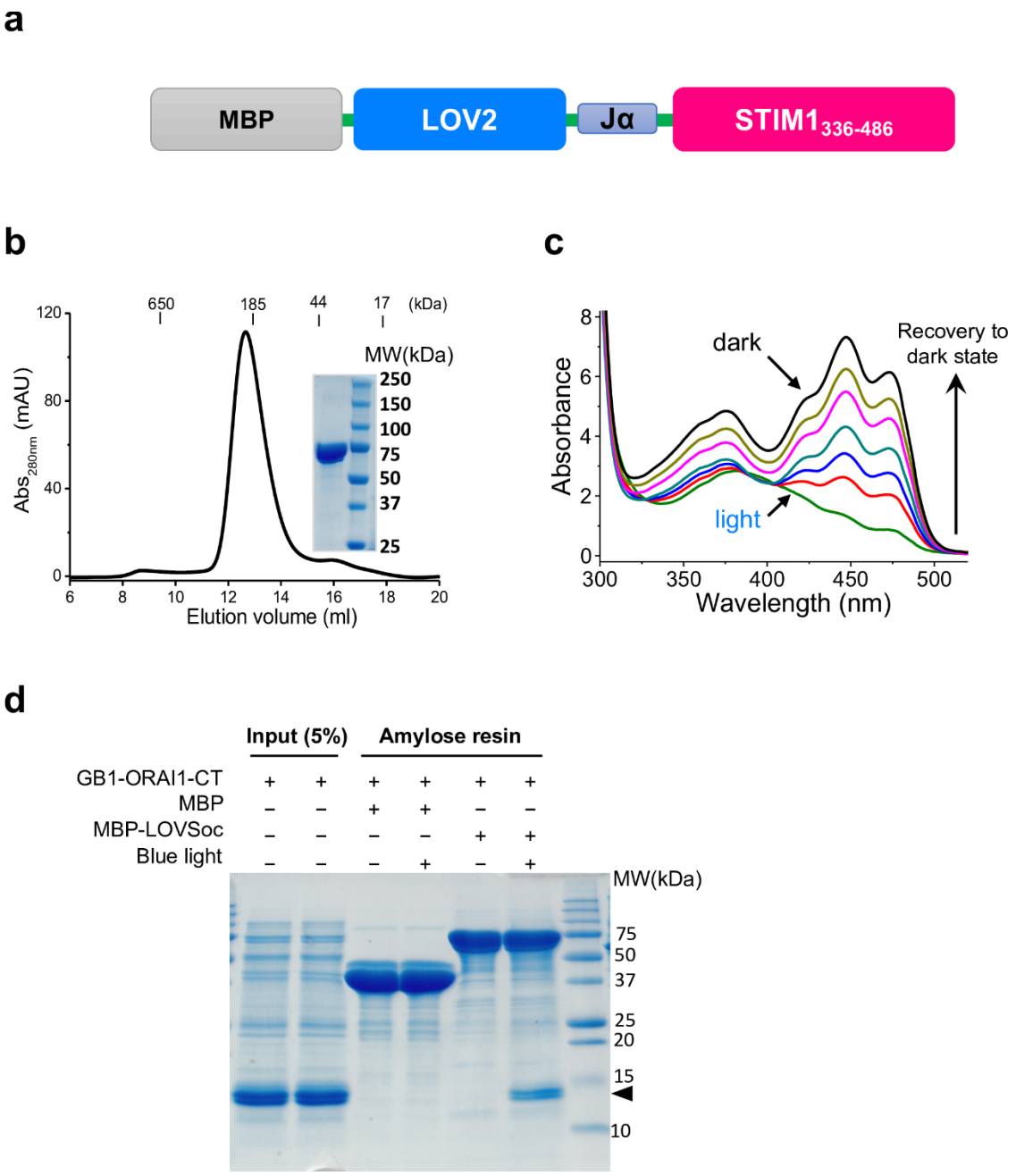

Figure 8. Purification and characterization of OptoSTIM1.
(a) MBP-tagged LOVSoc construct used for bacterial protein expression and *in vitro* analysis. **(b)** The elution profile of purified MBP-LOVSoc using size exclusion chromatography and SDS-PAGE of recombinant protein. **(c)** LOV2 domain photoexcitation was monitored by UV-Vis spectrophotometer. The signal was recorded every 25 s after 2 min blue light illumination. **(d)** *In vitro* pull-down assay using GB1-ORAI1-CT in solution and MBP-LOVSoc bound to amylose resin indicates the light-dependent association of these two proteins. MBP was used as a negative control. MBP, 43 kDa; GB1-ORAI1-CT, 13 kDa; MBP-LOVSoc, 76 kDa.

Spatial and temporal control of Ca^{2+} signals

Optogenetics confers spatial and temporal control over defined events, such as directing cell migration [51, 66, 67], with high precision. The spatial and temporal profiles of Ca^{2+} signals regulate different cellular pathways [68]. LOVSoc was transfected into HeLa cells to test if it can be photo-stimulated to generate various Ca^{2+} patterns. When the whole imaging field was exposed to light, we observed a global increase of cytosolic Ca^{2+} (**Figure 9a**). If we applied localized light stimulation toward defined areas, the Ca^{2+} influx was limited to the illuminated regions (**Figure 9b**). Thus, LOVSoc can be used to achieve spatial control over Ca^{2+} influx, providing a new method to generate Ca^{2+} microdomains and dissect their functions in various biological processes. In addition, the degree of Ca^{2+} influx could be tuned by varying the power density of input light (0.5-50 $\mu W/mm^2$).

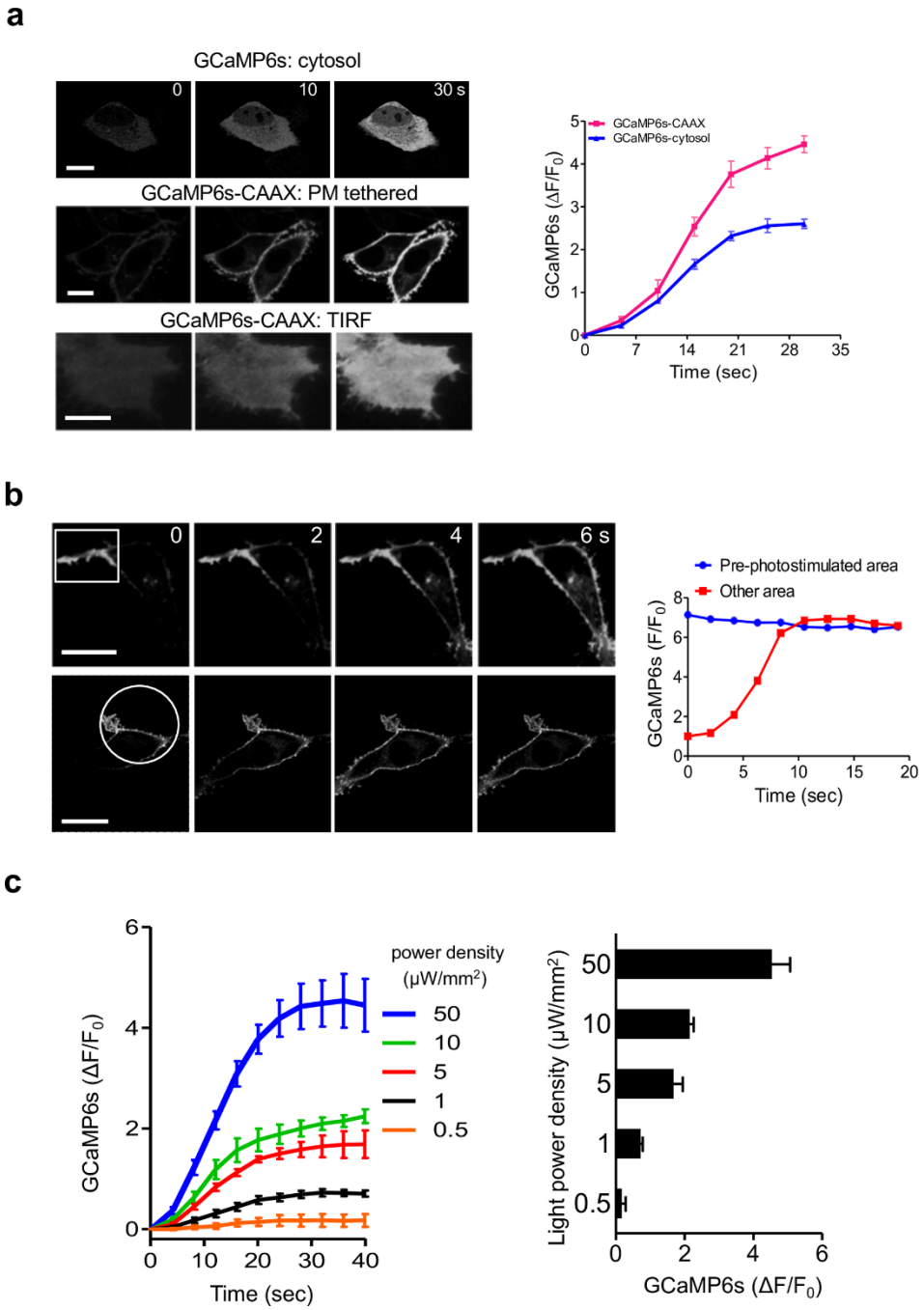

Figure 9. Spatial control and photo-tunable Ca^{2+} influx.
(a) Representative confocal and TIRF images show the global light-induced Ca^{2+} influx in HeLa cells, with GCaMP6s as Ca^{2+} readout. **(b)** Local Ca^{2+} influx in the defined area (boxed or circled areas were pre-exposed to light.). Representative confocal images of HeLa cells co-transfected with mCh-LOVSoc and GCaMP6s were shown. The high levels of GFP fluorescence intensities were shown in the pre-photostimulated areas, which indicated the preactivation of defined area Ca^{2+} influx. N=10, three independent trials. Error bars denote s.e.m. Scale bar, 10 μm. **(c)** The kinetics of Ca^{2+} signals (left) and fold-change of GCaMP6 fluorescence (right) at varying light power densities.

The light-triggered Ca^{2+} oscillation in HEK293T or HeLa cells were monitored by Fura-2, R-CaMP2 [69] and R-GECO1.2 (**Figure 10a-c**). LOVSoc could efficiently respond to 470 nm light but not to light excited at 561 nm (mCherry). We therefore used red color GECI as the readout for recording reversible changes in Ca^{2+} signals. The cytosolic Ca^{2+}-rise half-time ($t_{1/2,on}$) ranged from 23 s to 36 s, while the decay half-time was determined to be ~25-35 s (Table 2). The Ca^{2+} response kinetics are comparable to native SOCE under physiological conditions [4, 6, 19]. When fixing the light pulse at 30 sec with intervals varying from 0.5 to 4 min, we were able to generate different Ca^{2+} oscillation patterns as shown in **Figure 10d**. A shorter time interval is more prone to induce sustained Ca^{2+} influx, and a longer interval is likely to cause a transient Ca^{2+} elevation.

Table 2. Half-lives of activation and deactivation kinetics of LOVSoc

Calcium indicator	$t_{1/2,on}$ (s)	$t_{1/2,off}$ (s)
Fura-2 AM	36.4 ± 2.4	30.0 ± 1.1
R-GECO1.2	23.4 ± 4.2	24.9 ± 4.8
R-CaMP2	31.1 ± 4.9	34.7 ± 4.9

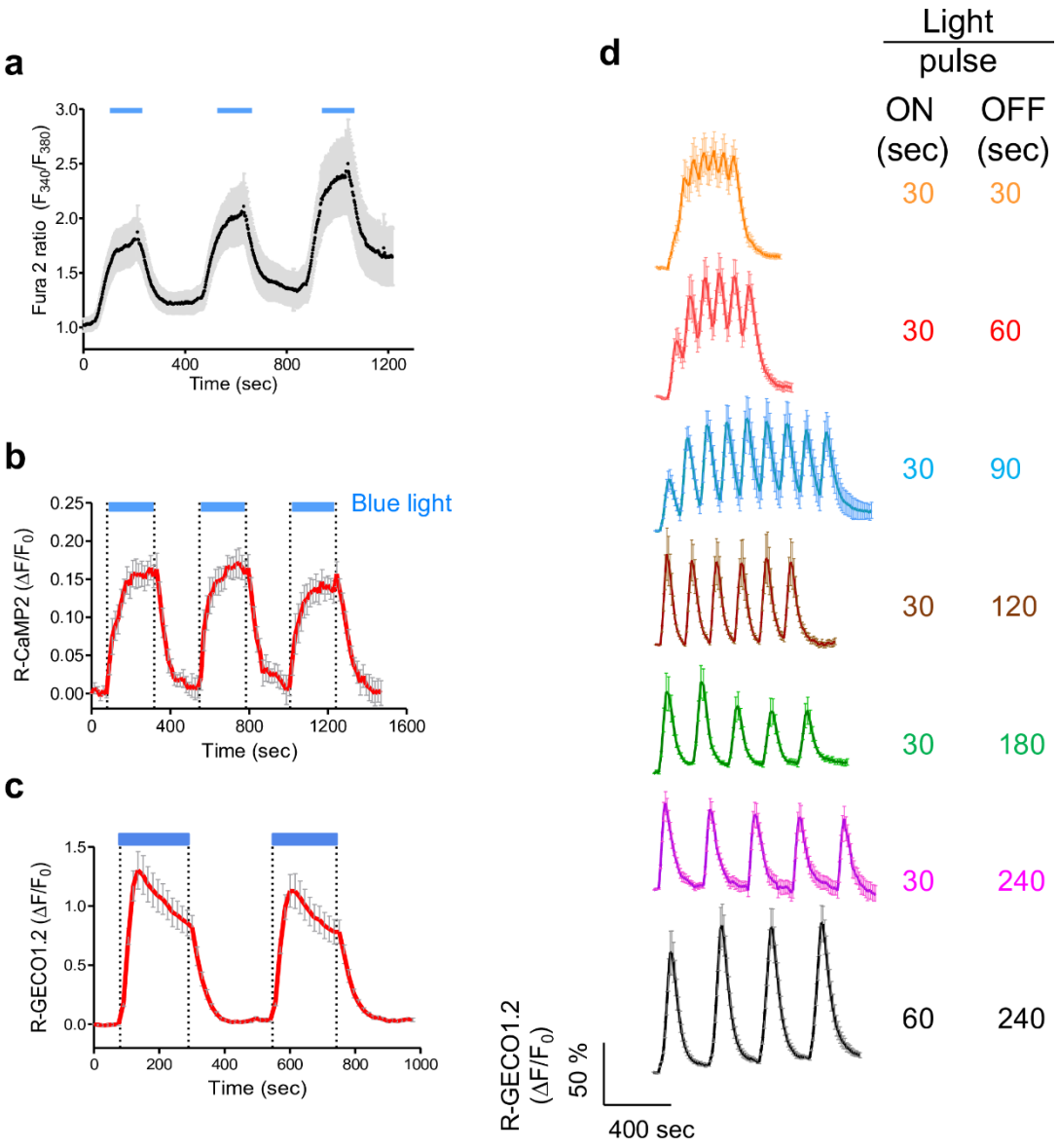

Figure 10. Light-dependent Ca^{2+} oscillations generated by OptoSTIM1 in HeLa cells.
Dark-light cycles were applied to cells, and the cytosolic Ca^{2+} signals were monitored by Ca^{2+} indicators (**a**, Fura2; **b**, R-CaMP2; **c-d**, R-GECO1.2).

Light tunable NFAT translocation and gene expression

Next, we asked if the Ca^{2+} patterns generated by the light pulse could tune the degree of downstream NFAFT translocation, as well as NFAT-dependent luciferase expression. When the light pulse was fixed at 30 sec, the efficiency of NFAT translocation decreased with an

increasing inter-pulse interval (**Figure 11a-b**). This finding suggested that a higher Ca^{2+} oscillation frequency could boost the efficiency of NFAT nuclear import. This observation agreed well with the reports that faster repetitive Ca^{2+} pulses were accompanied with increased NFAT activity [70]. The NFAT-dependent gene expression was further confirmed by the NFAT-driven luciferase (NFAT-Luc) report assay in HeLa cells. Consistent with the results from the NFAT translocation assay, a low NFAT-Luc activity was observed in cells exposed to low-frequency pulses (**Figure 11c**). Together, we demonstrated that feasibility of photo-tunable activation of NFAT by using LOVSoc in mammalian cells.

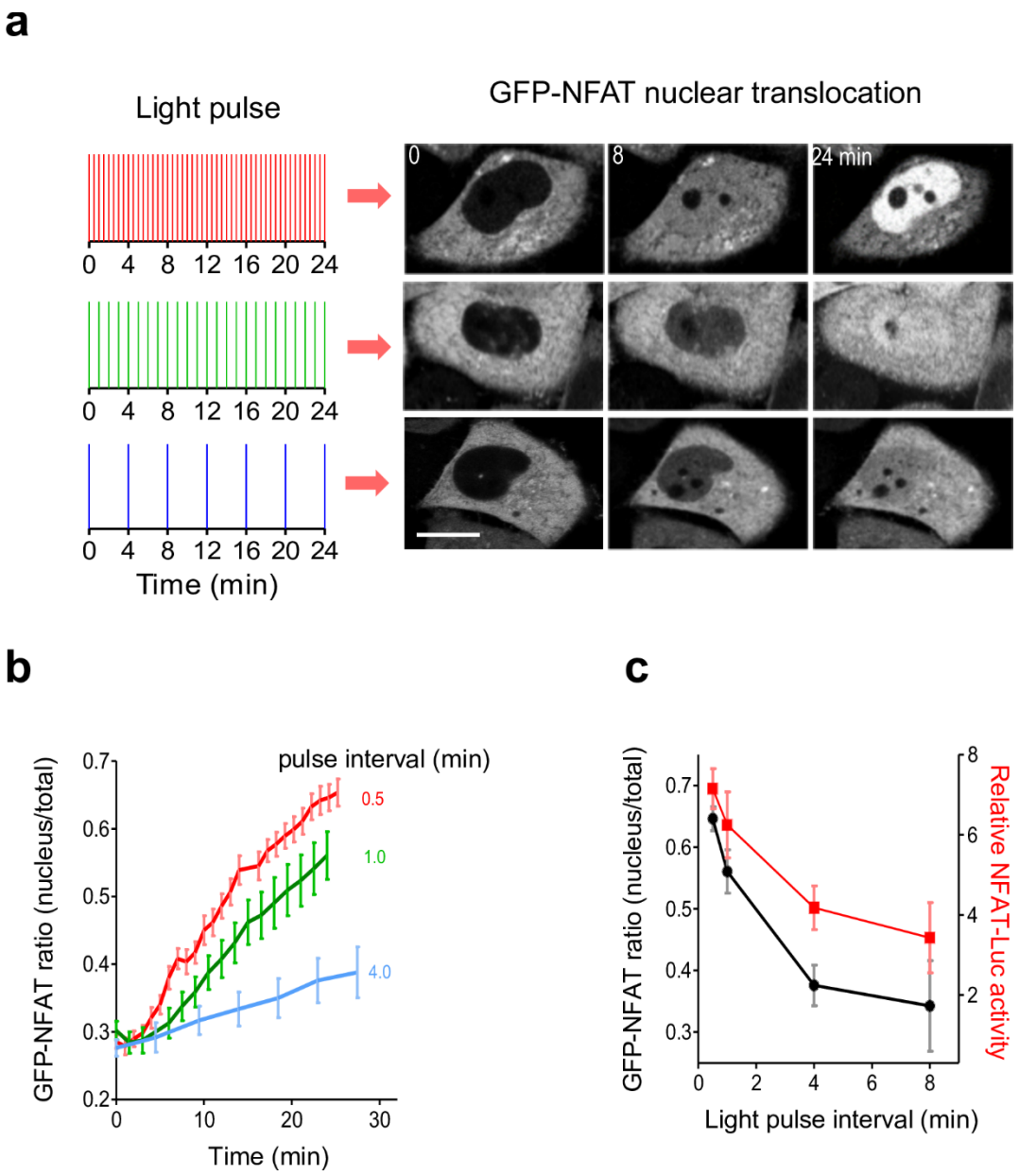

Figure 11. Light tunable NFAT$_{1\text{-}460}$-GFP nuclear translocation and NFAT-dependent luciferase gene expression.

(a-b) Confocal images and qualification of NFAT-GFP nuclear translocation. After transfection with mCh-LOVSoc, the NFAT$_{1\text{-}460}$-GFP stable HeLa cells were subjected to light pulse (30 sec stimulation with 0.5-4 min intervals). **(c)** The degree of NFAT nuclear translocation and NFAT dependent luciferase activity were plotted. The cells were treated with the same blue light pulse as in panels (a) and (b). NFAT responsible luciferase activity was assayed in HeLa cells.

Generation of customized Ca^{2+} patterns by LOVSoc

To customize the Ca^{2+} patterns, we generated additional five LOVSoc variants with various combination through ORAI1 co-expression, membrane tethering or tandem fusion. The light-induced cytosolic Ca^{2+} influx was dependent on the expression levels of LOVSoc and ORAI1. The endogens ORAI1, which is widely expressed in a variety of tissues with varying expression levels, is sufficient for LOVSoc to trigger notable Ca^{2+} influx upon blue light illumination. We introduced LOVSoc in the presence of ORAI1 with either an internal ribosome entry site (IRES) or self-cleaving 2A peptide (T2A) strategy. Under the same illuminated condition, the co-expression systems increased the intensity of GCaMP6s by ~1.4-fold compared to LOVSoc alone; while the activation kinetics remained similar (**Figure 12a**). Notably, PM tethered LOVSoc (Lyn11-LOVSoc) with the Src kinase Lyn [71] derived PM-targeting sequence accelerated the activation process by about 3.5-fold, which might be explained by the much closer positioning to the ORAI1 channels (**Figure 12b**). By contrast, the tandem LOVSoc with or without ORAI1 fusion substantially slowed down light inducible Ca^{2+} influx (4.5-fold slower than LOVSoc), but caused a higher Ca^{2+} elevation (~1.4-fold; **Figure 12c**). The fold-change of Ca^{2+} signals and activation half-times were summarized in **Figure 12d-e**. Collectively, we have created a full collection of OptoSTIM1 variants that can meet with varying needs to photo-manipulate intracellular Ca^{2+} signals.

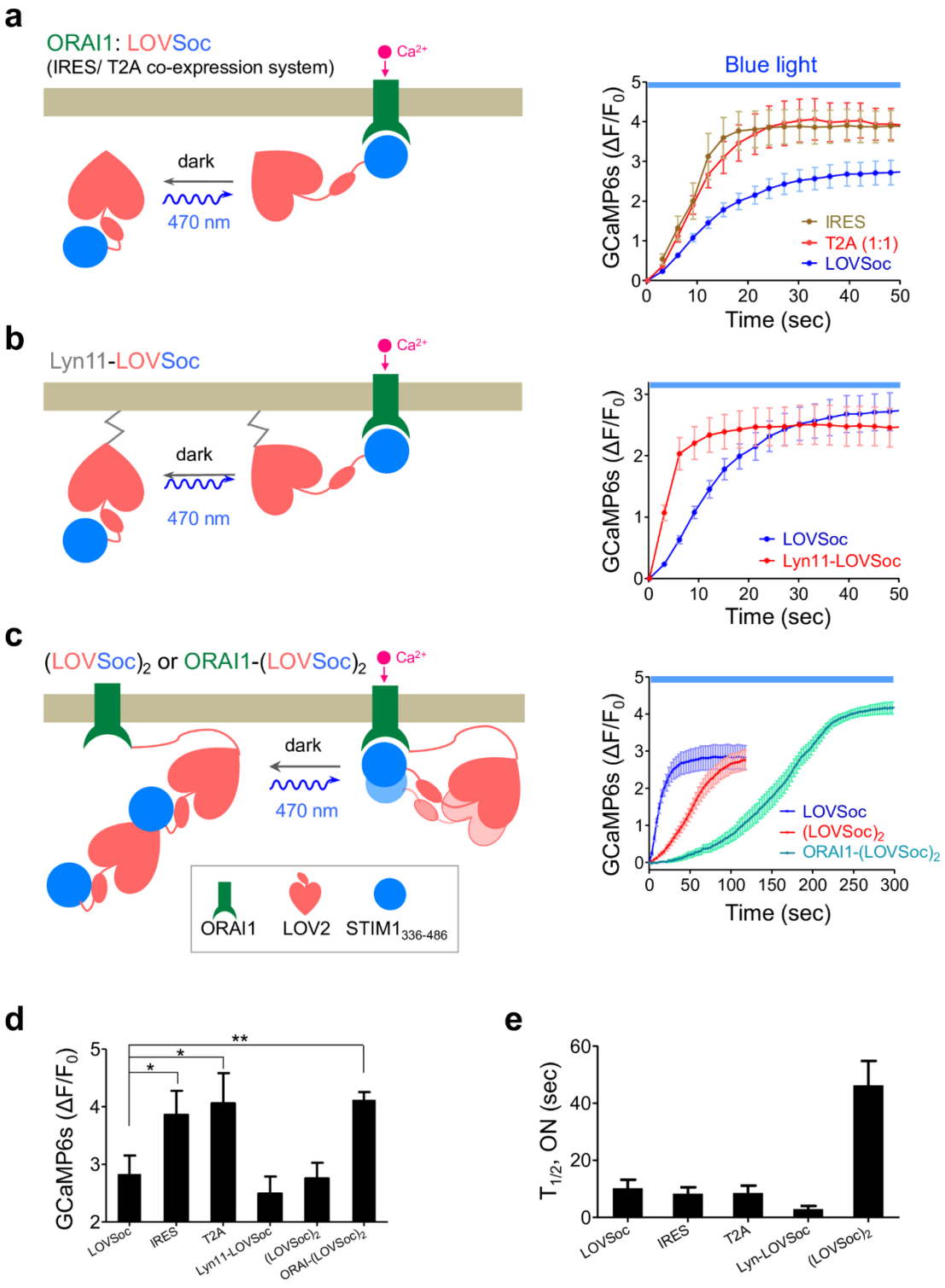

Figure 12. Schematic representation and characterization of OptoSTIM1 variants.
(a) Schematic representation of mCh-LOVSoc-IRES-ORAI (IRES) or ORAI1-T2A-mCh-LOVSoc (T2A), **(b)** Lyn11-mCh-LOVSoc and **(c)** mCh-(LOVSoc)2 or ORAI1-(LOVSoc)2 and the light-stimulated Ca^{2+} change with the blue light density of 40 µW/mm^2. **(d-e)** Comparison of the fold change of Ca^{2+} signals and half-times of Ca^{2+} rise.

Tighter control of LOVSoc through the combined use with Zdk

A small protein Zdark (Zdk) has been reported to interact with LOV2 domain only in the dark state and dissociate upon blue light stimulation [57, 58]. The reversible light-induced protein dissociation between LOV2 and Zdk will be used in this study to reduce the dark activity of LOVSoc further and to increase photo-excitable Ca^{2+} dynamic changes. Zdks showed over 150-fold changes in affinities for light-induced dissociation. Zdk1 is prone to interact with the C-terminal Jα helix, whereas Zdk2 binding to LOV2 is more likely independent on the C-terminal Jα helix [57]. By fusing Zdk to the C-terminus of LOVSoc, we anticipated that these new constructs (Z1-Z4; **Figure 13a-b**) would have a double locking mechanism to minimize dark activity. Longer GS linkers were included in Z1 and Z2 to provide more flexibility for LOV2-Zdk binding. To reduce the transfection bias, a cell line stably expressing cytosolic GCaMP6 was used to determine the fold-change in GCaMP6 signals before and after blue light illumination.

As seen in **Figure 13c**, the prototype LOVSoc, showed appreciable dark activity. The Z2 and Z3 constructs showed substantially reduced dark activity (**Figure 13c**). Moreover, this engineering strategy led to an increased dynamic range of Ca^{2+} signals (**Figure 13d**). The Z2 chimera turned out to be the best candidate with an activation half-life of 39.8 sec (Data not shown), but the activation half-time was slowed down by 4-fold when compared to LOVSoc.

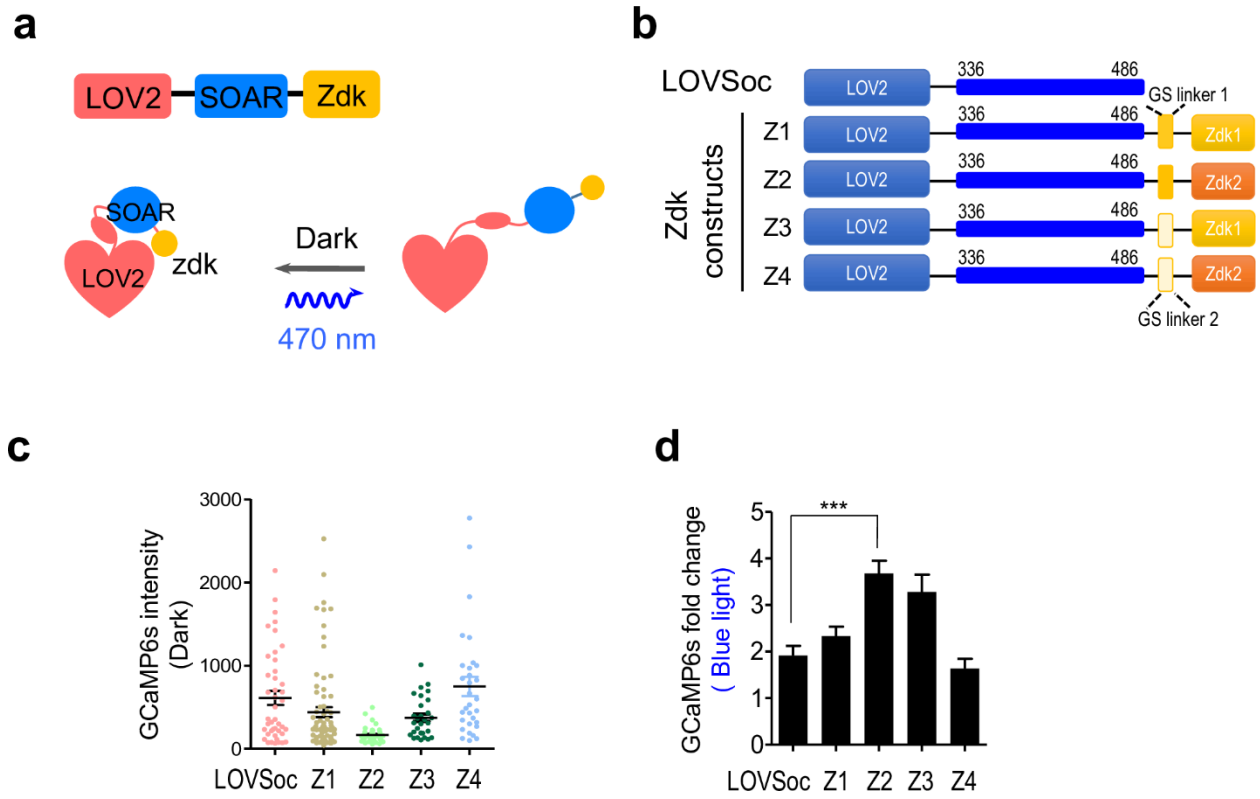

Figure 13. Combined use with Zdk to optimize OptoSTIM1.
(a-b) Design of Zdk-fused LOVSoc variants. The GCaMP6s-HeLa stable cells were transfected with the indicated constructs and the GCaMP6s basal dark activities were shown in **(c)** and the dynamic fold changes were plotted in **(d)**.

Discussion

In this study, we developed a serious of optogenetic tools that enabled light tunable Ca^{2+} entry. The optimized LOVSoc (LOV2-STIM1$_{336-486}$) chimera can generate sustained Ca^{2+} signals as well as user-defined Ca^{2+} patterns by controlling the intensity and pulses of input light. There are several distinctive features of the LOVSoc system: First, it is highly Ca^{2+} selective. The LOVSoc is directly engineered from one of the most Ca^{2+} selective ion channel, CRAC channel. The high Ca^{2+} selectivity (P_{Ca}/P_{Na}: >1000) makes it a better tool than ChR2 or its variants to control Ca^{2+} signaling [72]. The ChR-based tool has less ion selectivity and is permeable to Na^{+}, Ka^{+}, Ca^{2+}, and H^{+}. High proton permeability could perturb intracellular pH. Second, the Ca^{2+} influx generated by LOVSoc shows highly spatial-temporal resolution. With this tool in hand, we can manipulate the cytosolic Ca^{2+} levels in cardiac myocytes [73] and embryonic stem cells (ESC) to observe the functional consequences [74, 75]. Third, the magnitude and kinetics of LOVSoc Ca^{2+} signals are comparable to those generated under physiological conditions, such as antigen binding to the T cell receptor. The relatively slower kinetics of LOVSoc, compared with ChR, makes it suitable for modulating Ca^{2+} signaling events in non-excitable cells. Fourth, The LOVSoc tool is a single component system less than 900 bp with a relatively smaller size compared to ChR (2.2 kb), which is the ideal size for *in vivo* viral gene delivery system. Moreover, the endogenous level of ORAI1 is sufficient for LOVSoc to work in various cell types. We have succeeded in packaging the LOVSoc into retroviruses or lentiviruses for transduction of macrophages, primary T cells, and dendritic cells. Last but not least, by combining LOVSoc with red or near-infrared light-activatable optogenetic system such as PhyB-PIF[38, 76] or PpsR2-BphP1[77], it is feasible to achieve multi-signaling modulation through combined use of input lights.

We have generated a handful of LOVSoc constructs for generating customized Ca^{2+} signaling. For example, the PM-tethered Lyn11-LOVSoc shows similar kinetics as in the skeletal muscle cells, where the STIM1 is constantly observed to be localized in close proximity to the PM to rapidly activate Ca^{2+} entry upon store-depletion [78-80].

However, limitations and challenges remain for the OptoSTIM1 system. The LOV2 based optogenetic tools are activated by blue light, which have insufficient tissue penetration to limit its use for *in vivo* applications. Engineered or naturally occurring near-infrared red (NIR) light-sensitive photoreceptors with a similar property as LOV2 remain to be uncovered. Fortunately, an alternative approach was demonstrated for remote control of the Ca^{2+} signaling *in vivo* by coupling LOVSoc with upconversion nanoparticles (UCNP) [81, 82], which absorb relatively low energy light such as NIR and convert it into higher energy blue light. Tissue injected with UCNP could absorb NIR light and emit blue light to engineered cells to induce Ca^{2+} influx.

CHAPTER III

CIRCULARLY PERMUTED LOV2 AS A MODULAR DOMAIN FOR OPTOGENETIC ENGINEERING

Introduction

In the LOV2 domain based optogenetic tools, the effectors are always fused to the C-terminus of LOV2 and connected with Jα helix [45, 83]. This might cause problems for proteins requiring free N-termini for proper functions. In order to provide new opportunities for effector caging, especially for those proteins which should have free N termini to exert their functions, we set out to further engineer LOV2 to serve as a new photosensory scaffold. Based on the crystal structure of AsLOV2, we found that the N- and C-termini of LOV2 are closely positioned in space with a distance of approximately 10 Å [31]. This prompted us to engineer LOV2 through circular permutation (cpLOV2). Circular permutation (CP) is a common protein engineering method by connecting the native protein N- and C-termini via a covalent linker and reintroducing new termini through cleavage elsewhere in the protein sequence. As such, there are no amino acid substitutions in the existing protein, but the order of residues in the polypeptide sequence is reorganized. Hundreds of circularly permuted proteins have been found in nature, and these gene rearrangements work as a strategy for protein evolution [84-86]. Protein engineers adapted this method to make artificial CPs that manipulate protein structure and function [87-90]. Termini relocation in proteins can introduce conformational changes at the tertiary and quaternary structural levels, resulting in differences in ligand-binding activity, enzyme stability and substrate specificity [91]. The typical examples of the application of circular permutation are

genetically encoded Ca^{2+} indicators (e.g., GCaMP or R-GECO) which are designed based on cpGFP.

For circular permutated LOV2 (cpLOV2) design, there are two critical factors: peptide linker (linker length and composition) and the new terminus position. Usually, the linker connecting the native protein amino and carboxyl terminus should be flexible enough to allow for proper protein folding and stability, such as the Gly/Ser-rich sequences [92]. As a general rule, the new peptide backbone cleavage site should be located in the loop region that is far from the active site, which likely has less disruption to the overall protein structure. In our study, we re-connected the N/C-terminus of LOV2 with a linker, and in parallel, created new N/C termini between the core body and the C-terminal Jα helix to make several cpLOV2 variants. We examined the photoresponsiveness of cpLOV2 as the experiments did for LOV2 and Zdk [57]. cpLOV2 may keep the similar Zdk interaction interface and show a light dependent dissociation with Zdk. Then, the photosensory scaffold cpLOV2 will be used to create new photo-controllable STIM1 variants, as well as to cage other effectors such as nuclear localization signal (NLS), nuclear export signal (NES) and the ssrA peptide. We hypothesize that the cpLOV2 can serve as a new optogenetic platform for optogenetic control of protein function.

Materials and Methods

Plasmid construction

The circular permutated LOV2 gene fragments with six new termini (E412, P423, P456, S486, G504 and T517) were generated as IDT gblocks and inserted into mCherry2 (mCh2)-N1 vector (Addgene # 54517) between the HindIII and EcoRI restriction sites to yield the cpLOV2-mCh2 plasmids. The linker GGGSGGSGGG was used to connect the original LOV2 ends. The Venus-tagged mitochondrial anchored Zdk1 and Zdk2 plasmids pTriex-Ntom20-venus-Zdk1/Zdk2 were gifts form from Dr. Klaus M Hahn at University of North Carolina at Chapel Hill, USA. To generate cpLOV2 variants with truncations in the Jα helix, the PCR-amplified cpLOV2 fragments from the template cpLOV2(T517) or V6 were cloned into the same mCh2-N1 vector between HindIII and EcoRI sites. The KOD hot start DNA polymerase (EMD Millipore) was used for PCR amplification. All cpLOV2 or Zdk2 point mutations used in this study were generated by the QuickChange Lightning Multi Site-Directed Mutagenesis Kit (Agilent Technologies) by following the manufacturer's instructions. cpLOV2(T517)-V6-mCh2 was used as the template for site-directed mutagenesis. pTriEx-Ntom20-venus-Zdk2 was used as the template for Zdk2 mutagenesis. To make PM-tethered Lyn11-GFP-Zdk2, the PM-targeting sequence from the Src kinase Lyn was inserted into pcDNA3.1(+) between the KpnI and BamHI sites, followed by GFP(BamHI-EcoRI) and Zdk2 insertions (EcoRI-XhoI).

The sequence encoding STIM1 residents 336-486 were digested with NheI and HindIII and inserted at the N-terminus of cpLOV2(T517)-V6-mCh2 to make $STIM1_{336-486}$-cpLOV2-mCh2. The fragment between BamHI and BspEI in the linker region of cpLOV2 was replaced by $STIM1_{336-486}$ to make the cpLOV2($STIM1_{336-486}$)-mCh2, in which the gene insertion is between

cpLOV2 Jα helix, and core domains. The constructs $STIM1_{344-442}$-cpLOV2-mCh2 and cpLOV2($STIM1_{344-442}$)-mCh2 were made using a similar strategy. To make the $STIM1_{233-342}$-cpLOV2-$STIM1_{343-685}$-mCh2 construct, the cDNA sequences encoding $STIM1_{233-685}$ flanked by XhoI and EcoRI were inserted into the mCh2-N1 plasmid, followed by cpLOV2 fusion through Gibson Assembly. To generate mCh-Zdk2-$STIM1_{233-473}$-cpLOV2, the mCh fragment is introduced into a NheI restriction site at its 5' end and a BamHI at its 3' end. Zdk2, $STIM1_{233-473}$ and LOV2 fragments were digested with BamHI and EcoRI, EcoRI and XhoI or XhoI and XbaI respectively. The four parts were cloned into pcDNA3.1(+) as the following: pcDNA3.1(+)-NheI-mCh-BamHI-Zdk2-EcoRI-$STIM1_{233-473}$-XhoI-LOV2-XbaI.

To generate the blue light controllable nuclear import plasmid, the nuclear localization signal (NLS) from c-Myc (PAAKRAKLD) was merged into the Jα helix of cpLOV2(T517)-V6-mCh2 by extended PCR. An additional nuclear export signal (NES) from human protein kinase inhibitor-α (PKI- α) (LALKLAGLDI) was added between Jα helix and core domain (KpnI and XmaI restriction sites) to keep the expressed protein entirely in cytosol in the dark state. For the light-inducible nuclear export construct, the similar strategy was used. The NES from Super-PKI-2 (NIDELALKFAGLDL) was fused into Jα helix and an additional NLS from c-Myc was added so as to allow the full nuclear localization of the chimera. The nuclear marker H2B-GFP was obtained from Addgene (#11680).

The sequence encoding protein peptide SsrA was PCR amplified and inserted at the 5' of cpLOV2-mCh2 to make SsrA-cpLOV2-mCh2. To generate mCh-5-ptase/iSH2-SspB-T2A-SsrA-cpLOV2-CAAX, all the components with proper flanked restriction sites were cloned into a customized backbone based on pmCherry-N1 as following: HindIII-mCh-XhoI-5-ptase/iSH2-EcoRI-SspB-SacI-T2A-AgeI-SsrA-cpLOV2-KpnI-CAAX-XbaI. The inter-SH2(iSH2)-domain is

from human p85α and tbe 5-ptase domain (residues 214–644) is from human type IV 5-ptase enzyme with mutated C-terminal membrane targeting depletion. The CAAX plasma membrane targeting motif (residues 167-188) is derived from human Kras-4B. The GFP-$PH_{PLC\delta}$ (Addgene # 21179) and PH_{AKT}-GFP (Addgene # 18836) were used as the $PI(4,5)P_2$ and $PI(3,4,5)P_3$ marker, respectively. For SsrA-cpLOV2 and SspB regulated gene expression, 24xGCN4_v4-NLS-P2A-BFP was replaced by SsrA-cpLOV2 in pHRdSV40-NLS-dCas9-24xGCN4_v4-NLS-P2A-BFP-dWPRE (Addgene # 60910) to make dCas9-SsrA-cpLOV2. SspB flanking by BamHI and EcoRI, transcriptional activator VPR (VP64-p65-Rta) with ends EcoRI and XhoI were cloned into pcDNA3.1(+)-mCh through three parts ligation. The VPR was PCR amplified from the template SP-dCas9-VPR (Addgene # 63798). The luciferase reporter GAL4UAS-Luciferase was obtained from Addgene (#64125), also the sgRNAs used for luciferase promoter region targeting (Addgene #64157, #64158, #64159).

All the plasmids used in this chapter were listed in Table 3.

Table 3. Plasmids used in Chapter III

Given name	Plasmids	Source
V1	cpLOV2(E412)-mCherry2	This study
V2	cpLOV2(P423)-mCherry2	This study
V3	cpLOV2(P456)-mCherry2	This study
V4	cpLOV2(S486)-mCherry2	This study
V5	cpLOV2(G504)-mCherry2	This study
V6	cpLOV2(T517)-mCherry2	This study
V7	cpLOV2(520 truncation)-mCherry2	This study
V8	cpLOV2(525 truncation)-mCherry2	This study
V9	cpLOV2(530 truncation)-mCherry2	This study
V10	cpLOV2(535 truncation)-mCherry2	This study

Table 3. Continued

Given name	Plasmids	Source
V11	cpLOV2(540 truncation)-mCherry2	This study
V12	cpLOV2(No helix)-mCherry2	This study
V13	cpLOV2(No linker)-mCherry2	This study
	cpLOV2(T517)-mCherry2-I428V	This study
	cpLOV2(T517)-mCherry2-Y508F	This study
	cpLOV2(T517)-mCherry2-K544F	This study
	cpLOV2(T517)-mCherry2-K544I	This study
	cpLOV2(T517)-mCherry2-K544N	This study
	cpLOV2(T517)-mCherry2-K544Y	This study
	cpLOV2(T517)-mCherry2-I428V/K544F	This study
	cpLOV2(T517)-mCherry2-I427V	
	cpLOV2(T517)-mCherry2-Q513L	
	pTriex-Ntom20-venus-Zdk1	Gift from Dr. Klaus M Hahn
	pTriex-Ntom20-venus-Zdk2	Gift from Dr. Klaus M Hahn
	pTriex-Ntom20-venus-Zdk2-M9K	This study
	pTriex-Ntom20-venus-Zdk2-L10T	This study
	pTriex-Ntom20-venus-Zdk2-S11R	This study
	pTriex-Ntom20-venus-Zdk2-I31T	This study
	pTriex-Ntom20-venus-Zdk2-I31V	This study
	pTriex-Ntom20-venus-Zdk2-I31A	This study
	pTriex-Ntom20-venus-Zdk2-S33V/T35F	This study
	pTriex-Ntom20-venus-Zdk2-M9K/L10T/S11R	This study
	pcDNA3.1(+)-Lyn11-GFP-Zdk2	This study
	$STIM1_{336-486}$-cpLOV2(T517)-mCh2	This study
	$STIM1_{344-442}$-cpLOV2(T517)-mCh2	This study
	cpLOV2(T517,$STIM1_{336-486}$)-mCh2	This study
	cpLOV2(T517,$STIM1_{344-442}$)-mCh2	This study
	$STIM1_{233-342}$-cpLOV2-$STIM1_{343-685}$-mCh2	This study

Table 3. Continued

Given name	Plasmids	Source
	mCh-Zdk2-STIM1$_{233-473}$-cpLOV2	This study
	NLS-cpLOV2(T517)-mCh2	This study
	NES-cpLOV2(T517)--mCh2	This study
	H2B-GFP	Addgene #11680
	mCh-5-Ptase-SspB-T2A-SsrA-cpLOV2-CAAX	This study
	mCh-iSH2-SspB-T2A-SsrA-cpLOV2-CAAX	This study
	GFP-PH$_{PLC\delta}$	Addgene #21179
	PH$_{AKT}$-GFP	Addgene # 18836
	dCas9-SsrA-cpLOV2	This study
	pcDNA3.1(+)-mCh-SspB-VPR	This study
	GAL4UAS-Luciferase reporter	Addgene #64125
	sgRNA1_GAL4UAS-Luciferase reporter	Addgene #64157
	sgRNA2_GAL4UAS-Luciferase reporter	Addgene #64158
	sgRNA3_GAL4UAS-Luciferase reporter	Addgene #64159
	pGP-CMV-GCaMP6m	Addgene #40754
	pGP-CMV-NES-jRCaMP1b	Addgene # 63136

Cell culture, transfection and live-cell imaging

HeLa and HEK293T cells were cultured in 10% FBS-DMEM medium. For the cell transfections, appropriate vectors were transfected by Lipofectamine 3000 following the manufacturer's instruction. Four wells glass bottom dishes (D35C4-20-1.5-N, Cellvis) were used for live-cell imaging. The Nikon A1R confocal microscope equipped with tissue culture system

and NIE-elements confocal software was applied in this study. As the same equipment used in chapter II, the 40x and 60x oil objects were used for cell imaging.

For light-induced Zdk2 and cpLOV2 dissociation, images of cells co-transfected with pTriex-Ntom20-venus-Zdk2 and cpLOV2-mCh2 were acquired every 4 sec for 2min. Blue light excitation (488 nm) for GFP channel was also used for photostimulation of cpLOV2. For experiments examining the cycle stimulation for cpLOV2 and Zdk2 binding, the same mitochondrial anchored Zdk2 and cpLOV2-mCh2 were transfected, external blue light source (470 nm, 40 $\mu W/mm^2$, ThorLabs, Inc.) were performed a light cycle of 30 sec on and 100 sec off for 12 min. Time course imaging were recorded every 3 sec for stimulation period and every 15 sec for the dark recovery period. For fast and slow cpLOV2 recovery kinetics, cells were co-transfected with cpLOV2-mCh (WT/fast/slow) and PM tethered Lyn11-GFP-Zdk2 were pretreated with an external blue light source for two minutes. Then the images were acquired for red channel (561 nm) every 5, 10 or 30 sec depending on the cpLOV2 type, due to the difference of recovery time.

To measure the levels of Ca^{2+} influx presented in Figures 16-17, STIM1 fragments fused cpLOV2 or LOV2 constructs were transfected with either green color Ca^{2+} indicator GCaMP6s or red one jR-CaMP1b in HeLa cells. Ca^{2+} influx was induced by continuous blue light for 3 min, and fluorescent images were then acquired for 5 sec. Light stimulation was given 5 min for every 10 min in Figure 17b for Ca^{2+} oscillation.

For blue light-induced nuclear import or export assays, NLS-cpLOV2-mCh2 or NLS-cpLOV2-mCh2 was transfected with nuclear marker H2B-GFP. Time-lapse imaging was applied every 30 sec for 1 hour. Light pulse was given as shown in the figure.

Light-inducible phosphoinositide reprogramming in the plasma membrane was performed in HeLa cells. The single component mCh-5-ptase-SspB-T2A-SsrA-cpLOV2-CAAX was transfected and the PIP_2 sensor GFP- $PH_{PLC\delta}$ (Addgene # 21179); mCh-iSH2-SspB-T2A-SsrA-cpLOV2-CAAX was transfected with the PIP_3 sensor PH_{AKT}-GFP (Addgene # 18836). Cells were starved in FBS-free DMEM medium for 4 hours to deplete endogenous PIP_3 before imaging in the lateral group. Both red and green channel imagines were acquired before and after external blue light stimulation for 5 min.

Image analysis

Images were analyzed with the Nikon NIS-elements imaging software. For quantification of Zdk2 and cpLOV2 binding, we used ROI to define the cytosolic and mitochondrial region manually with 20-30 cells selected for analysis. The "Time Measurement" tool in Nikon imaging software was used to determine fluorescence intensity. Fluorescence intensity ratio of Mito/cyto for cpLOV2-mCh2 was calculated before and after photoexcitation. For fast and slow-cycling variants of cpLOV2, the cytosolic mCh2 intensity was measured, and the relative change was plotted by the Prism 5 software. The fluorescence intensity for GCaMP6s and jRCaMP1b was measured in the ROI. All the data are plotted by the Prism 5 graphing software as mean ± s.e.m. The half-time of activation or decay was calculated with the "One phase decay" tool in the Prism 5 software package.

Light-induced bioluminescence assay

The dCas9-SsrA-cpLOV2, SspB-VPR, sgRNAs targeted GAL4UAS and GAL4UAS-luciferase reporter were transfected at a 1:1:1:1 ratio in HEK293T cells plated in 24-well plate.

The dCas9-cpLOV2 was used to replace dCas9-SsrA-cpLOV2 for control. The ration of three sgRNAs was 1:1:1. Six hours after transfection, cells were stimulated with external blue light for 30 min in a culture hood. The control groups were kept at dark. After additional 18 hours of culture at 37°C in 5% CO2, cells were lysed, and bioluminescence measurements were performed using reagents from Promega (Dual Luciferase Reporter Assay System) and synergy luminescence microplate reader (BioTek).

Statistical analysis

Statistical analysis was performed using the Paired Student's *t*-test. *P<0.05; **P<0.01; ***P<0.001.

Results

Design and optimization of circularly permuted LOV2

To efficiently create LOV2 for promising circular permutation sites, the multiple cpLOV2 clones were generated by directly synthesizing the double strand DNA as gblock (IDT). The flexible glycine and serine-rich linker GGGSGGSGGG was used for fusing the N- and C-termini of wild type LOV2. The new termini were selected in the loop region to minimize perturbation to the host. As shown in **Figure 14a** for the highlighted purple color, six sites located in the core domain or between the core and Jα helix were chosen. The new cpLOV2 constructs were named as V1-V6 as shown in **Figure 14b**.

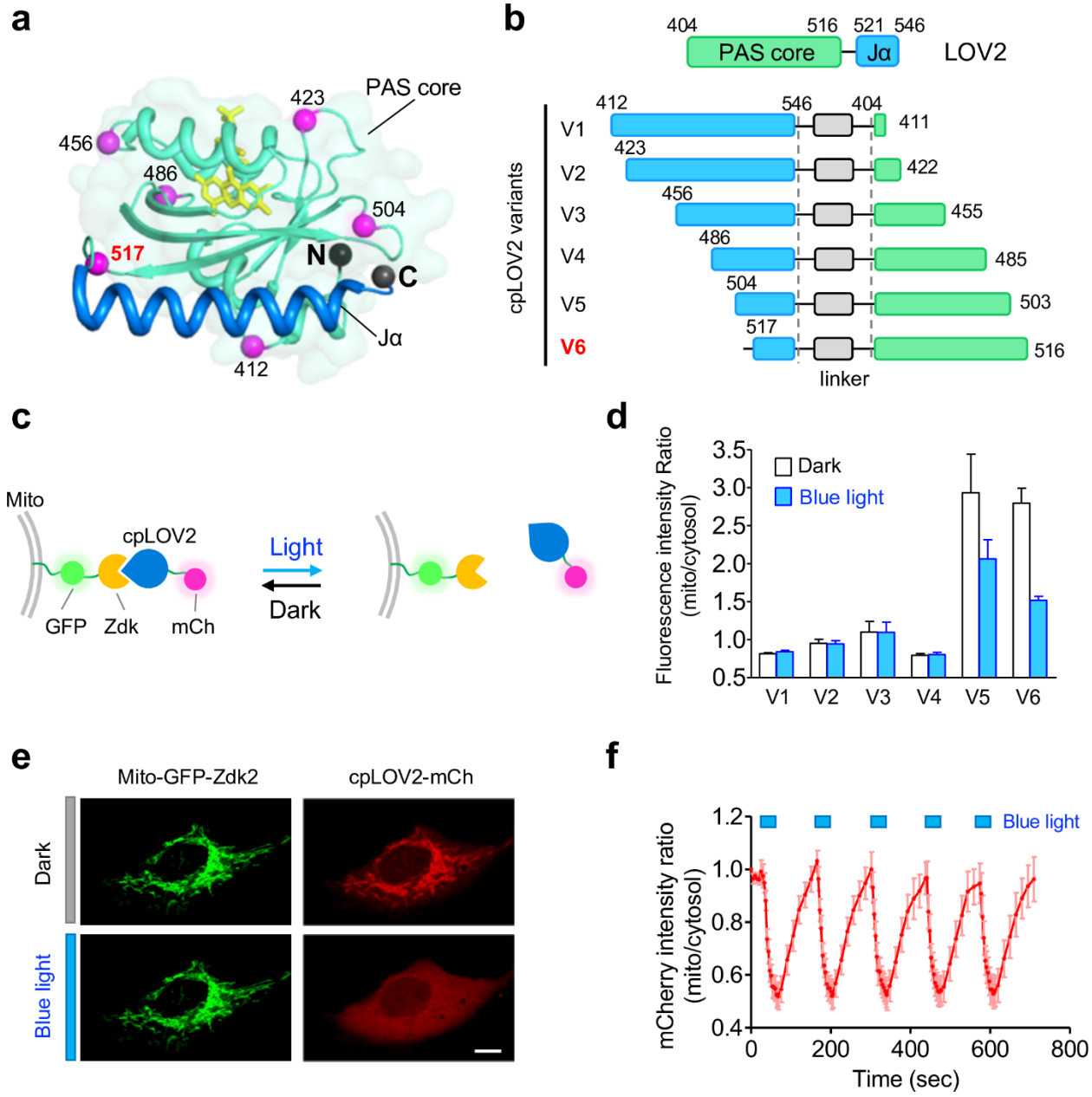

Figure 14. Design of photoswitchable circularly permuted LOV2 (cpLOV2).
(a-b) Generation of new N- and C-termini through circular permutation of LOV2. The N- and C-termini (black spheres) of LOV2 was separated by a distance of about 10Å. The locations of newly created N-termini (magenta spheres) were mapped to the X-ray crystal structure of LOV2 (a; PDB entry: 2V0W), with the corresponding domain architectures (b) shown on the right. **(c)** A Zdk2-based mitochondria dissociation assay to screen photo-responsive cpLOV2. A functional cpLOV2 is anticipated to dock toward mitochondria-tethered Zdk2 in the dark, but would rapidly dislodge from mitochondria and subsequently disperse into the cytosol. (**d**) Representative confocal images of HeLa cells co-expressing cpLOV2-mCh (V6, red) and mitochondria-tethered GFP-Zdk2 (green) before and after light illumination (470 nm; 40 μW/cm^2). Scale bar,10 μm. **(e)** Quantification of the fluorescence intensity ratio (mitochondria-over-cytosol) for cpLOV2-mCh before and after light illumination (n = 10-20 cells; mean ± s.e.m.) **(f)** Reversible binding of cpLOV2 (V6) to Zdk2 following repeated light-dark cycles (n = 12; mean ± s.e.m.).

To test the photo-responsiveness of cpLOV2, we used LOV2 binding partner of the dark state-Zdk. The Zdk is a small protein derived from immunoglobulin-binding staphylococcal protein A Z domain. Zdk has been shown to tightly interact with the LOV domain in the dark state and dissociate from LOV2 with light illumination [57, 58]. We reasoned that the cpLOV2 generated has the similar structure and function as wild type LOV2. To test this, the N terminus of Zdk (Zdk1 and Zdk2) were fused to the mitochondrial targeting fragment of TOM20 and fluorescent protein Venus; while the C terminus of cpLOV2 was fused to an mCherry2 fluorescent protein in the cytosol (**Figure 14c**). When the Zdk1/2 and cpLOV2 plasmids were co-expressed in HeLa cells, they had different behaviors. Zdk1 bound with LOV2's C-terminal Jα helix and had a significant difference in lit-dark affinity. However, Zdk1 showed no binding with cpLOV2 variants (data not shown). Zdk2 had a lower dissociation constant fold change than Zdk1 and bound to the N terminus of LOV2. Two of the cpLOV2 constructs (V5 and V6) showed the blue light-dependent binding and releasing with Zdk2 (**Figure 14d**). The V6 has more lit-dark fold change than V5. The cpLOV2-V6 has its Jα helix at N-terminus and the core domain at its C-terminus. The mitochondrially co-localized cpLOV2-mCh2-V6 quickly diffused into the cytosol after blue light irradiation (**Figure 14e**). The blue light illumination induced reversible Zdk2 dissociating and binding in a rapid manner (**Figure 14f**).

To further test if the Jα helix of cpLOV2 was necessary for Zdk2 binding, the N-terminus of cpLOV2 Jα helix was truncated (**Figure 15a**). Interesting, the three amino acids deletion at the cpLOV2-V6 N-terminus showed a decrease binding affinity with Zdk2 in the dark but the five more truncation (V8) one has similar lit-dark fold change as cpLOV2-V6. Further truncations in the Jα helix attenuated its ability to interact with Zdk2. The crystal structure of LOV2 and Zdk2 complexes are shown in **Figure 15b**. The residues situated at their interfaces were mutated to

interfere the cpLOV2-Zdk2 interaction. The cpLOV2 variants with the mutations sites at I428 and K544 demonstrated reduced dark binding with Zdk2. When the tyrosine at residue 508 was mutated to phenylalanine, less binding in the dark state and more releasing upon blue light illumination were observed. The isoleucine replacing tyrosine at Y508 abolished binding. Even more, double mutations (I428V/K544F) eliminated the interaction with WT Zdk2. Zdk2 mutations near the interface demonstrated the similar or reduced binding affinity with cpLOV2, while M9K showed stronger binding. Together, mutations perturbing the Zdk2-cpLOV2 interacting interfaces altered binding affinities or even disrupted the interaction.

For wild type cpLOV2, the deactivation half-life was determined to be 54.4 sec (**Figure 15c**). But the kinetics were tunable with the introduction of known fast- or slow-cycling mutations in LOV2 [93-95]. These mutations caused fast or slow deactivation kinetics with the half-lives of 23.9 sec and 494 sec, respectively. The tenability of photo-responsive kinetics will enable us to control cell signaling that span seconds to hours.

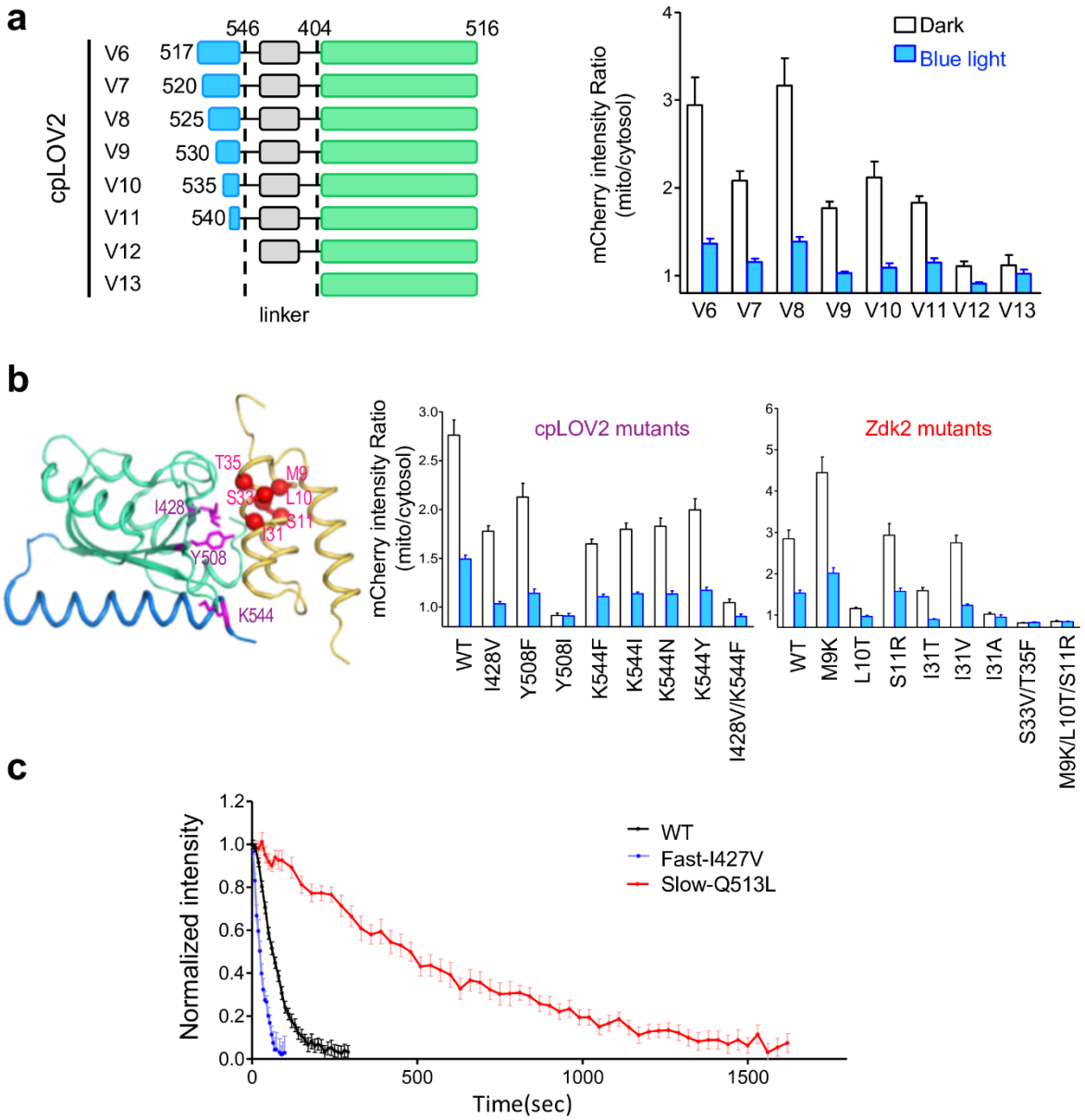

Figure 15. Design and optimization of cpLOV2 constructs.
(a) The Jα-helix of cpLOV2-V6 was further truncated, and the cpLOV2-Zdk light-dependent disassociation assay was used for quantification. **(b)** Mutational studies. Mutations were introduced to the binding interface, and the cpLOV2-mCh mitochondria/cytosol intensity ratio before and after blue light stimulation were recorded. **(c)** The fast- and slow-cycling mutations of cpLOV2.

cpLOV2 affords new interfaces for Ca^{2+} signaling controlling

In chapter II, we described the strategy of blue light inducible Ca^{2+} flux by fusing the STIM1 SOAR domain to the C-terminus of LOV2. The construct with the best performance contains the STIM1ct fragment 336-486. But the minimal ORAI1 interaction region of amino acids 344-442 was not photo-tunable even though several strategies were used for optimization. We speculated that the newly developed cpLOV2 would provide different interfaces for protein function caging. In this study, the two STIM1 fragments $STIM1_{336\text{-}486}$ and $STIM1_{344\text{-}442}$, in which the SOAR domain was included, were fused to LOV2 and cpLOV2. As shown on the top of **Figure 16**, the STIM1 effectors were fused to the C-terminus of wild type LOV2. For cpLOV2 photo-caging, the effector domain was either inserted upstream of the Jα helix or between the Jα helix and the core domain of cpLOV2. We anticipated that photoactivation of SOAR domain would enable it to translocate to the PM and open ORAI1 channel to induce Ca^{2+} entry as LOVSoc did. The light-inducible changes in fluorescence signals for $STIM1_{336\text{-}486}$-cpLOV2 was similar to the fold-change elicited by LOV2-$STIM1_{336\text{-}486}$ (LOVSoc) (**Figure 16a-b** middle panel). The insertion of this fragment between the Jα helix and the core domain failed to cause light-dependent changes in Ca^{2+} signals (**Figure 16c** middle panel). By comparison, for the case of $STIM1_{344\text{-}442}$ as an effector domain, we observed a totally different scenario: only the third strategy worked in the presence of Zdk2 (**Figure 16c** lower panel).

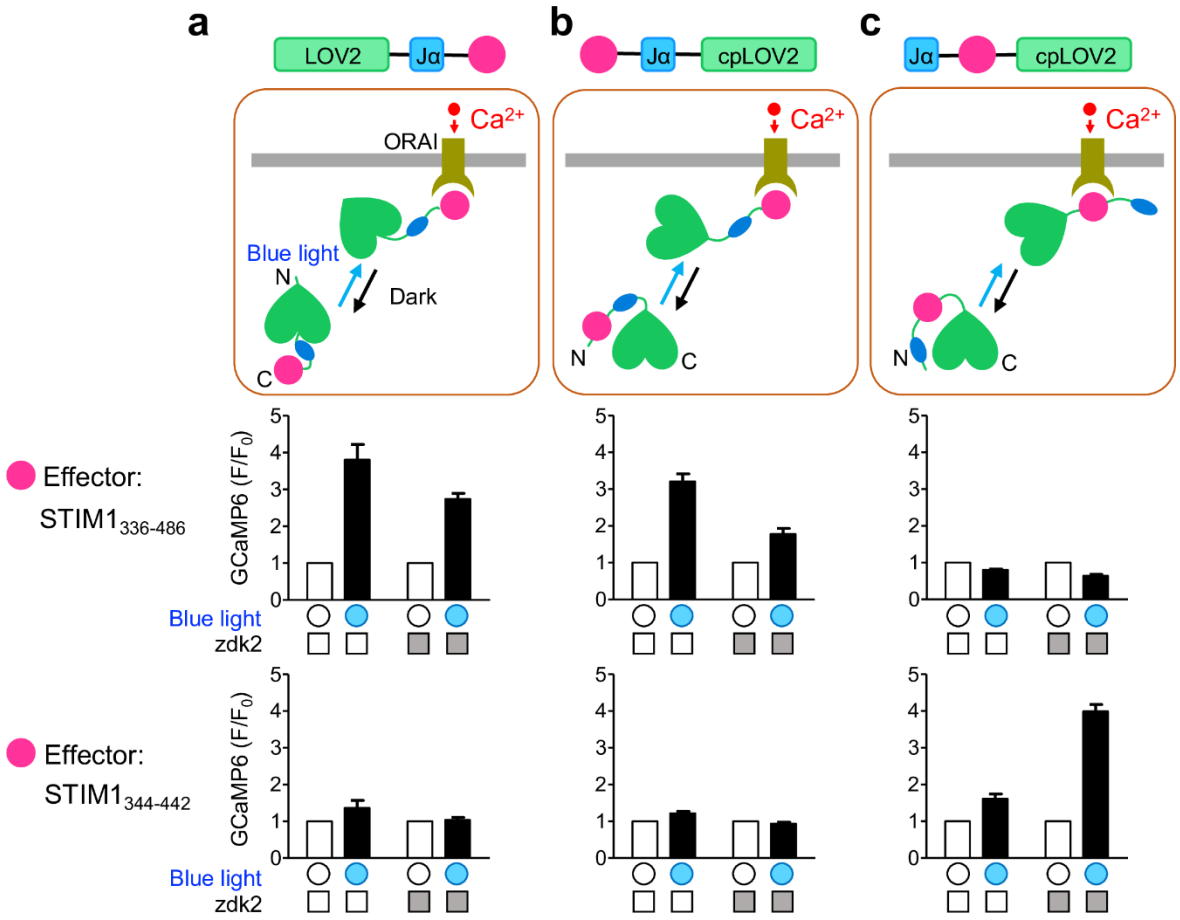

Figure 16. cpLOV2 affords new interfaces to cage STIM1 activity.
STIM1-mediated activation of the ORAI Ca^{2+} channel was utilized to test the caging capability. Light-induced Ca^{2+} influx through endogenous ORAI1 channels in HeLa cells was monitored by using the green Ca^{2+} indicator GCaMP6s. Two effector domains ($STIM1_{336-486}$ or $STIM1_{344-442}$) was individually fused to the C-terminus of LOV2 **(a)**, or placed at the N-terminus of cpLOV2 **(b)**, or inserted between the Ja helix and the PAS core of cpLOV2 **(c)**, in the presence or absence of Zdk2. Blue circle, blue light irradiation at 470 nm (power density: 40 $\mu W/cm^2$). Gray square, with Zdk2.

Design of ON and OFF switch for optical control of Ca^{2+} signals using cpLOV2

STIM1 CC1 domain (coiled-coil region, residue 234-343) was proposed to inhibit the function of SOAR domain or STIM1ct because deletion or point mutations in this region make the STIM1 constitutively active [96-99]. Here the cpLOV2 was used to interferes the CC1-SOAR interaction and then to achieve the light tunable activation of CRAC channels.

The cpLOV2 was inserted into the connection region between CC1 and SOAR (**Figure 17a**). After blue light absorption, the conformational changes within cpLOV2 seemed to disrupt the CC1-SOAR interaction to overcome STIM1 auto-inhibition to induce Ca^{2+} entry as seen in the **Figure 17a**. In contrast, the chimera with the Zdk2 fused at the N-terminus, and cpLOV2 fused at the C-terminus of CC1-SOAR (233-473) demonstrated repeated light-induced suppression of Ca^{2+} influx (**Figure 17b**). As a control, the relative fluoresce intensity for Ca^{2+} indicator jRCaMP1b was maintained at a constant level under the same light stimulation (Data not shown), ruling out the possibility of photobleaching. A plausible explanation for this finding is that the docking of Zdk2 to cpLOV2 interrupts the CC1-SOAR interaction to expose SOAR in the dark. Upon photostimulation to disrupt Zdk2-cpLOV2 association, the CC1-SOAR interaction was restored to terminate Ca^{2+} entry through ORAI channels.

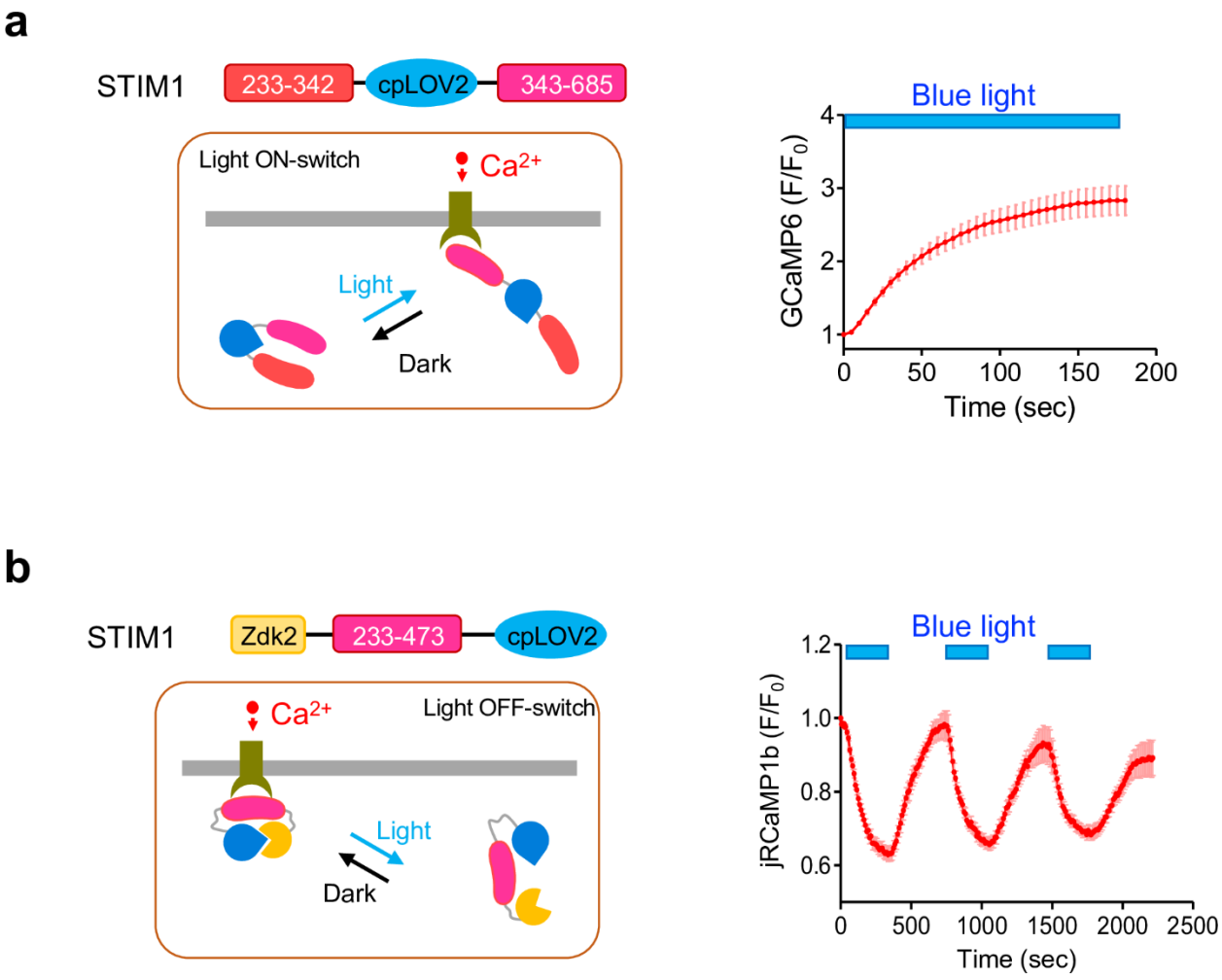

Figure 17. Control of STIM1 activity by cpLOV2/Zdk insertion.
(a) Insertion of cpLOV2 into a host protein (STIM1-CT) confers photosensitivity to CRAC channel. Light stimulation caused Ca^{2+} influx in cells transfected with $STIM1_{233-342}$-cpLOV2-$STIM1_{343-685}$ (n = 37; mean ± s.e.m.). **(b)** Photo-induced inhibition of Ca^{2+} influx in HeLa cells co-expressing jRCaMP1b and the indicated chimeras. (Left) Schematic illustration of the design. A STIM1-CT fragment (aa 233-473) was flanked by Zdk2 and cpLOV2 at its N- and C-termini, respectively. (Right) jRCaMP1b (red Ca^{2+} indicator) signals monitored over three repeated dark-light cycles (n = 32; mean ± s.e.m.).

Light-induced nuclear import or export by cpLOV2

The nuclear localization signal (NLS) or export signal (NES) peptides have been previously incorporated into the LOV2 domain to rapidly and reversibly control nuclear import/export of proteins [52, 100, 101]. We applied the same strategy by incorporating the NLS (NLS-cpLOV2) or NES (NES-cpLOV2) in the Jα helix situated at the N-terminus of cpLOV2 (**Figure 18**). The mCherry2 fused NLS-cpLOV2 was evaluated in HeLa cells, and the nucleocytoplasmic ratios upon blue light exposure were monitored with confocal microscopy. The NLS-cpLOV2-mCh2 was distributed in the cytosol in the dark and showed light-dependent nuclear import, with the co-expressed H2B-GFP serving as the nuclear marker (**Figure 18a**). The NLS-cpLOV2 demonstrated a blue light-dependent reversible nuclear importing with the import half-life of 67.9 sec and an export half-life of 65.7 sec.

For the light-induced nuclear export by cpLOV2, the NES-cpLOV2 was designed similarly to NLS-cpLOV2. The NES from Super-PKI-2 was put under the control of cpLOV2, and a C-Myc NLS was used to keep the protein within the nucleus. The NES-cpLOV2 shuttled between nuclear and cytosol following dark-light cycles, with an export half-life of 78.4 sec and an import half-life 262.4 sec (**Figure 18b**).

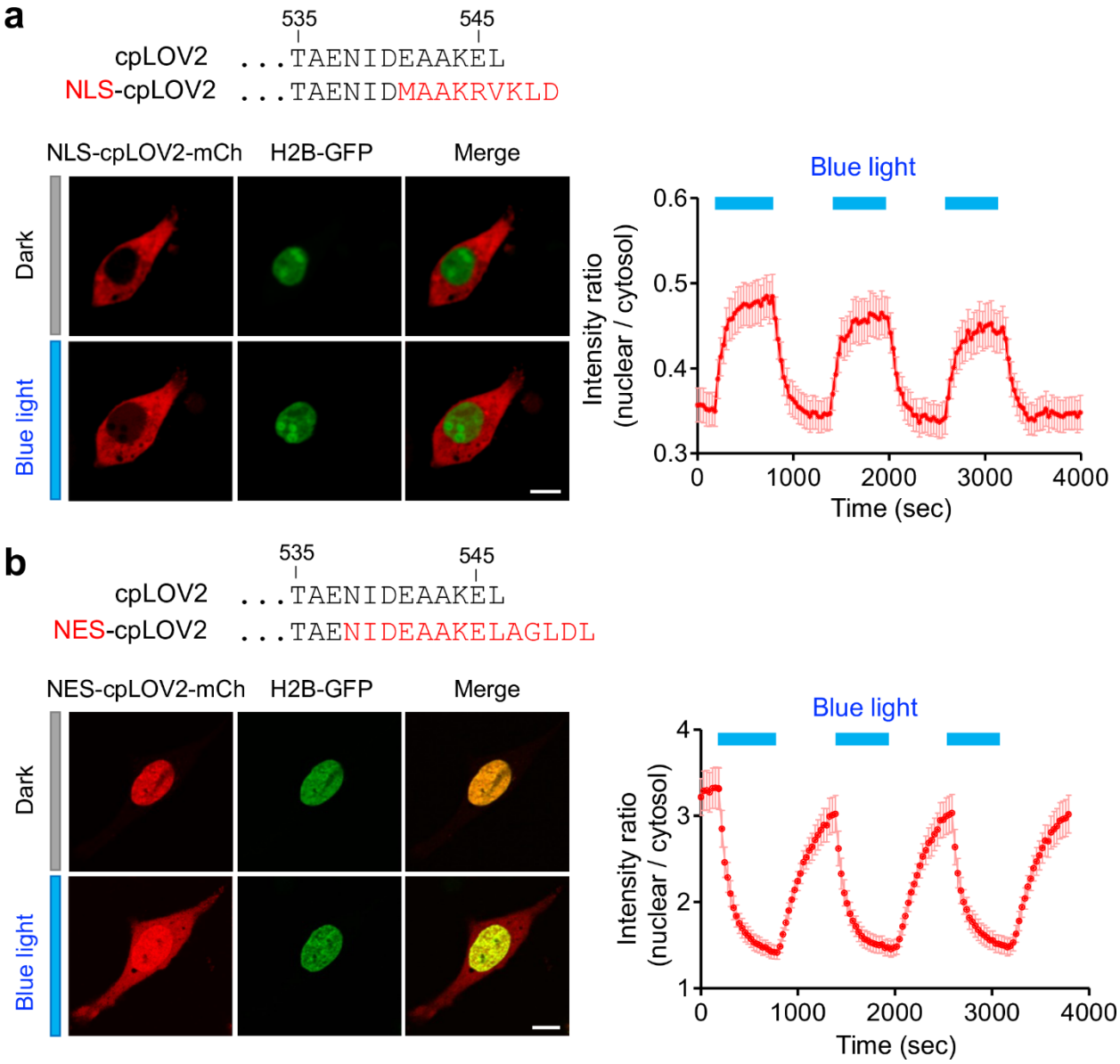

Figure 18. cpLOV2 for light-controllable nucleo-cytoplasmic shuttling in mammalian cells.
Design and representative confocal images of cplov2 caged **(a)** nuclear localization signal (NLS), NLS-cplov2 or **(b)** nuclear export signal (NES), NES-cpLOV2. H2B-GFP is used as a nuclear marker. The quantification of Nuclear over cytosolic mCh signals was shown on the right (n = 5).

Light-induced dimerization between SsrA-cpLOV2 and SspB for phosphoinositide reprogramming and transcriptional activation

In a recent study, an SsrA peptide from bacteria has been fused to LOV2 to enable light-inducible interaction with SspB. The LOV2-SsrA/Sspb pair (designated iLID) thus forms an optical dimerizer to photo-induce protein-protein interaction [33]. The design strategy was extended to cage SsrA by using cpLOV2. When anchoring SspB or SsrA-cpLOV2 to a subcellular location, the other component should exhibit light-induced heterodimerization and then show cellular translocation. If a protein of interest was fused, it could be used to localize protein in the cell and regulate signaling pathways.

Phosphoinositide (PI) lipids are important cellular membrane components and each of the PI species has specific cellular membrane distribution and mediates versatile signaling functions [102]. PI(4,5)P_2, the major phosphoinositide species in the PM, can be hydrolyzed to inositol trisphosphate and diacylglycerol as two important second messengers to mediate signal transduction [103]. Here, we fused a phosphoinositide 5-phosphatase (5-ptase) to SspB-mCh, while the SsrA-cpLOV2 was anchored on PM through a CAAX motif (**Figure 19a**). The confocal images demonstrated the rapid light inducible translocation of SspB-5-ptase-mCh to PM with subsequent depletion of PI(4,5)P_2, the latter of which was reflected in the dissociation of PI(4,5)P_2 maker GFP-$PH_{PLC\delta}$ from PM (**Figure 19b**). When the inter-SH2 domain (iSH2) of PI3K p85α regulatory subunit was connected with SspB, we observed light trigged SspB-iSH2-mCh PM targeting with consequent increase in PM-resident PI(3,4,5)P_3 as told by the PH_{AKT} – GFP sensor (**Figure 19c**). The endogenous PI3K catalytic subunit p110 was recruited by iSH2 to PM and generate PIP_3, which is monitored by the PIP_3 reporter PH_{AKT}-GFP. Collectively, SsrA peptide can be caged by cpLOV2 and has a light dependent interaction with SspB.

We next further combined the SsrA-cpLOV2/sspB system with CRISPR/Cas9 and transcriptional coactivators in the nuclear environment, with the goal of achieving photoactivatable transcription. The CRISPR-dCas9 systems have offered powerful tools for precise gene targeting and perturbation [104, 105]. The anchor probe contains dCas9 and SsrA-cpLOV2 bound to the targeted sequence guided by sgRNAs. Here we targeted SsrA-cpLOV2 to the upstream activator sequence (UAS) of firefly luciferase reporter. The activator probe includes SsrA binding partner SspB and synthetic transcriptional activation domains VP64-p65-Rta (VPR) (**Figure 19d**). In the absence of blue light, the dCas9-SsrA-cpLOV2 bound to the promoter region of the luciferase reporter. Upon blue light illumination, SsrA-cpLOV2 and SspB were heterodimerized and luciferase gene expression was initiated after recruiting the VPR module to the target gene. Indeed, we observed a significant increase in the luciferase activity after blue light stimulation (right, **Figure 19d**).

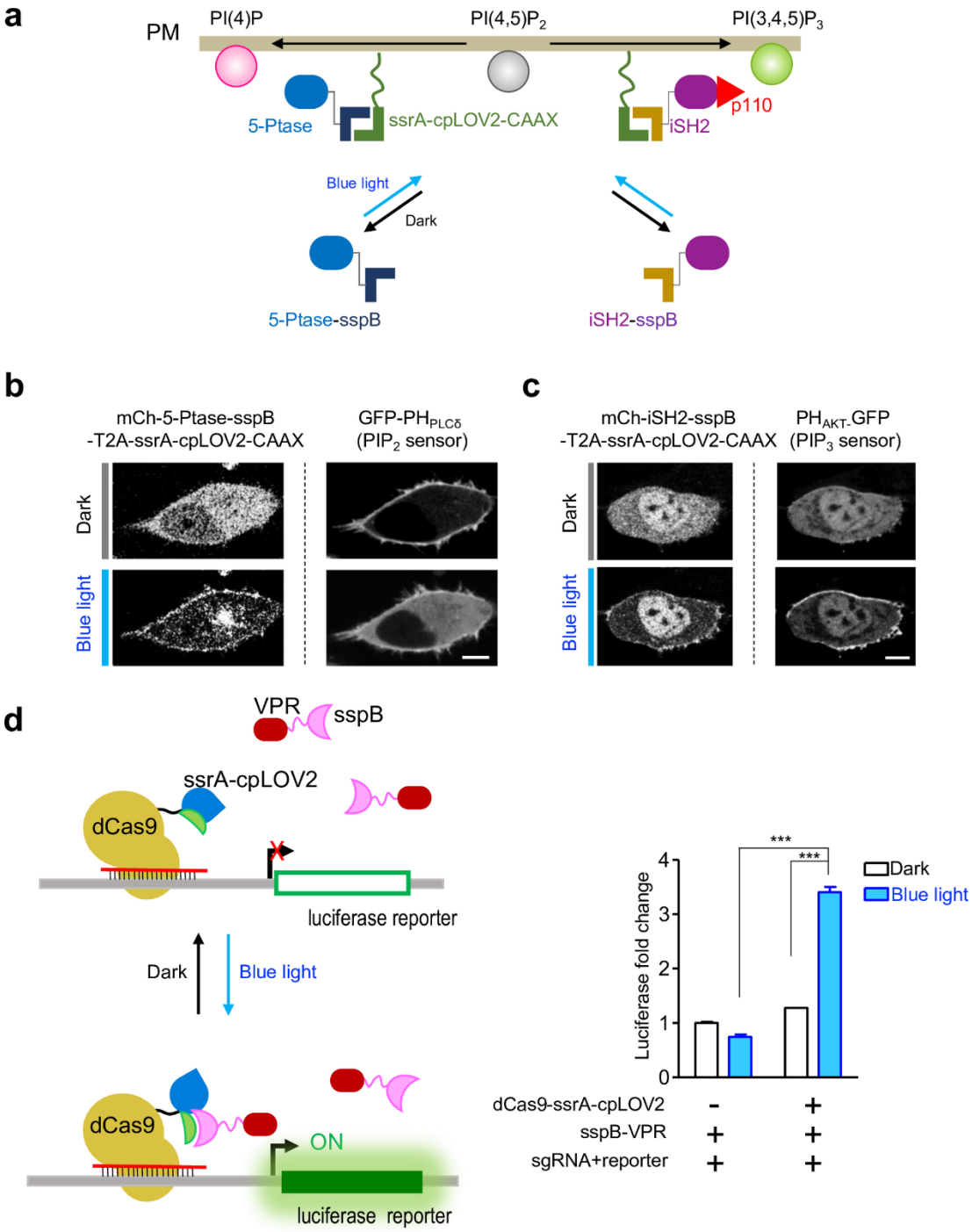

Figure 19. The reversible interaction between SspB and SsrA-cpLOV2 enables phosphoinositide reprogramming and light-inducible gene expression.
(a-b) The reversible interaction between PM-anchored Lyn11-GFP-SspB and SsrA-cpLOV2-mCh fused to effector domains (5-ptase or iSH2 of PI3K), which enables the light-inducible reprogramming of phosphoinositide metabolism in the plasma membrane. The membrane targeting of 5-ptase domain was abrogated with the C641A mutation. **(c)** Photoactivation of luciferase gene expression. Transcriptional activator VPR, VP64-p65-Rta.

Discussion

A novel aspect of this study was the use of the circularly permuted method to engineer the well-studied LOV2 to make cpLOV2. The LOV2 binder Zdk2 was used as the bait for screening photoresponsive cpLOV2 variants. We found the functional cpLOV2 with the new terminus in the loop region of core domain and Jα helix. The newly created cpLOV2 is different from wild type LOV2 because the Jα helix is located at N-terminus and core domain at C-terminus. In our study, Zdk2 shows light-induced association and disassociation with cpLOV2. This indicated that cpLOV2 keeps the similar structure and function as LOV2, at least for the Zdk2 binding region. Truncation of Jα helix reduced or abolished the Zdk2 binding, attesting to a critical role of Jα helix in mediating Zdk2-cpLOV2 interaction. cpLOV2 variants with mCh2 located at the N-terminus, C-terminus or Middle (between Jα helix and core domain) all show Zdk2 binding in the dark and releasing upon blue light absorption (Data not shown).

This newly developed cpLOV2 photosensory scaffold provides new opportunities for effectors engineering and caging, especially for proteins that should have free N termini to exert their functions. $STIM1_{336-486}$-cpLOV2 has similar light-induced Ca^{2+} fold change as LOVSoc. But for the $STIM1_{344-442}$ fragment, the photo-inducible Ca^{2+} influx only can be achieved by middle insertion in the prescence of Zdk2. More applications of cpLOV2 by inserting cpLOV2 into proteins or its combined use with Zdk2 will open more opportunities for optogenetic engineering. The cpLOV2-based photosensitive nucleocytoplasmic shuttling devices and the cpLOV2-iLID system provide a unique platform for remote interrogation of signal transduction and noninvasive control of gene expression.

To further extend the utility of cpLOV2, it is necessary to express and purify the protein *in vitro* for biophysical and structural characterization. Further research is needed for characterizing

the crystal structures of cpLOV2 in the dark and lit state. The understanding of the allosteric mechanism of cpLOV2 enables us to improve the design of optogenetic devices.

CHAPTER IV

PHOTOACTIVATABLE CONTROL OF CALCIUM SIGNALING THROUGH OPTOORAI1

Introduction

ORAI1 is a plasma membrane protein with four transmembrane domains and both the N and C termini facing the cytosol [106]. The CRAC channel is composed of six ORAI subunits, and the transmembrane 1 (TM1) helix form the calcium ion conduction pathway. The other transmembrane helices (TM2-4) are closely packed around the TM1 segment. After ER calcium store depletion, the calcium sensor STIM1 in ER migrates and accumulates at the ER-PM junction, where STIM1 engages and directly gates ORAI calcium channels in the plasma membrane [107]. STIM1 directly interacts with the cytoplasmic regions of ORAI1 and induce ORAI1 conformational changes, which leads to ORAI1 activation [4, 108-111]. The negatively charged E106 forms the Ca^{2+} coordinating pocket to confer high Ca^{2+} selectivity [106, 112, 113]. The six pore helix from each ORAI1 unit rotates from the pore axis after STIM1 binding [114]. Increased pore hydration allows the Ca^{2+} to flow through the hydrophobic pore and the CRAC channel opens. The Gill group recently described a model for STIM1-mediated gating of ORAI1 channels [115, 116]. STIM1 physically interacts with the helical extension of TM4 (TM4-ext) at the C-terminus of ORAI, which causes the TM4-ext hinge to flex, followed by hydrophobic coupling of L261 (TM4) to the closely apposed L174 (TM3). This conformational change propagates the rearrangement of the tightly associated TM3, TM2 and TM1 to open channel. Therefore, the activation of ORAI1 channel can be achieved by TM3 or TM4 rearrangement and signal transducing to TM1.

Bearing this model in mind, we attempted to create light controllable Ca^{2+} ORAI1 channels by directly pulling N- and C- terminus together through light inducible hetero-dimerization. However, these efforts failed and we detected no or little light-inducible Ca^{2+} influx. Here, instead of the traditional method by caging the effector at LOV2 C-terminus, we will insert LOV2 into the only intracellular loop of OARI1, with the goal of serving as an allosteric switch to photo-activate engineered ORAI1 channels. We propose to add LOV2 into constitutively active ORAI1 mutants. LOV2 insertion will cause ORAI1 structure rearrangement and pull the subdomain from the active position, especially for the TM3 after Jα helix. In this way, light-induced LOV2-Jα unfolding will exert an allosteric effect on ORAI1 to activate its activity.

Materials and Methods

Plasmid design and construction

For OptoORAI1 constructs, cDNA sequences encoding human ORAI1 were PCR amplified and subcloned into pcDNA3.1(+) vector with mKate2-P2A pre-inserted between NheI and BamHI sites. Sequence encoding ORAI1 was digested with BglII and XhoI, while the pcDNA3.1(+)-mKate2-P2A was lined by BamHI and XhoI for the complementary overhang sequences produced by BamHI and BglII. ORAI1 active mutations were introduced into the ORAI1 intracellular region (in pcDNA3.1(+)-mKate2-P2A-ORAI1 by QuickChange Lightning Multi Site-Directed Mutagenesis Kit (Agilent Technologies) following the manufacturer's instruction. The $AsLOV2_{404-546}$ fragment flanked with BamHI and BspEI sites was inserted into mCh-ORAI1 for WT or mutant ORAI1 through Gibson Assembly (NEBuilder® HiFi DNA Assembly Master Mix, NEW ENGLAND Biolabs Inc). For the best construct (OptoORAI1-V2) screened from ORAI1-error prone mutations and NFAT-GFP nuclear translocation assay, the same double mutations were introduced into mKate2-P2A-ORAI1, then LOV2 was inserted into other ORAI1 loop sites as indicated in Figure 22a by Gibson Assembly. ORAI1 fragments (with LOV2 insertion) from OptoORAI1-V2 was cloned into pcDNA3.1(+)-mCh or mCh-N1 vectors to make mCh-OptoORAI1(1-301), mCh-OptoORAI1(65-301), mCh-OptoORAI1(65-301) and OptoORAI1(1-301)-mCh by using proper restriction sites. All plasmids vectors were confirmed by DNA sequencing. See **Table 4** for all the plasmids used in this chapter.

Table 4. Plasmids used in Chapter IV

Given name	Plasmids	Source
	pcDNA3.1(+)-mKate2-P2A-ORAI1(LOV2, WT)	This study
	pcDNA3.1(+)-mKate2-P2A-ORAI1(LOV2, H174G)	This study
	pcDNA3.1(+)-mKate2-P2A-ORAI1(LOV2, G183D)	This study
OptoORAI-V1	pcDNA3.1(+)-mKate2-P2A-ORAI1(LOV2, P245T)	This study
	pcDNA3.1(+)-mKate2-P2A-ORAI1(LOV2, LV>AN)	This study
	pcDNA3.1(+)-mKate2-P2A-ORAI1(LOV2, ANSGA)	This study
	pcDNA3.1(+)-mKate2-P2A-ORAI1(LOV2, H171D, P245T)-S1	This study
	pcDNA3.1(+)-mKate2-P2A-ORAI1(LOV2, H171D, P245T)-S2	This study
	pcDNA3.1(+)-mKate2-P2A-ORAI1(LOV2, H171D, P245T)-S3	This study
	pcDNA3.1(+)-mKate2-P2A-ORAI1(LOV2, H171D, P245T)-S4	This study
	pcDNA3.1(+)-mKate2-P2A-ORAI1(LOV2, H171D, P245T)-S5	This study
	pcDNA3.1(+)-mKate2-P2A-ORAI1(LOV2, H171D, P245T)-S6	This study
OptoORAI-V2	pcDNA3.1(+)-mKate2-P2A-ORAI1(LOV2, H171D, P245T)-S7	This study
	pcDNA3.1(+)-mKate2-P2A-ORAI1(LOV2, H171D, P245T)-S8	This study
	pcDNA3.1(+)-mKate2-P2A-ORAI1(LOV2, H171D, P245T)-S9	This study
	pcDNA3.1(+)-mKate2-P2A-ORAI1(LOV2, R91W, H171D, P245T, R91W)-S7	This study
OptoORAI-V3	pcDNA3.1(+)-mCh-ORAI1$_{65-301}$(LOV2, H171D, P245T)	This study
	pcDNA3.1(+)-mCh-ORAI1$_{65-286}$(LOV2, H171D, P245T)	This study
	ORAI1$_{1-301}$(LOV2, H171D, P245T)-mCh	This study
	pcDNA3.1(+)-mCh-ORAI1$_{65-301}$(LOV2, R91W, H171D, P245T)	This study
	pcDNA3.1(+)-mCh-ORAI1$_{65-301}$(LOV2, E106A,H171D, P245T)	This study
	HA-NFAT1$_{1-460}$-GFP	Addgene #11107
	pGP-CMV-GCaMP6m	Addgene #40754

Confocal live cell imaging and images analysis

To test light-induced Ca^{2+} influx for OptoORAI1 variants, HeLa cells seeded on 35 mm glass bottom dishes were transiently transfected with OptoORAI1 and GCaMP6 at 20-24 h before imaging. Imaging was acquired on a Nikon Eclipse A1R microscope mounted onto a Nikon Eclipse T1 body. An incubation cage was installed to maintain the temperature, humidity and CO_2 supplies. Lipofectamine 3000 was used for transfection following the manufacturer's protocol. GCaMP6 and mKate2 images (with 40x oil objects) were acquired every 5 sec for 2-3 min depending on the experimental requirements. The 488 nm laser was used for photoactivation with 5% input. For the OptoORAI1 cycle stimulation by GCaMP6 or R-GECO1.2, blue light pulse was given as indicated in Figure 20c and Figure 22g.

For NFAT-GFP translocation testing, OptoORAI1 vectors were transfected into HeLa cells with stable expression of NFAT-GFP. Images were acquired every 1 min for 15 min under blue light stimulation (470 nm, 40 $\mu W/mm^2$, ThorLabs, Inc.). The mKate2 positive cells were used for analysis.

Generation of OptoORAI mutant library by error-prone PCR

The ORAI1 fragment (residues 160-233) containing the partial intracellular loop, transmembrane 3 (TM3) and the second extracellular loop were used for randomized mutagenesis. To achieve a high mutational ratio, we chose to use the GeneMorph II Random Mutagenesis Kit (Agilent). To perform error-prone PCR for the designed ORAI1 region, I used 10 ng of the template plasmid (mKate2-T2A-OptoORAI1(P245T)-V1) in a total reaction volume of 50 µl. 33 PCR cycles were used to increase the mutational frequency. The restriction sites BspEI, which is introduced by LOV2 insertion at the C-terminus of LOV2, and endogenous

XmaI at the second extracellular loop end of ORAI1 were used for insertion of mutant fragments into the mKate2-T2A-OptoORAI1(P245T)-V1 template. The PCR products flanked by BspEI and XmaI were sub-cloned into the template vector to replace the corresponding segment to yield a sublibrary for screening an optimized OptoORAI.

High-throughput NFAT translocation assay and data analysis

HeLa cells stably expressing $NFAT_{1-460}$-GFP were seeded into 384-well glass bottom dishes at a density of 2000 cell/25 μl medium/well by a Multidrop Dispensers (Thermo Fisher Scientific). On the second day, the OptoORAI mutants were individually transfected into seeded cells at a concentration of 25 ng/well by using Lipofectamine 3000. Four wells were repeated for each plasmid, with two repeat for the dark and lit conditions, respectively. 24 hours after transfection, cells were either shielded from the dark or subjected to blue light illumination with an external LED (470 nm, 40 $\mu W/mm^2$, ThorLabs, Inc) for 20 min. Next, cells were fixed with 4% PFA and stained with DAPI following the standard fixing and DAPI staining protocol. All the staining and washing steps were operated by the Hydrospeed (Tecan Diagnostics) and Multidrop Dispensers. The images for mKate2, GFP and DAPI channels were acquired by IN Cell Analyzer 6000 (GE-Healthcare Life Sciences) with a 10x object with 2 fields for each well. A total of 8 different imaging fields were acquired for each plasmid and each treatment.

The high-throughput image data was analyzed by Pipeline Pilot. Reid Powell at Institute of Biosciences and Technology-Texas A&M University wrote the code and analyzed the data. The NFAT translocation index was used to indicate the degrees of nuclear translocation of NFAT, and high number means a high level of translocation.

Results

Engineering of light-gated Ca^{2+} specific ORAI1 channel

We chose to insert LOV2 in the loop region of ORAI1 to keep the TM helices intact. The constitutively active mutations, most of which are located in the TM regions, cause partial of full activation of ORAI1 channels. Here we inserted the LOV2 into the ORAI1 intracellular loop and presumably could exert allosteric actions on the nearby TM3 and TM4 regions (**Figure 20a**). The constitutively active mutants in TM3-4 are chosen for LOV2 insertion. The ORAI1-P245T-LOV2 chimera indeed showed significant calcium influx upon blue light irradiation (**Figure 20b**) while the LV>AN mutant only showed a slight increase. Interestingly, we observed a modest decrease of GCaMP6 signals in cells expressing the chimeric mutant G183D. We named the LOV2-inserted P245T mutant as OptoORAI1-V1 and measured the calcium kinetics (**Figure 20c**). The light-induced Ca^{2+} influx is reversible. Additionally, the V1 construct showed a biphasic response in light-induced calcium response (an initial drop within 12 sec followed by the increase of signals), which makes it more complicated for data interpretation and less practical for future applications in biological systems. The stable GCaMP intensity after photostimulation indicated that the calcium decreases is not caused by GCaMP photobleaching. Nonetheless, results from the $NFAT_{1\text{-}460}$-GFP translocation assay suggested a relatively high pre-activation of the V1 construct, although there was an increased nuclear translocation after blue light induction. It is possible that the OptoORAI1 assumes an intermediate state (between the open and closed states) and is very sensitive to local structural perturbation elicited by the LOV2 conformational switch (with a free energy of 3.8 kcal/mol) (88). We therefore focused on

improving the OptoORAI to eliminate the biphasic response, reduce the dark activation and enhance the dynamic range of calcium signals.

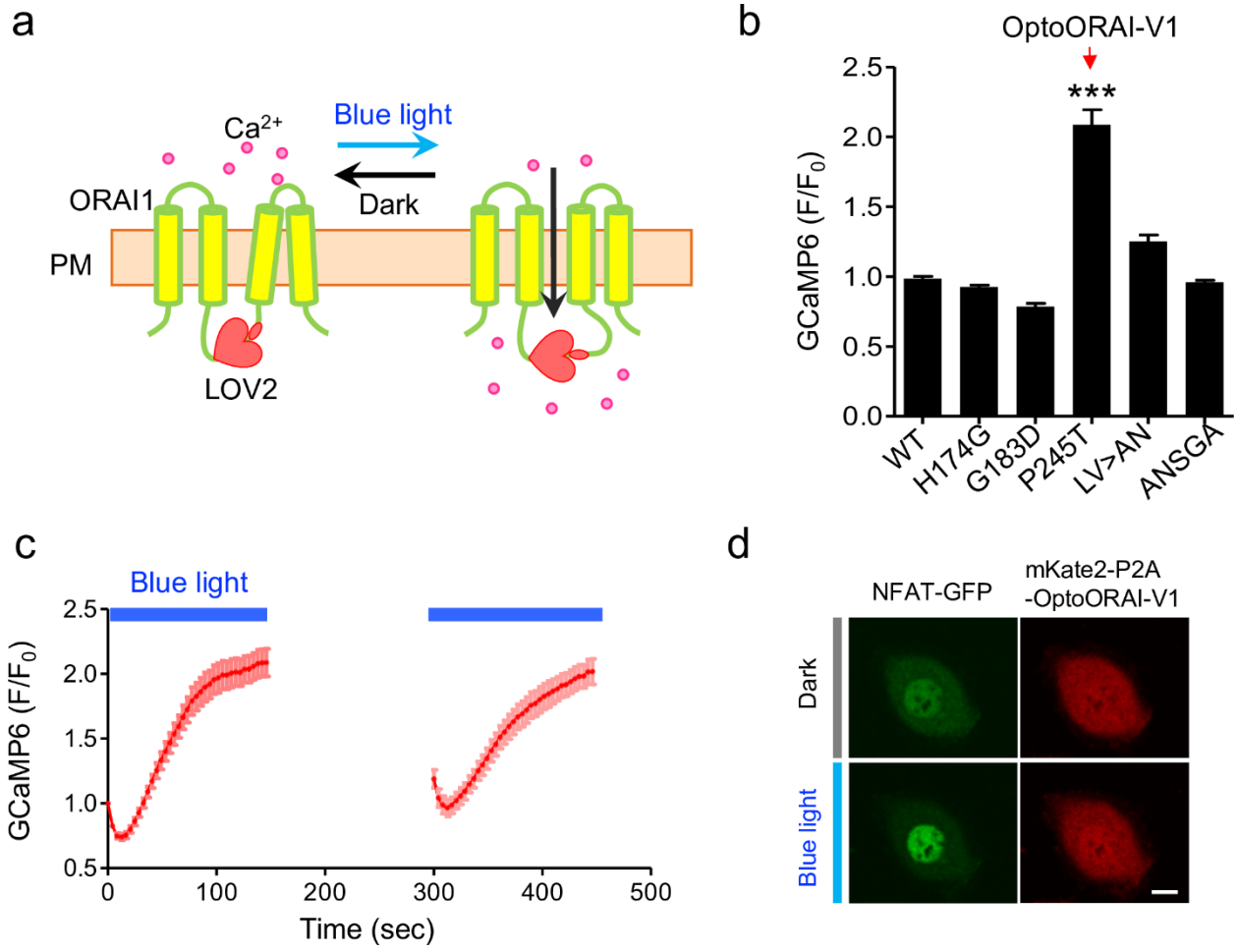

Figure 20. Design and characterization of OptoORAI.
(a) Schematic of blue light inducible Ca^{2+} influx through OptoORAI. The LOV2 domain was inserted into the intracellular loop of active ORAI1 and silenced the constitutively active ORAI1. Upon blue light exposure, the conformational change of ORAI that follow LOV2-Jα photo activation triggers Ca^{2+} influx through ORAI channel. **(b)** The fold-change of calcium response was indicated by GCaMP6 for OptoORAI variants. The LOV2 domain was inserted into WT and selected constitutively active mutations of ORAI1. **(c)** Light-tunable Ca^{2+} entry reported by GCaMP6s in HeLa cells transfected with OptoORAI-V1. Blue bar: 470 nm light. **(d)** Blue light drove $NFAT_{1-460}$-GFP nuclear translocation in the cell expressing mkate2-P2A-OptoORAI-V1. High degree of pre-activation was observed as indicated by nuclear GFP-NFAT in the dark.

Engineering next generation OptoORAI-V2 through error-prone PCR screening

To make OptoORAI1 as a strictly controlled optogenetic device, it is important to minimize dark-state pre-activation. For long-time use, an overload of Ca^{2+} in the cells will cause cell death. We thus turned to directed random mutagenesis to improve the light-caging efficiency of OptoORAI1 and increase the Ca^{2+} dynamic range. We reasoned that specific mutations in ORAI1 might keep the TM regions away from the activation position. Based on the OptoORAI with the P245T mutation, we set out to improve the light gating by directly evolving the region between LOV2 insertion site and Orai1-P245T (approximately 70 residues), which includes the TM3/4 and the 2nd extracellular loop. The error-prone PCR was used to amplify this region to generate a mutant library (**Figure 21a**). The Mn^{2+}-containing buffer and unequal concentrations of nucleotides contribute to mutagenic conditions for *Taq* DNA polymerase. The amplified mutant products were sub-cloned into OptoORAI to replace the original TM3-loop region.

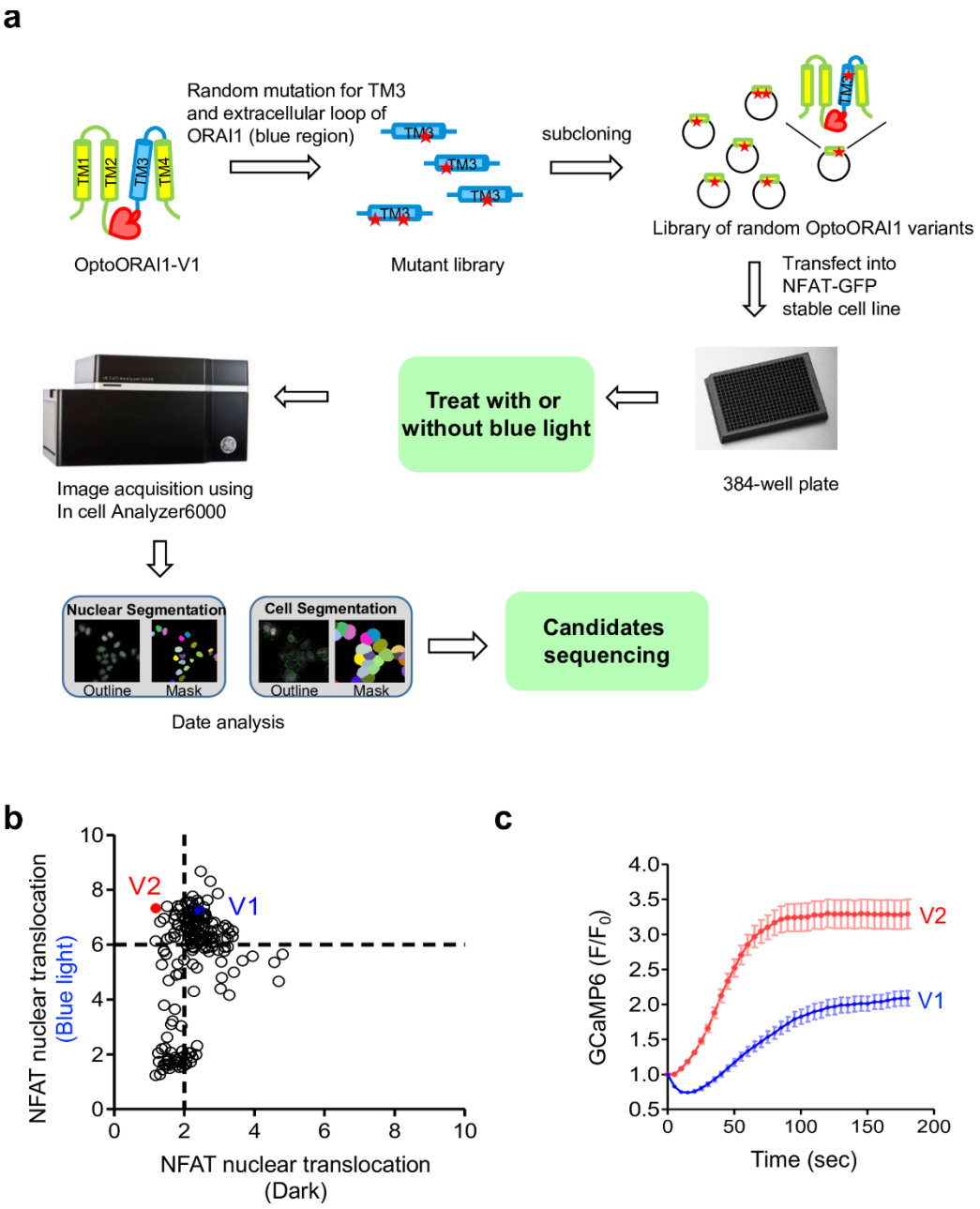

Figure 21. Optimization of OptoORAI.
(a) The TM3 and extracellular region (highlighted in blue) was amplified by error-prone PCR to introduce random mutations between the LOV2 insertion site and P245T in TM4. The mutant fragments were subcloned into OptoORAI (P245T) to replace the same region. The OptoORAI1 variants were transfected into a NFAT$_{1\text{-}460}$-GFP stable cell line and illuminate the plate to induce calcium-stimulated NFAT translocation after 24 h expression. The duplicate plate with the same transfection was kept in the dark to test the pre-activation of OptoORAI. Acquire images by in cell Analyzer 6000 and analyze data by Pipeline Pilot. The variants with low NFAT translocation in the dark state and high NFAT translocation in the lit state have be selected as OptoORAI candidates. Last, characterize the candidates by sequencing. **(b)** Validation of OptoORAI variants in NFAT$_{1\text{-}460}$-GFP stable cells. NFAT nuclear translation degrees were plotted as dark VS light. The original V1 was highlighted in blue; the best construct with low dark activation and high light activation was indicated in red as V2. **(c)** Qualification and comparison of Ca^{2+} signals generated by OptoORAI V1 and V2.

The mutant constructs were further selected by high-throughput NFAT nuclear translocation screening. The cytosolic Ca^{2+} elevation was anticipated to induce NFAT-GFP nuclear translocation. To perform positive selection for the efficient Ca^{2+} flux induced NFAT nuclear translocation in the presence of blue light, the transfected cells were incubated under a light source for 15 min. We also performed negative selection for the less Ca^{2+} leakage constructs in the absence of blue light. The qualified NFAT index (degree of NFAT nuclear translocation) was plotted for each construct of both dark and light state (**Figure 21b**). As we expected, the introduction of random mutations improved the OptoORAI1. The best performance at the upper left corner was designated as OptoORAI1-V2, which has less dark activation and high light-induced NFAT translocation. Sanger's sequencing revealed that the best candidate contained the H171D mutation located at the TM3, in addition to the P245T substitution at TM4. The Ca^{2+} dynamic change was 3-fold of V2 compared to 2-fold for V1 (**Figure 21c**). From the Ca^{2+} activation kinetics, we observed that the V2 exhibited a single-phase light-inducible Ca^{2+} increase compared. The GCaMP6s Ca^{2+} signal statured after about 90 sec of blue light illumination; while the V1 took about 130 sec.

Functional characterization of OptoORAI1

To determine if the LOV2 can be inserted at other loop sites for the double mutation (H171D, P245T) ORAI1 screened above, eight more sites (site1-9, site7 is the original LOV2 insertion site) were chosen for every 2 or 3 residues. The sites were shown in **Figure 22a,** and the light excited Ca^{2+} fold changes were plotted in **Figure 22b**. The OptoORAI1-V2 (S7) displayed the most robust response. Most of the LOV2 insertion variants showed no obvious Ca^{2+} change. Three variants were found to be activated by light. The S9 insertion site close to

TM3 has a moderate Ca^{2+} dynamic change (2.2-fold). Interestingly, one variant (S8) had the opposite response, which showed light-dependent inhibition of Ca^{2+} influx.

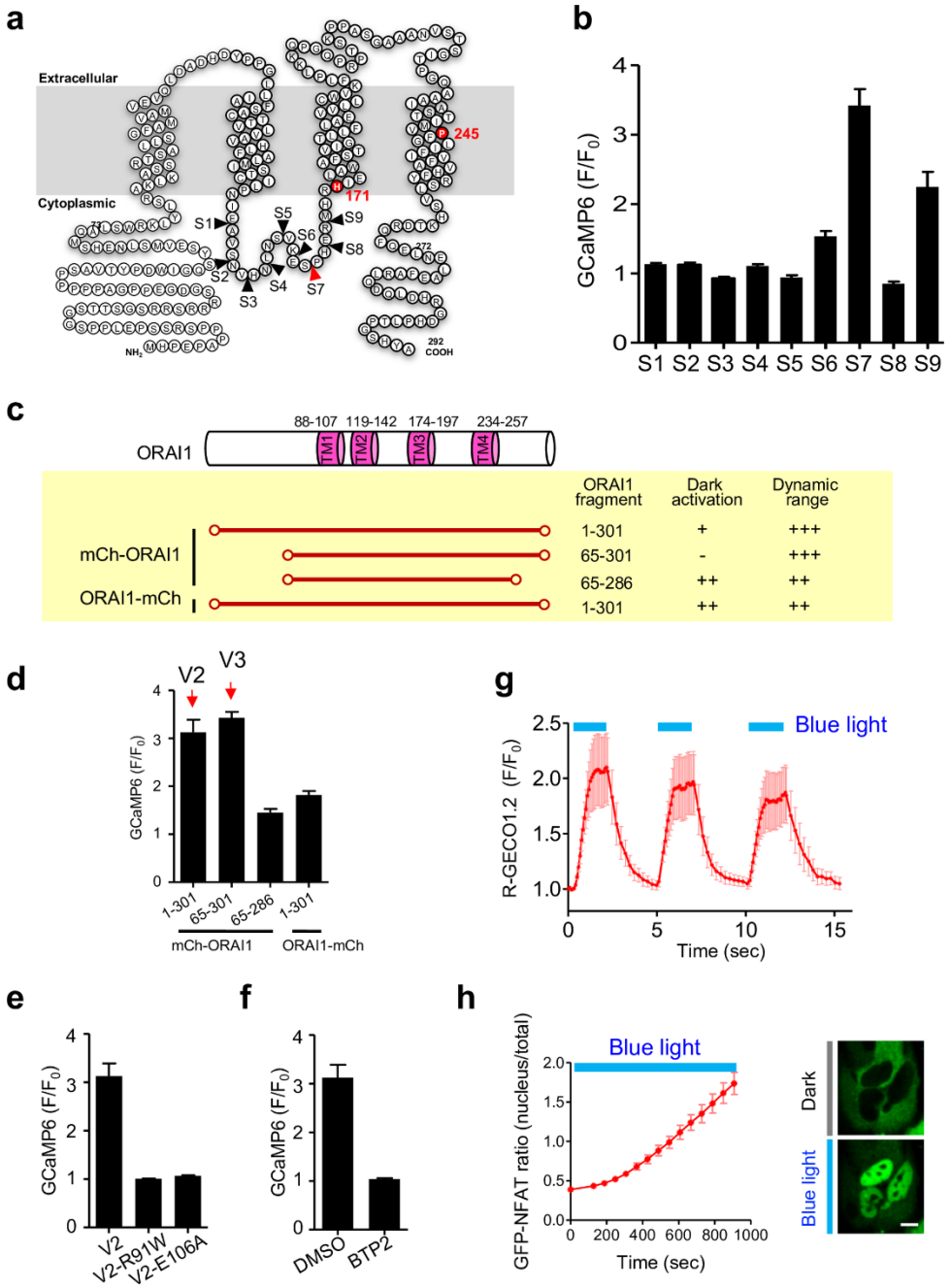

Figure 22. Characterization of OptoORAI1-V2.
(a) LOV2 insertion sites in ORAI1 were further optimized based on the ORAI1 mutations obtained from error-prone screening. **(b)** The bar graph showed the light-induced Ca^{2+} dynamic change for constructs indicated in (a). **(c-d)** ORAI1 fragments and mCherry position influenced Ca^{2+} influx in OptoORAI. Dark activation is fined as the GFP intensity ratio of mCh-OptoOARI1 transfected cells over non-transfected ones in GCaMP6 stable cells. The mCh-OptoORAI1(65-301) (V3) showed a reduced dark activation and increased Ca^{2+} dynamic change. **(e)** Blue light tunable Ca^{2+} influx by OptoORAI1-V3. Ca^{2+} sensor R-GECO1.2 was used to monitor the cytosolic Ca^{2+} change **(f-g)** ORAI1 dead mutations (R91W or E106A) and ORAI1 channel inhibitor BTP2 blocked the calcium entry of OptoORAI. **(h)** Blue light-induced $NFAT_{1\text{-}460}$-GFP nuclear translocation in OptoORAI1-V3 transfected cells stably expressing $NFAT_{1\text{-}460}$-GFP.

It has been reported that the truncated ORAI1 (65-301) still forms the functional Ca^{2+} channel and retains much of the activity [62, 117]. The ORAI1 (1-285) behaves as WT with deletion of the C-terminal residues 286-301. Therefore, the truncations of OptoORA1-V2 with mCherry fused to its N or C-terminus were made. The light-activated Ca^{2+} change was measured by GCaMP6 (**Figure 22c-d**). The mCherry-OptoORAI1-V2 variant behaved similarly to mKate2-T2A-OptoORAI1-V2. When the mCherry tag was placed to the C-terminus, we only observed a moderate light-induced Ca^{2+} elevation. The truncated mCh-OptoORAI1 (65-301) variant showed a robust Ca^{2+} increase upon photostimulation similar to V2, but had less dark activity as monitored by the NFAT nuclear translocation assay. We designed this optimized version as V3. Further truncations in the ORAI1 C-terminus on V3 reduced the photo-responsiveness, thus highlighting the importance of the ORAI1 carboxyl end in our study. To further confirm the blue light-induced Ca^{2+} influx through OptoORAI1, the ORAI1 dead mutations R91W [118, 119] or E106A [120] were introduced into OptoORAI1-V3. The data showed that Ca^{2+} influx was eliminated with these constructs (**Figure 22e**). The CRAC channel inhibitor BTP2 also abolished the OptoORAI-V3 activity, further validating that the light-induced effect was specifically mediated by ORAI channels.

The OptoORAI1-V3 could repeatedly be activated by blue light with activation and decay half-time of 34 sec and 21 sec, respectively (**Figure 22g**). The light stimulation was given as indicated in the figure. The OptoORAI1-V3 induced NFAT-GFP nuclear translocation kinetics and images were shown in **Figure 22h**. Almost no NFAT-GFP was observed in the nuclei in the dark state and a strong nuclear translocation was detected after 15 min blue light photoexcitation for the improved OptoORAI1-V3.

Discussion

In conclusion, we have developed a photo-switchable Ca^{2+} selective channel by combining a blue-light sensor LOV2 and a Ca^{2+} specific ORAI1 channel. The resulting OptoORAI1 is fully genetically encoded. The FMN cofactor for lightswitch LOV2 is ubiquitously present in mammals, and therefore, no external factors are needed. This promising tool has several desirable properties:

First, it is a single component Ca^{2+} specific channel with reversibility. Besides, there are very limited reports for combining the photosensory into naturally-occurring ion channels to make it light controllable. There is only one precedent reporting the fusion the LOV2 to a small viral K^+ channel Kcv to generate a blue-light-inducible K^+ channel (BLINK1) [121]. Our tool provides a unique way to control Ca^{2+} signaling and Ca^{2+}-modulated biological functions.

Second, this OptoORAI created is more "ORAI1" specific. For the OptoSTIM1[122] or its variants described in the previous chapters, it gates not only the ORAI1, but also the isoforms ORAI2 and ORAI3 [111, 123], as well as other unknown binding targets. Both OptoSTIM1 and OptoORAI are single-component tools, the efficacy of OptoSTIM1 is dependent on the endogenous ORAI levels. By comparison, OptoORAI1 obviates the requirement of endogenous ORAI, making it a more attractive tool to photo-manipulate tissues/cells with no or little ORAI expression.

Third, the successful photoactivation suggested that the strategy of allosteric control of ORAI1 might be applied to manipulate other ion channels with light. Our successful example illustrates a broadly applicable method to design and control membrane protein activity.

Finally, the OptoORAI1 can be used for screening specific chemical modulators of ORAI1 channel, particularly ORAI1 blockers. Currently, the most widely used

immunosuppressant agents in patients are targeted to calcineurin, which is the downstream effector of CRAC channel but upstream of NFAT. Because calcineurin is shared by many signaling pathways, calcineurin targeted immunotherapy causes serious side effects, such as hypertension, nephrotoxicity and liver damage [124, 125]. The ORAI1 channel is specific for Ca^{2+} influx and ORAI1 inhibitors might have fewer side effects in immunosuppression. Indeed, in mice depleted of ORAI1, very mild extra-immunological symptoms are observed, further attesting that targeting ORAI channel might be a more attractive strategy. Traditional NFAT nuclear translocation assay cannot distinguish whether compounds directly binding to ORAI1 or other proteins in the CRAC/Calcineurin/NFAT signaling cascade. By combing the OptoORAI1 with high throughput platform, we will develop an all-optical screening platform to search for ORAI1 channel specific modulators.

CHAPTER V

SUMMARY

Calcium signaling regulates nearly every aspect of cellular life. We engineered one of the highly Ca^{2+} selective CRAC channel, which has an important function in immune response. In this study, the light sensor was used to control the functions of STIM1 and ORAI1, which form the two elementary components in the store-operated calcium entry pathway. We developed the OptoCRAC system (OptoSTIM1 and OptoORAI1) for blue light inducible Ca^{2+} influx and optimized them with less background activation but higher dynamic calcium change.

In the first part of this study, we used lightswitch LOV2 to cage the function of the minimal ORAI1 activation region within STIM1. The tunable Ca^{2+} oscillation patterns can affect the efficiency of NFAT translocation and NFAT-related gene expression. More variants of OptoSTIM1 by PM anchoring, or combination with Zdk2 are available to provide a full cassette of genetically encoded calcium actuators with varying kinetics and dynamics for broad applications.

In the second part of this study, a circularly permuted LOV2 was module was developed as the new optogenetic platform for protein caging. The created cpLOV2 maintained similar structure and function as WT LOV2. Upon blue light absorption, the cpLOV2 underwent light-induced conformational change by releasing the Jα helix. In the functional study, the cpLOV2 showed similar caging effects for $STIM1_{336\text{-}486}$, NLS, NES and SsrA, as LOV2. The docking sites of N-terminus and middle (Jα helix and core domain) provides new caging interfaces for protein docking.

In the third part of this study, the LOV2 was inserted into ORAI1 as the allosteric switch to photo-trigger Ca^{2+} entry. The LOV2 insertion into ORAI1 with P245T mutation showed a light-induced Ca^{2+} increase. However, it exhibited a relatively high dark activity, promoting us to further improve the tool through randomized mutagenesis. The optimized OptoORAI1-V2 and its shorter version OptoORAI1-V3 showed better performance in Ca^{2+} influx and NFAT nuclear translocation. This OptoORAI tool is compatible with tissues having low or no endogenous ORAI proteins.

In summary, our creation of a full collection of OptoCRAC tools will enable us to study the function of Ca^{2+} signaling and CRAC channels at an unprecedented spatiotemporal resolution. The development of optics-based platform will enable the fast and easy high throughput screening of calcium channel-specific inhibitors, thus providing drug candidates for developing therapeutics to treat autoimmune disorders, allergy and cancer.

REFERENCES

1. Berridge, M.J., P. Lipp, and M.D. Bootman, *The versatility and universality of calcium signalling.* Nat Rev Mol Cell Biol, 2000. **1**(1): p. 11-21.
2. Clapham, D.E., *Calcium signaling.* Cell, 2007. **131**(6): p. 1047-58.
3. Berridge, M.J., *The Inositol Trisphosphate/Calcium Signaling Pathway in Health and Disease.* Physiol Rev, 2016. **96**(4): p. 1261-96.
4. Prakriya, M. and R.S. Lewis, *Store-Operated Calcium Channels.* Physiol Rev, 2015. **95**(4): p. 1383-436.
5. Lewis, R.S., *Store-operated calcium channels: new perspectives on mechanism and function.* Cold Spring Harb Perspect Biol, 2011. **3**(12).
6. Soboloff, J., B.S. Rothberg, M. Madesh, and D.L. Gill, *STIM proteins: dynamic calcium signal transducers.* Nat Rev Mol Cell Biol, 2012. **13**(9): p. 549-65.
7. Feske, S., *Calcium signalling in lymphocyte activation and disease.* Nat Rev Immunol, 2007. **7**(9): p. 690-702.
8. Parekh, A.B., *Store-operated CRAC channels: function in health and disease.* Nat Rev Drug Discov, 2010. **9**(5): p. 399-410.
9. Buckley, R.H., *Molecular defects in human severe combined immunodeficiency and approaches to immune reconstitution.* Annu Rev Immunol, 2004. **22**: p. 625-55.
10. Feske, S., R. Draeger, H.H. Peter, K. Eichmann, and A. Rao, *The duration of nuclear residence of NFAT determines the pattern of cytokine expression in human SCID T cells.* J Immunol, 2000. **165**(1): p. 297-305.
11. Gwack, Y., S. Srikanth, M. Oh-Hora, P.G. Hogan, E.D. Lamperti, et al., *Hair loss and defective T- and B-cell function in mice lacking ORAI1.* Mol Cell Biol, 2008. **28**(17): p. 5209-22.
12. Oh-Hora, M., M. Yamashita, P.G. Hogan, S. Sharma, E. Lamperti, et al., *Dual functions for the endoplasmic reticulum calcium sensors STIM1 and STIM2 in T cell activation and tolerance.* Nat Immunol, 2008. **9**(4): p. 432-43.
13. Shaw, K.T., A.M. Ho, A. Raghavan, J. Kim, J. Jain, et al., *Immunosuppressive drugs prevent a rapid dephosphorylation of transcription factor NFAT1 in stimulated immune cells.* Proc Natl Acad Sci U S A, 1995. **92**(24): p. 11205-9.
14. Hogan, P.G., L. Chen, J. Nardone, and A. Rao, *Transcriptional regulation by calcium, calcineurin, and NFAT.* Genes Dev, 2003. **17**(18): p. 2205-32.
15. Tian, C., L. Du, Y. Zhou, and M. Li, *Store-operated CRAC channel inhibitors: opportunities and challenges.* Future Med Chem, 2016. **8**(7): p. 817-32.
16. Bohm, J., F. Chevessier, C. Koch, G.A. Peche, M. Mora, et al., *Clinical, histological and genetic characterisation of patients with tubular aggregate myopathy caused by mutations in STIM1.* J Med Genet, 2014. **51**(12): p. 824-33.
17. Bohm, J., F. Chevessier, A. Maues De Paula, C. Koch, S. Attarian, et al., *Constitutive activation of the calcium sensor STIM1 causes tubular-aggregate myopathy.* Am J Hum Genet, 2013. **92**(2): p. 271-8.

18. Hulot, J.S., J. Fauconnier, D. Ramanujam, A. Chaanine, F. Aubart, et al., *Critical role for stromal interaction molecule 1 in cardiac hypertrophy.* Circulation, 2011. **124**(7): p. 796-805.
19. Hogan, P.G., R.S. Lewis, and A. Rao, *Molecular basis of calcium signaling in lymphocytes: STIM and ORAI.* Annu Rev Immunol, 2010. **28**: p. 491-533.
20. Palty, R., Z. Fu, and E.Y. Isacoff, *Sequential Steps of CRAC Channel Activation.* Cell Rep, 2017. **19**(9): p. 1929-1939.
21. Putney, J.W., *Pharmacology of store-operated calcium channels.* Mol Interv, 2010. **10**(4): p. 209-18.
22. Deisseroth, K., *Optogenetics.* Nat Methods, 2011. **8**(1): p. 26-9.
23. Yizhar, O., L.E. Fenno, T.J. Davidson, M. Mogri, and K. Deisseroth, *Optogenetics in neural systems.* Neuron, 2011. **71**(1): p. 9-34.
24. Fenno, L., O. Yizhar, and K. Deisseroth, *The development and application of optogenetics.* Annu Rev Neurosci, 2011. **34**: p. 389-412.
25. Nagel, G., T. Szellas, W. Huhn, S. Kateriya, N. Adeishvili, et al., *Channelrhodopsin-2, a directly light-gated cation-selective membrane channel.* Proc Natl Acad Sci U S A, 2003. **100**(24): p. 13940-5.
26. Zhang, F., V. Gradinaru, A.R. Adamantidis, R. Durand, R.D. Airan, et al., *Optogenetic interrogation of neural circuits: technology for probing mammalian brain structures.* Nat Protoc, 2010. **5**(3): p. 439-56.
27. Kleinlogel, S., K. Feldbauer, R.E. Dempski, H. Fotis, P.G. Wood, et al., *Ultra light-sensitive and fast neuronal activation with the Ca(2)+-permeable channelrhodopsin CatCh.* Nat Neurosci, 2011. **14**(4): p. 513-8.
28. Huang, X., P. Yang, X. Ouyang, L. Chen, and X.W. Deng, *Photoactivated UVR8-COP1 module determines photomorphogenic UV-B signaling output in Arabidopsis.* PLoS Genet, 2014. **10**(3): p. e1004218.
29. Bugaj, L.J., A.T. Choksi, C.K. Mesuda, R.S. Kane, and D.V. Schaffer, *Optogenetic protein clustering and signaling activation in mammalian cells.* Nat Methods, 2013. **10**(3): p. 249-52.
30. Taslimi, A., B. Zoltowski, J.G. Miranda, G.P. Pathak, R.M. Hughes, et al., *Optimized second-generation CRY2-CIB dimerizers and photoactivatable Cre recombinase.* Nat Chem Biol, 2016.
31. Halavaty, A.S. and K. Moffat, *N- and C-terminal flanking regions modulate light-induced signal transduction in the LOV2 domain of the blue light sensor phototropin 1 from Avena sativa.* Biochemistry, 2007. **46**(49): p. 14001-9.
32. Strickland, D., Y. Lin, E. Wagner, C.M. Hope, J. Zayner, et al., *TULIPs: tunable, light-controlled interacting protein tags for cell biology.* Nat Methods, 2012. **9**(4): p. 379-84.
33. Guntas, G., R.A. Hallett, S.P. Zimmerman, T. Williams, H. Yumerefendi, et al., *Engineering an improved light-induced dimer (iLID) for controlling the localization and activity of signaling proteins.* Proc Natl Acad Sci U S A, 2015. **112**(1): p. 112-7.
34. Zoltowski, B.D., B. Vaccaro, and B.R. Crane, *Mechanism-based tuning of a LOV domain photoreceptor.* Nat Chem Biol, 2009. **5**(11): p. 827-34.
35. Nash, A.I., R. McNulty, M.E. Shillito, T.E. Swartz, R.A. Bogomolni, et al., *Structural basis of photosensitivity in a bacterial light-oxygen-voltage/helix-turn-helix (LOV-HTH) DNA-binding protein.* Proc Natl Acad Sci U S A, 2011. **108**(23): p. 9449-54.

36. Motta-Mena, L.B., A. Reade, M.J. Mallory, S. Glantz, O.D. Weiner, et al., *An optogenetic gene expression system with rapid activation and deactivation kinetics.* Nat Chem Biol, 2014. **10**(3): p. 196-202.
37. Sawa, M., D.A. Nusinow, S.A. Kay, and T. Imaizumi, *FKF1 and GIGANTEA complex formation is required for day-length measurement in Arabidopsis.* Science, 2007. **318**(5848): p. 261-5.
38. Levskaya, A., O.D. Weiner, W.A. Lim, and C.A. Voigt, *Spatiotemporal control of cell signalling using a light-switchable protein interaction.* Nature, 2009. **461**(7266): p. 997-1001.
39. Burgie, E.S. and R.D. Vierstra, *Phytochromes: an atomic perspective on photoactivation and signaling.* Plant Cell, 2014. **26**(12): p. 4568-83.
40. Zhou, X.X., H.K. Chung, A.J. Lam, and M.Z. Lin, *Optical control of protein activity by fluorescent protein domains.* Science, 2012. **338**(6108): p. 810-4.
41. Grusch, M., K. Schelch, R. Riedler, E. Reichhart, C. Differ, et al., *Spatio-temporally precise activation of engineered receptor tyrosine kinases by light.* EMBO J, 2014. **33**(15): p. 1713-26.
42. Heintz, U. and I. Schlichting, *Blue light-induced LOV domain dimerization enhances the affinity of Aureochrome 1a for its target DNA sequence.* Elife, 2016. **5**: p. e11860.
43. Taslimi, A., J.D. Vrana, D. Chen, S. Borinskaya, B.J. Mayer, et al., *An optimized optogenetic clustering tool for probing protein interaction and function.* Nat Commun, 2014. **5**: p. 4925.
44. Reichhart, E., A. Ingles-Prieto, A.M. Tichy, C. McKenzie, and H. Janovjak, *A Phytochrome Sensory Domain Permits Receptor Activation by Red Light.* Angew Chem Int Ed Engl, 2016.
45. Lungu, O.I., R.A. Hallett, E.J. Choi, M.J. Aiken, K.M. Hahn, et al., *Designing photoswitchable peptides using the AsLOV2 domain.* Chem Biol, 2012. **19**(4): p. 507-17.
46. Christie, J.M., M. Salomon, K. Nozue, M. Wada, and W.R. Briggs, *LOV (light, oxygen, or voltage) domains of the blue-light photoreceptor phototropin (nph1): binding sites for the chromophore flavin mononucleotide.* Proc Natl Acad Sci U S A, 1999. **96**(15): p. 8779-83.
47. Huala, E., P.W. Oeller, E. Liscum, I.S. Han, E. Larsen, et al., *Arabidopsis NPH1: a protein kinase with a putative redox-sensing domain.* Science, 1997. **278**(5346): p. 2120-3.
48. Jarillo, J.A., H. Gabrys, J. Capel, J.M. Alonso, J.R. Ecker, et al., *Phototropin-related NPL1 controls chloroplast relocation induced by blue light.* Nature, 2001. **410**(6831): p. 952-4.
49. Salomon, M., J.M. Christie, E. Knieb, U. Lempert, and W.R. Briggs, *Photochemical and mutational analysis of the FMN-binding domains of the plant blue light receptor, phototropin.* Biochemistry, 2000. **39**(31): p. 9401-10.
50. Swartz, T.E., S.B. Corchnoy, J.M. Christie, J.W. Lewis, I. Szundi, et al., *The photocycle of a flavin-binding domain of the blue light photoreceptor phototropin.* J Biol Chem, 2001. **276**(39): p. 36493-500.
51. Wu, Y.I., D. Frey, O.I. Lungu, A. Jaehrig, I. Schlichting, et al., *A genetically encoded photoactivatable Rac controls the motility of living cells.* Nature, 2009. **461**(7260): p. 104-8.

52. Yumerefendi, H., A.M. Lerner, S.P. Zimmerman, K. Hahn, J.E. Bear, et al., *Light-induced nuclear export reveals rapid dynamics of epigenetic modifications.* Nat Chem Biol, 2016. **12**(6): p. 399-401.
53. Yumerefendi, H., D.J. Dickinson, H. Wang, S.P. Zimmerman, J.E. Bear, et al., *Control of protein activity and cell fate specification via light-mediated nuclear translocation.* PloS one, 2015. **10**(6): p. e0128443.
54. Renicke, C., D. Schuster, S. Usherenko, L.O. Essen, and C. Taxis, *A LOV2 domain-based optogenetic tool to control protein degradation and cellular function.* Chem Biol, 2013. **20**(4): p. 619-26.
55. Kyung, T., S. Lee, J.E. Kim, T. Cho, H. Park, et al., *Optogenetic control of endogenous Ca(2+) channels in vivo.* Nat Biotechnol, 2015. **33**(10): p. 1092-6.
56. Ma, G., M. Wei, L. He, C. Liu, B. Wu, et al., *Inside-out Ca 2+ signalling prompted by STIM1 conformational switch.* Nature communications, 2015. **6**: p. 7826.
57. Wang, H., M. Vilela, A. Winkler, M. Tarnawski, I. Schlichting, et al., *LOVTRAP: an optogenetic system for photoinduced protein dissociation.* Nat Methods, 2016. **13**(9): p. 755-8.
58. Wang, H. and K.M. Hahn, *LOVTRAP: A Versatile Method to Control Protein Function with Light.* Curr Protoc Cell Biol, 2016. **73**: p. 21 10 1-21 10 14.
59. Wang, X., Y. Wang, Y. Zhou, E. Hendron, S. Mancarella, et al., *Distinct Orai-coupling domains in STIM1 and STIM2 define the Orai-activating site.* Nature communications, 2014. **5**: p. 3183.
60. Zhou, Y., P. Srinivasan, S. Razavi, S. Seymour, P. Meraner, et al., *Initial activation of STIM1, the regulator of store-operated calcium entry.* Nat Struct Mol Biol, 2013. **20**(8): p. 973-81.
61. Zhou, Y., S. Ramachandran, M. Oh-Hora, A. Rao, and P.G. Hogan, *Pore architecture of the ORAI1 store-operated calcium channel.* Proc Natl Acad Sci U S A, 2010. **107**(11): p. 4896-901.
62. Zhou, Y., P. Meraner, H.T. Kwon, D. Machnes, M. Oh-hora, et al., *STIM1 gates the store-operated calcium channel ORAI1 in vitro.* Nat Struct Mol Biol, 2010. **17**(1): p. 112-6.
63. Chen, T.W., T.J. Wardill, Y. Sun, S.R. Pulver, S.L. Renninger, et al., *Ultrasensitive fluorescent proteins for imaging neuronal activity.* Nature, 2013. **499**(7458): p. 295-300.
64. Wu, J., L. Liu, T. Matsuda, Y. Zhao, A. Rebane, et al., *Improved orange and red Ca(2)+/- indicators and photophysical considerations for optogenetic applications.* ACS Chem Neurosci, 2013. **4**(6): p. 963-72.
65. Strickland, D., X. Yao, G. Gawlak, M.K. Rosen, K.H. Gardner, et al., *Rationally improving LOV domain-based photoswitches.* Nature methods, 2010. **7**(8): p. 623-6.
66. Kim, J.M., M. Lee, N. Kim, and W.D. Heo, *Optogenetic toolkit reveals the role of Ca2+ sparklets in coordinated cell migration.* Proc Natl Acad Sci U S A, 2016. **113**(21): p. 5952-7.
67. Dagliyan, O., M. Tarnawski, P.H. Chu, D. Shirvanyants, I. Schlichting, et al., *Engineering extrinsic disorder to control protein activity in living cells.* Science, 2016. **354**(6318): p. 1441-1444.
68. Giorgi, C., A. Danese, S. Missiroli, S. Patergnani, and P. Pinton, *Calcium Dynamics as a Machine for Decoding Signals.* Trends Cell Biol, 2018.

69. Inoue, M., A. Takeuchi, S. Horigane, M. Ohkura, K. Gengyo-Ando, et al., *Rational design of a high-affinity, fast, red calcium indicator R-CaMP2.* Nature methods, 2015. **12**(1): p. 64-70.
70. Dolmetsch, R.E., K. Xu, and R.S. Lewis, *Calcium oscillations increase the efficiency and specificity of gene expression.* Nature, 1998. **392**(6679): p. 933-6.
71. Inoue, T., W.D. Heo, J.S. Grimley, T.J. Wandless, and T. Meyer, *An inducible translocation strategy to rapidly activate and inhibit small GTPase signaling pathways.* Nature methods, 2005. **2**(6): p. 415-8.
72. Hoth, M. and R. Penner, *Calcium release-activated calcium current in rat mast cells.* J Physiol, 1993. **465**: p. 359-86.
73. Fearnley, C.J., H.L. Roderick, and M.D. Bootman, *Calcium signaling in cardiac myocytes.* Cold Spring Harb Perspect Biol, 2011. **3**(11): p. a004242.
74. Apati, A., K. Paszty, L. Hegedus, O. Kolacsek, T.I. Orban, et al., *Characterization of calcium signals in human embryonic stem cells and in their differentiated offspring by a stably integrated calcium indicator protein.* Cell Signal, 2013. **25**(4): p. 752-9.
75. Tonelli, F.M., A.K. Santos, D.A. Gomes, S.L. da Silva, K.N. Gomes, et al., *Stem cells and calcium signaling.* Adv Exp Med Biol, 2012. **740**: p. 891-916.
76. Uda, Y., Y. Goto, S. Oda, T. Kohchi, M. Matsuda, et al., *Efficient synthesis of phycocyanobilin in mammalian cells for optogenetic control of cell signaling.* Proc Natl Acad Sci U S A, 2017. **114**(45): p. 11962-11967.
77. Kaberniuk, A.A., A.A. Shemetov, and V.V. Verkhusha, *A bacterial phytochrome-based optogenetic system controllable with near-infrared light.* Nat Methods, 2016. **13**(7): p. 591-7.
78. Luik, R.M., M.M. Wu, J. Buchanan, and R.S. Lewis, *The elementary unit of store-operated Ca2+ entry: local activation of CRAC channels by STIM1 at ER-plasma membrane junctions.* J Cell Biol, 2006. **174**(6): p. 815-25.
79. Franzini-Armstrong, C., F. Protasi, and V. Ramesh, *Shape, size, and distribution of Ca(2+) release units and couplons in skeletal and cardiac muscles.* Biophys J, 1999. **77**(3): p. 1528-39.
80. Luik, R.M. and R.S. Lewis, *New insights into the molecular mechanisms of store-operated Ca2+ signaling in T cells.* Trends Mol Med, 2007. **13**(3): p. 103-7.
81. Shen, J., L. Zhao, and G. Han, *Lanthanide-doped upconverting luminescent nanoparticle platforms for optical imaging-guided drug delivery and therapy.* Advanced drug delivery reviews, 2013. **65**(5): p. 744-55.
82. Chen, G., H. Qiu, P.N. Prasad, and X. Chen, *Upconversion nanoparticles: design, nanochemistry, and applications in theranostics.* Chem Rev, 2014. **114**(10): p. 5161-214.
83. Zimmerman, S.P., B. Kuhlman, and H. Yumerefendi, *Engineering and Application of LOV2-Based Photoswitches.* Methods Enzymol, 2016. **580**: p. 169-90.
84. Cunningham, B.A., J.J. Hemperly, T.P. Hopp, and G.M. Edelman, *Favin versus concanavalin A: Circularly permuted amino acid sequences.* Proc Natl Acad Sci U S A, 1979. **76**(7): p. 3218-22.
85. Lo, W.C., C.C. Lee, C.Y. Lee, and P.C. Lyu, *CPDB: a database of circular permutation in proteins.* Nucleic Acids Res, 2009. **37**(Database issue): p. D328-32.
86. Lindqvist, Y. and G. Schneider, *Circular permutations of natural protein sequences: structural evidence.* Curr Opin Struct Biol, 1997. **7**(3): p. 422-7.

87. Baird, G.S., D.A. Zacharias, and R.Y. Tsien, *Circular permutation and receptor insertion within green fluorescent proteins.* Proc Natl Acad Sci U S A, 1999. **96**(20): p. 11241-6.
88. Daugherty, A.B., S. Govindarajan, and S. Lutz, *Improved biocatalysts from a synthetic circular permutation library of the flavin-dependent oxidoreductase old yellow enzyme.* J Am Chem Soc, 2013. **135**(38): p. 14425-32.
89. Lindberg, M., J. Tangrot, and M. Oliveberg, *Complete change of the protein folding transition state upon circular permutation.* Nat Struct Biol, 2002. **9**(11): p. 818-22.
90. Nakai, J., M. Ohkura, and K. Imoto, *A high signal-to-noise Ca(2+) probe composed of a single green fluorescent protein.* Nat Biotechnol, 2001. **19**(2): p. 137-41.
91. Qian, Z., J.R. Horton, X. Cheng, and S. Lutz, *Structural redesign of lipase B from Candida antarctica by circular permutation and incremental truncation.* J Mol Biol, 2009. **393**(1): p. 191-201.
92. Yu, Y. and S. Lutz, *Circular permutation: a different way to engineer enzyme structure and function.* Trends Biotechnol, 2011. **29**(1): p. 18-25.
93. Pudasaini, A., K.K. El-Arab, and B.D. Zoltowski, *LOV-based optogenetic devices: light-driven modules to impart photoregulated control of cellular signaling.* Front Mol Biosci, 2015. **2**: p. 18.
94. Kawano, F., Y. Aono, H. Suzuki, and M. Sato, *Fluorescence imaging-based high-throughput screening of fast- and slow-cycling LOV proteins.* PloS one, 2013. **8**(12): p. e82693.
95. Nash, A.I., W.H. Ko, S.M. Harper, and K.H. Gardner, *A conserved glutamine plays a central role in LOV domain signal transmission and its duration.* Biochemistry, 2008. **47**(52): p. 13842-9.
96. Cui, B., X. Yang, S. Li, Z. Lin, Z. Wang, et al., *The inhibitory helix controls the intramolecular conformational switching of the C-terminus of STIM1.* PloS one, 2013. **8**(9): p. e74735.
97. Korzeniowski, M.K., I.M. Manjarres, P. Varnai, and T. Balla, *Activation of STIM1-Orai1 involves an intramolecular switching mechanism.* Sci Signal, 2010. **3**(148): p. ra82.
98. Yang, X., H. Jin, X. Cai, S. Li, and Y. Shen, *Structural and mechanistic insights into the activation of Stromal interaction molecule 1 (STIM1).* Proc Natl Acad Sci U S A, 2012. **109**(15): p. 5657-62.
99. Yu, J., H. Zhang, M. Zhang, Y. Deng, H. Wang, et al., *An aromatic amino acid in the coiled-coil 1 domain plays a crucial role in the auto-inhibitory mechanism of STIM1.* Biochem J, 2013. **454**(3): p. 401-9.
100. Niopek, D., P. Wehler, J. Roensch, R. Eils, and B. Di Ventura, *Optogenetic control of nuclear protein export.* Nature communications, 2016. **7**: p. 10624.
101. Niopek, D., D. Benzinger, J. Roensch, T. Draebing, P. Wehler, et al., *Engineering light-inducible nuclear localization signals for precise spatiotemporal control of protein dynamics in living cells.* Nature communications, 2014. **5**: p. 4404.
102. Di Paolo, G. and P. De Camilli, *Phosphoinositides in cell regulation and membrane dynamics.* Nature, 2006. **443**(7112): p. 651-7.
103. Rebecchi, M.J. and S.N. Pentyala, *Structure, function, and control of phosphoinositide-specific phospholipase C.* Physiol Rev, 2000. **80**(4): p. 1291-335.

104. Gilbert, L.A., M.H. Larson, L. Morsut, Z. Liu, G.A. Brar, et al., *CRISPR-mediated modular RNA-guided regulation of transcription in eukaryotes.* Cell, 2013. **154**(2): p. 442-51.
105. Qi, L.S., M.H. Larson, L.A. Gilbert, J.A. Doudna, J.S. Weissman, et al., *Repurposing CRISPR as an RNA-guided platform for sequence-specific control of gene expression.* Cell, 2013. **152**(5): p. 1173-83.
106. Hou, X., L. Pedi, M.M. Diver, and S.B. Long, *Crystal structure of the calcium release-activated calcium channel Orai.* Science, 2012. **338**(6112): p. 1308-13.
107. Liou, J., M.L. Kim, W.D. Heo, J.T. Jones, J.W. Myers, et al., *STIM is a Ca2+ sensor essential for Ca2+-store-depletion-triggered Ca2+ influx.* Curr Biol, 2005. **15**(13): p. 1235-41.
108. Derler, I., P. Plenk, M. Fahrner, M. Muik, I. Jardin, et al., *The extended transmembrane Orai1 N-terminal (ETON) region combines binding interface and gate for Orai1 activation by STIM1.* J Biol Chem, 2013. **288**(40): p. 29025-34.
109. Stathopulos, P.B., R. Schindl, M. Fahrner, L. Zheng, G.M. Gasmi-Seabrook, et al., *STIM1/Orai1 coiled-coil interplay in the regulation of store-operated calcium entry.* Nat Commun, 2013. **4**: p. 2963.
110. Muik, M., I. Frischauf, I. Derler, M. Fahrner, J. Bergsmann, et al., *Dynamic coupling of the putative coiled-coil domain of ORAI1 with STIM1 mediates ORAI1 channel activation.* J Biol Chem, 2008. **283**(12): p. 8014-22.
111. Yuan, J.P., W. Zeng, M.R. Dorwart, Y.J. Choi, P.F. Worley, et al., *SOAR and the polybasic STIM1 domains gate and regulate Orai channels.* Nat Cell Biol, 2009. **11**(3): p. 337-43.
112. Gudlur, A., A. Quintana, Y. Zhou, N. Hirve, S. Mahapatra, et al., *STIM1 triggers a gating rearrangement at the extracellular mouth of the ORAI1 channel.* Nat Commun, 2014. **5**: p. 5164.
113. McNally, B.A., M. Yamashita, A. Engh, and M. Prakriya, *Structural determinants of ion permeation in CRAC channels.* Proc Natl Acad Sci U S A, 2009. **106**(52): p. 22516-21.
114. Yamashita, M., P.S. Yeung, C.E. Ing, B.A. McNally, R. Pomes, et al., *STIM1 activates CRAC channels through rotation of the pore helix to open a hydrophobic gate.* Nat Commun, 2017. **8**: p. 14512.
115. Zhou, Y., X. Cai, R.M. Nwokonko, N.A. Loktionova, Y. Wang, et al., *The STIM-Orai coupling interface and gating of the Orai1 channel.* Cell calcium, 2017. **63**: p. 8-13.
116. Zhou, Y., X. Cai, N.A. Loktionova, X. Wang, R.M. Nwokonko, et al., *The STIM1-binding site nexus remotely controls Orai1 channel gating.* Nat Commun, 2016. **7**: p. 13725.
117. Li, Z., J. Lu, P. Xu, X. Xie, L. Chen, et al., *Mapping the interacting domains of STIM1 and Orai1 in Ca2+ release-activated Ca2+ channel activation.* J Biol Chem, 2007. **282**(40): p. 29448-56.
118. Feske, S., M. Prakriya, A. Rao, and R.S. Lewis, *A severe defect in CRAC Ca2+ channel activation and altered K+ channel gating in T cells from immunodeficient patients.* J Exp Med, 2005. **202**(5): p. 651-62.
119. Feske, S., Y. Gwack, M. Prakriya, S. Srikanth, S.H. Puppel, et al., *A mutation in Orai1 causes immune deficiency by abrogating CRAC channel function.* Nature, 2006. **441**(7090): p. 179-85.

120. Navarro-Borelly, L., A. Somasundaram, M. Yamashita, D. Ren, R.J. Miller, et al., *STIM1-Orai1 interactions and Orai1 conformational changes revealed by live-cell FRET microscopy.* J Physiol, 2008. **586**(22): p. 5383-401.
121. Cosentino, C., L. Alberio, S. Gazzarrini, M. Aquila, E. Romano, et al., *Optogenetics. Engineering of a light-gated potassium channel.* Science, 2015. **348**(6235): p. 707-10.
122. He, L., Y. Zhang, G. Ma, P. Tan, Z. Li, et al., *Near-infrared photoactivatable control of Ca(2+) signaling and optogenetic immunomodulation.* Elife, 2015. **4**.
123. Frischauf, I., M. Muik, I. Derler, J. Bergsmann, M. Fahrner, et al., *Molecular determinants of the coupling between STIM1 and Orai channels: differential activation of Orai1-3 channels by a STIM1 coiled-coil mutant.* J Biol Chem, 2009. **284**(32): p. 21696-706.
124. Burdmann, E.A., T.F. Andoh, L. Yu, and W.M. Bennett, *Cyclosporine nephrotoxicity.* Semin Nephrol, 2003. **23**(5): p. 465-76.
125. Hoorn, E.J., S.B. Walsh, J.A. McCormick, A. Furstenberg, C.L. Yang, et al., *The calcineurin inhibitor tacrolimus activates the renal sodium chloride cotransporter to cause hypertension.* Nat Med, 2011. **17**(10): p. 1304-9.